MSc Thesis Project

BCP Lithography Defined Arrays of InAs NWs Grown Using MOVPE with Au Seeds

2015.11.30
(Corrected 2016.04.17)

Björn Landeke-Wilsmark

LUND
UNIVERSITY

Supervisor: Ivan Maximov (ivan.maximov@ftf.lth.se)
Co-supervisor: Nicklas Nilsson (nicklas.nilsson@ftf.lth.se)
Examiner: Carina Fasth (carina.fasth@ftf.lth.se)

ABSTRACT

In this report we outline a detailed process flow for a quick and inexpensive implementation of large dense arrays of InAs *nanowires* (NWs) grown in the *reactive ion etching/*etched (RIE) pores of a SiO_2/SiN_x mask on top of an InAs/Si(111) substrate. The self-assembled (hexagonally close-packed) pattern of *poly(methyl-methacrylate)* (PMMA) cylinders in a *poly(styrene)* (PS) matrix adopted by a linear diblock *poly(styrene-block-methyl-methacrylate)* P(S-b-MMA) *block-copolymer* (BCP) was transferred to the dielectric stack (consisting of a ≈10 nm *plasma enhanced chemical vapour deposition/deposited* (PECVD) SiN_X layer topped by a thin *atomic layer deposition/deposited* (ALD) SiO_2 film) using a two-step RIE procedure. Gold particles were then selectively deposited at the bottom of the etched cylinders by means of electrodeposition and were later used as catalytic seeds in the subsequent *metal-organic vapour-phase epitaxy* (MOVPE) growth of InAs NWs.

The P(S-b-MMA) BCP was used in conjunction with a graftable hydroxyl end-functionalized P(S-r-MMA) brush layer and the conditions for *rapid thermal processing* (RTP) grafting and various annealing techniques were evaluated. RTP was found to be a rapid, effective and convenient way of performing both the brush layer graft and the BCP anneal. This project was a successful proof-of-concept but each step in the process flow still needs further optimization to improve the fidelity of our version of BCP lithography.

Contents

Acknowledgements

First of all I like to thank my supervisor Ivan Maximov (Assoc. Prof.) and Lars-Erik Wernersson (Prof.) for instigating this project and for entrusting me with it. I am furthermore grateful to them for giving me the freedom to explore and delve into esoterica while still keeping me en route towards the larger goal. I also like to convey my deep-felt gratitude to Nicklas Nilsson, Reza Jafari Jam and Mariusz Graczyk for tutelage, inspiring discussions and advice in all things big and nano. It is safe to say that they share a stake in any 'successes' of this project however I greedily claim full credit for all follies and wrong turns. I like to point out that Reza was instrumental by expertly operating the machinery for all processing steps involving PECVD, ALD and electrodeposition – of course under my stern supervision. Johannes Svensson must also be included for providing advice regarding and performing the crowning MOVPE NW growth.

The acknowledgement would not be complete without mentioning Dmitry Suyatin, Håkan Lapovski and George Rydnemalm for all manners of practical assistance in the lab and finally Federico Ferrarese Lupi for resolving to a number of important processing queries through e-mail correspondence.

List of Abbreviations and Symbols

A#.#	**Appendix #.#**
AA	Acetic Acid
B67	P(S-b-MMA), $M_n = 67$ kg/mol
B82	P(S-b-MMA), $M_n = 82$ kg/mol
BCP	Block-copolymer
D	Total DUV dose at $\lambda = 254$ nm
d_{cyl}	Cylinder diameter
DSC	Differential scanning calorimetry
EBL	Electron Beam Lithography
ER	Etch rate
f_A	Volumetric fraction of block "A"
FC	Faraday cage
γ_A	Surface energy of block A (at an interface)
GT	Growth test
h_{BCP}	BCP layer thickness
IPA	Isopropanol, 2-Propanol
M_n	Number average molecular weight
M_w	Weight average molecular weight
MOVPE	Metal-organic vapour phase epitaxy
N	Degree of polymerization
NW	Nanowire
$N\chi_{AB}$	Degree of immiscibility between the A and B block in the BCP
PDI	Polydispersity index
PECVD	Plasma enhanced chemical vapour deposition
P(S-b-MMA)	Poly(styrene-block-methyl-metacrylate)
PP	Plasma Preen
RCP	Random co-polymer
RTP	Rapid Thermal Processing (Equipment)
SB	Soft-Bake
SC	Spin-coat(-ing)
SiN_x	Silicon Nitride
SVA	Solvent vapour anneal
T_g	Glass transition temperature
T_{graft}/T_a	RTP set-point temperature used brush graft and BCP annealing respectively.
THF	Tetrahydrofuran
TMIn	Tri-methyl indium
VA	Vacuum anneal
VO/C	Vacuum oven/chamber
VOA	Vacuum oven anneal
VCA	Vacuum chamber anneal
χ_{AB}	Flory-Huggins interaction parameter between monomer A and B

List of Important/Noteworthy Samples

BCP Anneal

Sample #	Description	Location
W15E	Best order achieved (of any sample) using RTP annealing	A1.1 (p. 17)
W15F	Sample with largest area of defect free ordering.	A2.2 (p. 18)
W40D	Slightly too high T_a for t_a =1 h	A2.2 (p. 19)
W24A,C	Too low h_{B82} for continuous surface coverage (when RTP annealed at $T_a = 250$°C for $t_a = 1$h)	A2.8 (p. 29)
W39B	Best ordering achieved on samples annealed in vacuum oven	A2.18 (p. 43)
W35B	Sample suspected to be damaged by the presence of an oxygen contain atmosphere during an extended thermal anneal	A2.19 (p. 44)
W27E	Best sample in the SVA evaluation	A2.22 (p. 49)
WN1C, WN5A	Best ordering on a SiNx surface	A4.4 (p. 76), A4.8 (p. 79)

Electrodeposition

Sample #	Description	Location
BL9777_01K	Best electrodeposition with regards to Au amount and distribution.	A5.2 (p. 92)

MOVPE

Sample #	Description	Location
BL9777_01I	Highest yield of NWs after MOVPE	A6 (p. 97)

Part I
Theory

1.1 Introduction

1.1.1 Background

Block-copolymer (BCP) lithography is a still maturing technology but it has been included in the *international technology roadmap for semiconductors* (ITRS) as one of the lithographic methods with the potential to enable the next generation of transistor nodes *[1]*. It is based on the principle that a polymer chain containing two, or more, covalently linked immiscible blocks will given the right circumstances self-organize so as to minimize the total free energy of the system *[2] [3]*. The blocks themselves contain only a single type of monomer residue but since they are covalently linked this imposes constrains on the entropic configurations available to the system. The immiscibility will cause 'microphase separation' (traditional nomenclature - regardless of feature size) i.e. the formation of separate 'homopolymer domains'. However, this entails stretching of the polymer chains (that otherwise adopt a random coil conformation) thus causing an energetically costly loss of entropy. Essentially, in the bulk state there are two competing forces at play: i) the unfavourable interaction between different monomers that drives them apart and ii) an entropic 'spring-like' restoring force *[2]*. The practical consequence is that a set of different, highly ordered, morphologies can be adopted in a BCP film by judiciously choosing the size and composition of the polymer and the conditions the cast film is subjected to. One of the more interesting morphologies obtainable from a diblock BCP is an array of hexagonally close packed cylinders, formed from one type of block from multiple polymer chains, in a matrix composed of the polymer in the other type of block. Differing properties of the polymer blocks, aside from their immiscibility, can then be harnessed in the implementation of more advanced nanostructures. If the property in question is etch resistance the polymer film can be used as an etch mask and thus make it possible to transfer the self-organized pattern to underlying layers. Essentially, BCP lithography entails utilizing the self-organized pattern of domains with differing physical properties in the manufacturing of periodic nanoscale features/structures.

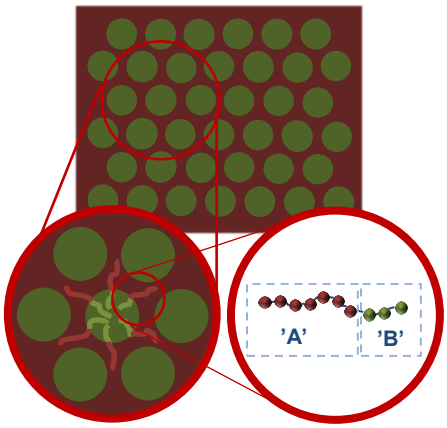

Figure 1: Schematic illustration of a single linear di-block BCP-chain and a top-view of an example of the resultant self-organized pattern formed in a polymer sample containing countless chains.

BCP lithography has several advantageous traits such as versatility, cost-effectiveness and perhaps most of all the potential for high resolution. The versatility stems from the fact that there is a vast number of monomer combinations to choose from and modern routes of chemical synthesis allow for the formation of not only linear polymer chains but also branched, star-shaped etc. Furthermore, a specific BCP can be subjected to post-synthesis modification to e.g. add/remove a functional group that adds/subtracts a certain property to one or both of the blocks e.g. lending the BCP tailored mechanical, optical, electrical, ionic, ligand-binding, species selective transporting, semiconducting or barrier properties *[2] [4]*. The main cost of using BCP lithography is the synthesis of the polymer; the polymer application and annealing steps might require specialized equipment but which in comparison to e.g. *electron beam lithography* (EBL) or *nanoimprint lithography* (NIL) is fairly inexpensive to buy and operate. The main strength however is the parallelism of the technology, stemming from the self-assembly of the BCP pattern, which is in stark contrast to EBL - the nanolithographic workhorse of choice today. EBL creates a pattern by serially exposing areas of an e^--beam sensitive resist which later is developed; the exposure renders the resist either more or less soluble in the developer depending on type of resist. The serial exposure is very time consuming and severely limits the size of patterned area

that can be realized in a given timeframe. EBL also requires large investments in highly expensive equipment and suffers from proximity effects in the implementation of small features and/or dense patterns. Proximity effects are caused by the scattering of the e^--beam as it interacts with the substrate and intrinsically limits the obtainable resolution and pattern density. This particular issue is not a problem in BCP lithography where theoretically both higher resolution and pattern densities are possible. See Table 1 below for a summarized comparison of alternative nanolithographic techniques.

Lithographic technique	Pros.	Cons.
Electron Beam Lithography (EBL)	i. Versatility ii. Process Control iii. Reproducibility	i. Proximity Effects ii. Serial Process iii. Expensive machine
Nanoimprint Lithography (NIL)	i. High Resolution ii. Parallel process	iii. Expensive machine + stamps
Molecular Self-assembly: Block-Copolymer (BCP) Lithography	i. Parallel Process ii. High resolution iii. High pattern density iv. Fast + inexpensive v. No proximity effects vi. No stamp needed	i. Polymer Synthesis ii. Limited pattern versatility iii. Process calibration iv. Process conditions

Table 1: A summarized comparison of advantages and disadvantages of alternative nanolithographic techniques.

Despite the impression that might have been conveyed above BCP lithography has, of course, drawbacks of its own. Among these are the need to identify the specific polymer composition and the conditions under which the BCP film will self-assemble into the desired morphology with the correct orientation relative to the substrate. These parameters will be polymer-specific and laborious calibration might be necessary for even small alterations to the polymer or substrate.

However, it is the author's view that the various nanolithographic techniques not ought to be pinned against one another but rather to see the ways in which they complement each other. It is not likely that the true pattern versatility of EBL ever can be matched by pure BCP lithography but when it comes to implementing large arrays techniques like NIL and BCP lithography will more than likely have the upper hand. Perhaps the most interesting applications of BCP lithography might be used in conjunction with the other lithographic methods in what is referred to as *directed self-assembly* (DSA). DSA entails using a pattern (physical, chemical or otherwise) to form conditions of e.g. confinement or wetting that will force the BCP pattern to locally have a certain orientation. DSA might also be a prerequisite in achieving long range order i.e. to minimize defects and create large grains (the 2D equivalent of crystal grains). Such a combined approach might be a convenient way to achieve a higher resolution and reap the benefits of parallelism inherent to the BCP while at the same time availing itself of the versatility and precision of traditional techniques such as EBL.

The continual strive for smaller feature sizes has been the staple of micro/nanotechnology since its inception. The premier engine of change is the ongoing scaling of MOSFET transistors in CMOS technology, the reason being that scaling allows for higher transistor operating frequencies and device densities. Unfortunately, this comes at the cost of a reduced electrostatic control of the transistor channel. This in turn translates into leakage currents i.e. an inability to completely switch of the transistor by applying a gate-voltage (the magnitude of which must not exceed the break-down voltage which is also affected by scaling). The presence of appreciable static leakage currents, now also in CMOS, means both a higher power consumption and local heat build-up. The increased power consumption is particularly detrimental in mobile applications with a limited battery capacity. The increased heat generation will limit the device density if it cannot be off-set by an improved heat dissipation. There are two main approaches for scaling these hurdles and push transistor performance even further: i) a move from the planar to a 'higher dimensional' gate/channel geometry and ii) substitute the traditional Si for a semiconductor with a higher carrier mobility e.g. III-V compounds. By "a higher dimensional gate/channel geometry" is here meant a transistor structure where the gate-channel interface area is increased by having the gate partially or completely surround the channel. Ideally the gate should wrap around the entire channel since this ensures the best possible electrostatic

control of the current through the channel. Perhaps the easiest way of implementing such a transistor geometry is by starting with a substrate with grown or etched vertical III-V NWs and it is here that this BCP lithography project enters the scene.

III-V NWs are interesting in their own right for combining the advantages of III-V semiconductors, such as direct band-gap, high carrier mobility, potential for advanced band-structure engineering with whose inherent to the nanoscale 1D geometry i.e. the free-standing nature, quantum confinement effects and an effective lateral strain relaxation. The latter allowing for implementation of highly lattice mismatched heterostructures - further extending the scope of band-structure engineering and/or integration directly onto Si substrates *[5]*.

1.1.2 Aims of the project

The main aim of this MSc project is the implementation of an array of Au seed particles, using BCP lithography, for subsequent epitaxial growth of III-V nanowires. Achieving this goal entails figuring out how to deal with a number of subsidiary milestones: i) choosing an appropriate polymer system, ii) achieving the desired morphology and orientation on top of a SiN_x-layer, iii) transferring the self-organized polymer pattern into the underlying SiN_x, iv) selective Au deposition in the resultant pores of the SiN_x layer and finally iv) *metal-organic vapour phase epitaxy* (MOVPE) of the III-V NWs. All of these steps can of course be broken down further and requires calibration to work as intended. The purpose of the SiN_x-layer is to immobilize the deposited Au dots on the substrate surface and as masking during the MOVPE i.e. to keep the Au seeds well separated and suppress epitaxial growth everywhere except beneath the Au dots. A schematic processing flow summary is outlined in Figure 2.

Since SiN_x can be deposited by means of low temperature techniques such as *plasma enhanced chemical vapour deposition* (PECVD) our hope is that the process flow developed during the course of this project will be transferable and thus applicable to several different III-V substrates. Furthermore, what makes this project particularly interesting is that it, to the author's knowledge, will be a proof-of-concept. BCP lithography has previously [6] been used to define pores in a SiN_x layer deposited on top of a GaAs substrate, where MOVPE was subsequently employed to grow InAs NWs in the defined openings by means of *selective area epitaxy* (SAE) i.e. without metal seed particles.

If arrays of III-V NWs can be realized with our method the NWs could then be further processed into the aforementioned vertical MOSFETs with wrap-around gates or used in e.g. optoelectrical applications such as LEDs or solar cells if heterojunctions are incorporated during the MOVPE growth.

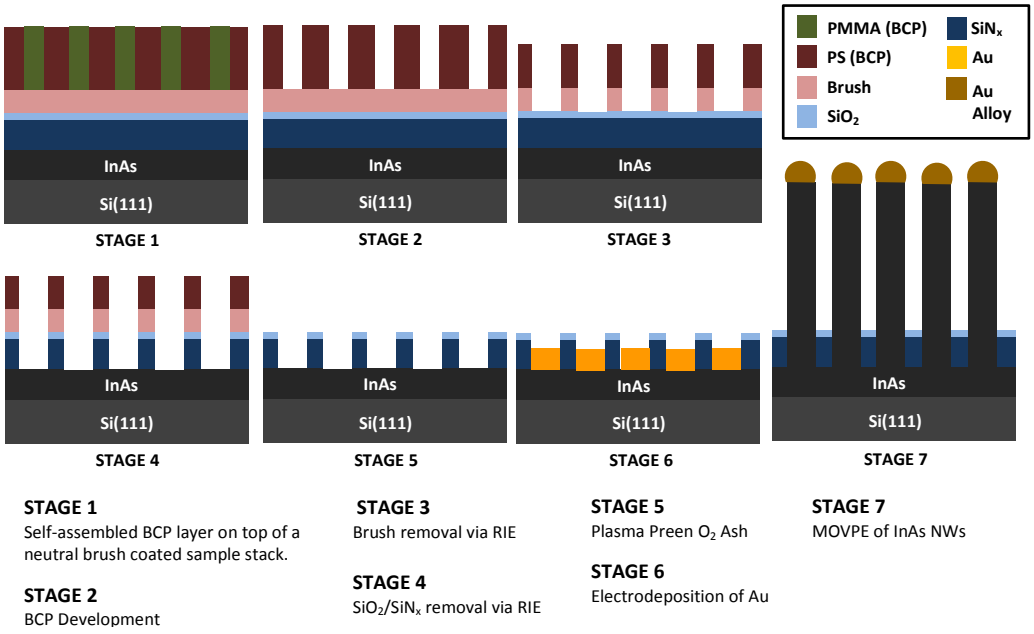

Figure 2: Schematic process flow for implementing InAs NWs using BCP lithography.

1.2 General BCP Theory

1.2.1 BCP Theory of Bulk Melts

As mentioned above, BCPs are a family of polymers whose chains consist of two or more homopolymer blocks that are covalently linked to each other. The homopolymer blocks themselves, as the name suggests, only contain of a single type of monomer residue. The molecular structure of a BCP can in principle be varied in perpetuity with designs including linear, branched, grafted and radiating star-like permutations *[2]*. This project only includes and deals with linear diblock BCPs which furthermore is the most researched configuration, partly because of the relative ease of synthesis and pattern usability. More intricate molecular designs require complex routes of chemical synthesis and mapping out phase/morphology diagrams with respect to e.g. relative internal composition is a laborious endeavour.

There are several parameters of interest used to characterize a BCP and which to a certain extent can be used to predict the thermodynamically stable morphology it will adopt in the bulk state. All polymers can be assigned *number (M_n) and weight (M_w) average molecular weights (MWs)* which of course is related to the size and composition of the polymer chains. In general when synthesizing a polymer the end product is not a collection of identical polymer chains but rather a distribution of chains of various lengths. One way of quantizing the width of this distribution is the *polydispersity index* (PDI) which simply is the ratio of M_w to M_n i.e. $PDI = M_w/M_n$. $PDI = 1$ means that all chains are of identical length and distributions with $PDI \leq 1.10$ can generally be considered narrow but that is of course dependent on the intended application. Another size-related parameter extensively used in BCP theory is the *degree of polymerization* (N) which is the total number of monomer residues included in the polymer chain. A noteworthy principle difference is that both M_n and M_w refers to a distribution whereas N describes a specific polymer chain. The initial attempts to describe and simulate the behaviour of BCP melts generally used an idealized scenario with a perfect delta distribution with respect to molecular weight (i.e. $PDI = 1$), position of polymer terminations in domains etc.. As computational power dropped in price, attempts has been made to address these shortcomings *[7]* but a general understanding and predictive power can still be gleaned from the idealized case where all polymer chains have an identical N. That is the case in the scenario described below.

A schematic linear diblock BCP containing monomers A and B will be used to illustrate the morphological phase diagram of a melt of this type of BCP. f_A and f_B are the volumetric fractions of the A and B block respectively in relation to the whole polymer chain and depends on the volume occupied by a single monomer residue as well as the number of residues (N_A resp. N_B) in the respective blocks. The volumetric relationship between the blocks is one of the most influential parameters affecting which available morphology will be the thermodynamically stable in a bulk BCP melt. However, as previously mentioned in order to obtain any degree of self-assembly the polymer blocks must be immiscible and a common way to quantize this immiscibility is through the use of the composite parameter called *degree of immiscibility* ($N\chi_{AB}$) where χ_{AB} is the *Flory-Huggins interaction parameter*. χ_{AB} describes the interaction between A and B type monomers and a higher value means that the interaction between the two types is more unfavourable as compared to if the monomers where to interact only with others of their own kind *[2] [8]*. A larger $N\chi_{AB}$ thus means a higher thermodynamic drive of the BCP melt to phase separate i.e. form micro-/nanodomains formed from a single type of block *[2]*. A diblock BCP system is usually characterized by a single χ_{AB}–parameter but this is not necessarily sufficient as the free energy cost from placing an A monomer in a surrounding of B monomers is not always the same as when placing a B monomer in an environment of A monomers *[2]*. Essentially, $N\chi_{AB}$ can be increased either by choosing a material system with a higher χ_{AB}-parameter or, for a given material system, increasing the length of the polymer chain i.e. N.

Self-consistent mean field theory (SCMFT) (a version of *mean field theory* (MFT)) has been used to model BCP melts and according to this $N\chi_{AB}$ needs to exceed ≈10.5 (for a symmetric BCP) for organized phase separation to take place – usually referred to as the segregation limit *[2] [8]*. Noteworthy is that χ_{AB} is inversely proportional ($\chi_{AB} \propto 1/T$) to the *temperature* (T) which means that the morphology of a bulk BCP melt can be pushed from an organized morphology into a disorganized state simply by increasing T (i.e. move along a vertical line in *Figure 3* b) *[2] [4]*; the *order to disorder transition* (ODT) occurs at T_{ODT} which in turn also is dependent on N and f_A. This fact can limit the available processing window in which the BCP can self-assemble into practically useful patterns. The definite upper temperature limit is otherwise the temperature at which the thermal energy is sufficient to break monomer-monomer bonds in the polymer backbone and thus decompose the polymer chain.

A high χ_{AB} is also desirable since it is conducive to sharper interfaces between the polymer domains. In this project the desirable morphology is that of hexagonally close packed cylinders and the point could be illustrated by making a cross-section of the film along the central axis of the cylinders. For a low χ_{AB} the interfaces between domains would be somewhat diffuse and if you were to plot the content of e.g. monomer A along the cross-section the curve would be reminiscent of a periodic sine function *[9]*. However, with increasing χ_{AB} this plot will more and more take on the appearance of a tophat (square-wave) function – something that for our purposes would be beneficial.

Thus far we have only seen the benefits of increasing $N\chi_{AB}$ but for various reasons you might not be free to choose the material system and then χ_{AB} will be fixed (T-dependence aside). Your only other option to up the $N\chi_{AB}$ is to increase N by making the polymer chain longer. Unfortunately this brings to bare one of the shortcomings with using a linear diblock BCP, namely that the size of the domains will grow correspondingly. Since $N\chi_{AB} \geq 10.5$ is a prerequisite for organized phase separation there is an intrinsic resolution limit for a given BCP i.e. a low χ_{AB} material system will never be able to achieve the same degree of resolution as one with a higher χ_{AB} *[9] [10]*. A high χ_{AB} usually occurs for fairly dissimilar monomers e.g. polar/non-polar or hydrophilic/hydrophobic. A lot of interest has, of late, been devoted to BCPs composed of one organic and one inorganic type of monomer *[11] [12]* e.g. P(S-b-DMS) for the dual potential of relatively high i) χ_{AB} and ii) dry etch selectivity obtainable.

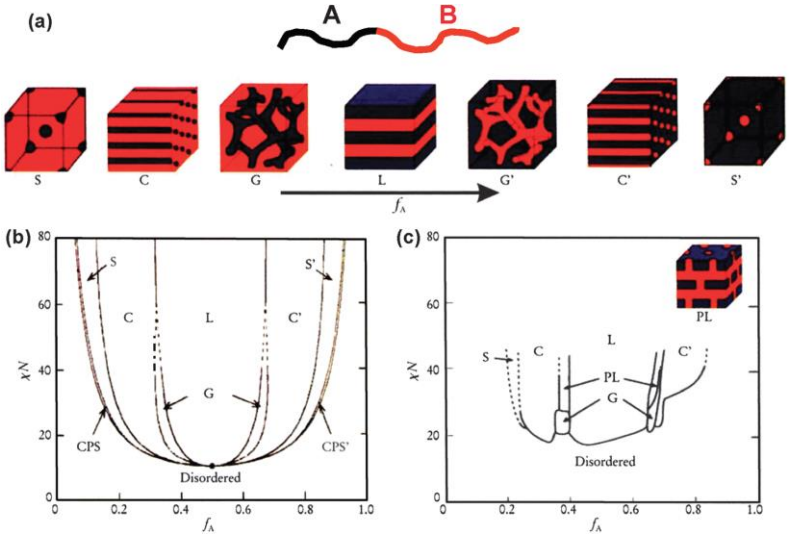

Figure 3: a) Thermodynamically stable morphologies of a diblock BCP melt. Simulated b) and experimentally obtained c) phase diagrams of a linear diblock BCP bulk melt. [8]

The SCMFT simulation of thermodynamically stable morphologies available to a diblock BCP melt and the compositions for which they occur are summarized in *Figure 3* b). As f_A is increased (for a fixed $\chi_{AB}N$) the morphology transitions from disorganized, to close-packed spheres of A in a matrix of B (CPS), to *body-centered cubically* (BCC) packed spheres (S), to cylinders of A (C), to gyroid (G), to lamellar (L), to the inverted gyroid (G'), to cylinders of B in a matrix of A (C') , to BCC spheres of B (S'), to CPS' and finally back to disorganized, see *Figure 3* a). The gyroid morphology is a cubic bi-continuous (both phases are continuous throughout the melt) network *[2] [4]*. The melt adopt these morphologies as a consequence of the attempt to minimize the free energy of the system. This entails minimizing the interfacial area between blocks but under the simultaneous condition of not causing too severe stretching of the polymer chains since this means an energetically costly loss of entropy *[2]*. The covalent bond between blocks in the polymer backbone is of course paramount since the same morphologies would not spontaneously be adopted if two homopolymers with the same M_n as the corresponding blocks were to be mixed in an equivalent ratio. Such a mix would *macro*phase separate i.e. the two types of homopolymers would agglomerate into two distinct layers, one on top of the other, in the same way as a dispersion of oil in water eventually will.

More diblock BCP morphologies than those outlined in *Figure 3* b) have been observed experimentally, generally for a very narrow set of conditions and most of these are deemed metastable or transition stages between more stable states - one example is *perforated lamellae* (PL). When comparing the

idealized phase-diagram in *Figure 3* b) to one experimentally obtained for the poly(isoprene-block-styrene) material system, see *Figure 3* c), three things become apparent: i) the basic predicted structure is present, ii) there is a marked loss of symmetry and iii) the disordered phase is stable beyond $\chi_{AB}N = 10.5$. There are several likely explanations why this is the case: i) f_A is defined as N_A/N here and the shape and volume occupied by a styrene monomer are different from those of isoprene monomers and ii) again a single χ_{AB} might not be sufficient *[2]*. The idealized version furthermore only considers the thermodynamics and not the kinetic limitations that have to be factored in, in a real world scenario. Kinetic considerations are particularly important in polymer physics since we are dealing with very large macromolecules that have a limited mobility - in part because of entanglements and molecular interactions between neighbouring chains. Polymers can for example have the thermodynamic potential to form a perfect crystal but the kinetics of the ordering process make such an outcome exceedingly unlikely given a finite timeframe.

1.2.2 Extension of theory to account for thin film conditions

The bulk state BCP theory accounted above needs to be amended if it is to serve as guidance in nanolithographic applications. The BCP is usually applied to a substrate through the means of e.g. spin- or dip-coating with the intent to form a 'thin' film. The morphological impact of the interactions at the air/polymer as well as the substrate/polymer interfaces is far greater for a thin film than in a thicker more bulk-like structure. Moreover, there now also exists an important orientational aspect e.g. in this project where the desired morphology is "C" it is essential for the cylinders to be oriented perpendicular to the substrate for them to be of practical use. Typically a preferential wetting behaviour of one of the polymer blocks towards the substrate is observed for a BCP system [4]. The fact that one block has a higher affinity for the substrate can make parallel cylinders the thermodynamically most stable orientation, at least close to the surface [4]. The influence of the polymer-air and polymer-substrate interfaces decays with the distance from the interface but in the thin film case the effect can be profound throughout the film due to the limited thickness of the polymer layer [13] [14]. The difference in wetting behaviour at the substrate can be quantized and described in terms the *differential surface energy* ($\delta\gamma = \gamma_A - \gamma_B$) between the two types of blocks towards the substrate surface. The *surface (or interface) energy* (γ_A) between the substrate and monomer A is a measure of the free energy cost associated with the interface (per unit area) as compared to the bulk state [15]. Since the entire BCP system strives to minimize the total free energy the substrate interaction with the block with the lowest γ will be favored and that block will tend to cluster at the interface. A similar process occurs at the air-polymer interface but the terminology used is instead *differential surface tension* since it is a liquid (alt. solid)-gas interface. Again, if there is a marked difference in surface tension between the blocks the one with the lower surface tension will preferentially migrate to the surface [13] . Without any substrate modifications the PMMA block will wet a Si oxide surface while the PS block will exhibit a stronger affinity for the free surface [3].

Various experimental approaches to coax or force a perpendicular orientation, of a given morphology, in a BCP film have been investigated. The directional property of strong electric or magnetic fields [4] can be used if there is a difference in response between the monomer residues to such fields. Attempts to utilize viscoelasticity related differences by subjecting the film to a shear induced strain have also been made as well as various forms of *zone annealing* (ZA) and directional solidification [4]. However, the most prevalent technique found in literature is the use of a brush layer in combination with control of the *BCP layer thickness* (h_{BCP}). A brush layer is layer introduced between the substrate and the BCP with, in our case, the intention to minimize $\delta\gamma$ and thus create so called *neutral wetting conditions*. Neutral wetting conditions is the nomenclature primarily used in literature but in actuality this is something of a misnomer and it is more accurate to state that the brush has an affinity for the particular composition found in the BCP thus creating a preference for the perpendicular orientation [16]. In this report however we will adhere to the language used in literature. Multiple types of materials have been tried for this purpose, including homopolymers (and blends thereof), *self-assembled monolayers* (SAMs) of silanes and *random-copolymers* (RCPs) and even other BCPs [4]. A RCP is polymer in which the monomer residues are not neatly ordered into discrete blocks but occur randomly along the length of the chain but in a chosen ratio. The synthesis of a RCP occurs from a common pool of monomers and is therefore generally easier than the synthesis of BCPs where, for example, one block first is synthesized from a single type of monomer before the chain is continued by synthesizing the other block in a separate step, see *Appendix 0* (A0). The ratio between monomer residues in a RCP can be controlled by choosing the composition in the reaction vessel during synthesis and/or by affecting the kinetics of the

polymerization reaction. Usually the types of monomers used are the same as the ones in the subsequently applied BCP but not necessarily in the same compositional ratio.

From a processing point of view there are two practical issues involved in the use of brush layers. The first is that the integrity of the layer has to be maintained during the application of the BCP e.g. the RCP must not be dissolved (during the spin-coating of the BCP) by the solvent used to solve the BCP [4]. For a RCP composed of the same type of monomers as the BCP this can be particularly challenging. The second issue if that the RCP cannot be allowed to migrate into the BCP layer during the order-inducing step e.g. thermal or solvent anneal [4]. If it was to do this it could potentially interfere with the self-assembly process of the BCP by its interaction and the fact that the neutral wetting condition will be lost at the substrate surface.

There are two principle strategies for combating these issues: by functionalizing the RCP to enable i) grafting and/or ii) cross-linking. Grafting means that the RCP chain is covalently linked to the substrate surface and thus immobilized. This can be accomplished by incorporating/terminating with a monomer residue with a reactive functional group e.g. a hydroxyl group (-OH) that can react with –OH-groups present on the surface in a condensation reaction. In the condensation reaction between two –OH groups H_2O is a by-product and an oxygen bridge (-O-) is established that anchors the RCP chain. The required activation energy for the reaction is generally supplied by heating of the brush covered sample to high temperatures ($\geq$170°C). All RCP chains not grafted to the surface need to be washed off before the application of the BCP. The second strategy is to incorporate a small amount of a monomer, in the RCP, with the ability to cross-link. After the RCP has to be subjected to the cross-linking stimuli e.g. heat or DUV it will form a non-solvable network where the RCP chains once again are immobilized with respect to large scale translation.

Both methods have pros and cons: the efficacy of grafting is highly substrate dependent due to the required presence of reactive groups e.g. –OH on the surface. If the density of these groups is low then the coverage of RCP after the wash will be sparse. Furthermore, the time required to allow for a sufficiently high number of –OH groups on the surface to react might be considerable.

The RTP grafting process can be divided into two regimes: i) the diffusion or reaction limited adsorption regime where the –OH group on the RCP has to come into juxtaposition to a corresponding group on the surface and later ii) the penetration limited regime where access to the substrate of additional RCP chains is limited due to the already grafted chains. If the new RCP molecules are to reach the surface the chains already present need to adopt a less favourable conformation i.e. there is an entropic penalty [17] [18].

On the pro side, grafting can generate very thin brush layers which can be beneficial for later lithographic steps. The principle benefit of using a cross-linkable RCP is the insensitivity to type of sample i.e. it could be used on a host of substrates as long as the wetting behaviour allows for a uniform film of the polymer to be applied. The downside is that it might be hard to form very thin uniform layers by spin-coating i.e. without the formation of pinholes or larger break-ups of the film. The physical stability of the cross-linked network might moreover be compromised if the film is made to thin. The monomer residue ratio in the RCP will also have to be adjusted to compensate for the introduction of the third cross-linkable monomer [14].

An important consideration is that the surface energies are temperature dependent which means that a brush layer only might be effective in a certain temperature range if γ_A and γ_B exhibit divergent behaviour as a function of temperature. Tailoring the atmosphere at the air/polymer interface could in principle play a similar role as that of the brush layer but the author has not found reliable literature investigating this.

The *BCP layer thickness* (h_{BCP}) is also considered important in achieving the perpendicular morphology. [3] refers to this as a *commensurability condition* between h_{BCP} and the interdomain distance (L_0) (in our case the center-to-center distance between adjacent cylinders). L_0 is here primarily related to the length of the BCP chain (for a linear di-block BCP) i.e. a chain of higher molecular weight results in a larger L_0. The exact volume ratio between the blocks also affect L_0 but to a far more limited extent. For a neutrally wetting substrate a h_{BCP}-window, in which the perpendicular geometry is obtained for a cylinder-forming BCP, is known to be located at $h_{BCP} \approx L_0$ [3]. Here the physical confinement in the

vertical dimension makes the perpendicular arrangement of cylinders energetically more favourable than that of parallel ones due to the strain that this would entail. However, vertical cylinders have been observed even at $h_{BCP} \neq L_0$ and specifically at $h_{BCP} = \frac{1}{2}L_0$ [3]. In thick films, i.e. on the order of multiple L_0, you run the risk of obtaining mixed morphologies long the film thickness, not sufficiently straight or even discontinuous cylinders. Such BCP films would be of limited use - if any.

In our case of a linear cylinder-forming diblock BCP the *diameter* (d_{cyl}) of the features as well as L_0 are determined by N and the exact f_A ratio [9]. This is of course in the ideal scenario with a perfect pattern and no influence from strain caused by confinement.

1.2.3 The P(S-b-MMA) material system and P(S-r-MMA) brush polymer

Both BCPs (B82 and B67) used in this MSc project belong to the *poly(styrene-block-methyl-metacrylate)* [P(S-b-MMA)] material system but differ on M_n and to a lesser extent f_{PS} (volume fraction of polystyrene in the BCP chain). Both are linear PMMA cylinder-forming diblock BCPs and the "B" in the nomenclature "Bxx" indicates that it is indeed a BCP while the number represents the *number average molecular weight* (M_n) in kg/mol. They were purchased from *Polymer Source Inc*. which also supplied some of the polymer characterization data stated here and everything in A0. Both were synthesized by means of a living anionic polymerization in *tetrahydrofuran* (THF) at -78°C by the use of an initiator (cumyl potassium and sec. butyl-Li for B82 and B67 respectively) and in the presence of LiCl. The *poly(styrene)* (PS) blocks were synthesized first and end-capped with diphenyl ethylene before the MMA monomers were added. *Size exclusion chromatography* (SEC) was used on both the PS homopolymer blocks as well as the complete BCPs in order to obtain M_n and M_w at both stages. The composition was determined by *proton nuclear magnetic resonance* (^{1}H-NMR) spectroscopy by comparing the peak area corresponding to the PMMA protons and that of the 'aromatic protons' of PS. *Polymer Source Inc.* also carried out a thermal analysis by using a *differential scanning calorimeter* (DSC, TA Q100) and a heating rate of 15°C/min.
The characterization data is summarized in Table 2.

SAMPLE	M_n^* /[kg·mol^{-1}]	M_w^* /[kg·mol^{-1}]	PDI^*	T_g^* /[°C]	f_{PS}^{**} *(vol.)*	d_{cyl}^{**} /[nm]	$L_{0,GISAXS}^{**}$ /[nm]	$L_{0,SEM}^{**}$ /[nm]
B82 - PS Block	57	60	1.05	106	-	-	-	-
B82 - PMMA Block	25	-	-	127	-	-	-	-
B82 - Complete BCP	87	-	1.07	-	0.7212	19.0 ± 2.0	43.9 ± 0.7	42.9 ± 0.7
B67 - PS Block	46.1	49.5	1.07	105	-	-	-	-
B67 - PMMA Block	21.0	-	-	128	-	-	-	-
B67 - Complete BCP	67.1	-	1.09	-	0.7135	17.0 ± 1.0	34.4 ± 0.4	35.0 ± 1.0
R10.5 - Complete RCP	10.5	12.0	1.15	91	0.66*	-	-	-

* = *Polymer Source Inc.*
** = [19]

Table 2: Characterization data for the BCPs and RCP used. PDI = polydispersity index, T_g = Glass transition temperature, f_{PS} = volume fraction PS, d_{cyl} = diameter of PMMA cylinders, $L_{0,GISAX}$ and $L_{0,SEM}$ are the mean interdomain spacing measured using grazing incidence angle x-ray scattering (GISAXS) and SEM respectively.

The PMMA block in both B82 and B67 is highly rich in syndiotactic content (>78% and >80% respectively) i.e. a large portion of the MMA monomer residue side groups are arranged in the syndiotactic configuration where the side groups have alternating orientation with regards to the polymer backbone. The immiscibility between blocks is greater if the PMMA block is syndiotactic rather than isotactic or atactic [20].

The brush polymer (R10.5) used in this project is a RCP composed of S and MMA monomer residues i.e. [P(S-r-MMA)] terminated in one end by a hydroxyl group and a "Tempo" moiety (a remnant functional group from the polymer synthesis) in the other. It was also purchased from *Polymer Source Inc.*, was synthesized by free radical polymerization at 135°C and has a S content of 66 mol-% (established by ^{1}H-NMR spectroscopy). Other relevant data is found in Table 2 (DSC heating rate unknown).

The choice of the P(S-b-MMA) material system was based on the amount of research already conducted on and with it. The use of it is well documented and from a processing standpoint it has, at least, four

things speaking in its favour: i) price and availability, ii) relatively low $\Delta\gamma_{PS,PMMA}$ at the air/polymer interface, iii) highly selective domain removal possible and iv) potential for combined use with *sequential infiltration synthesis* (SIS). Even though the P(S-b-MMA) material system cannot achieve feature sizes below ≈ 12 nm its resolution limit is sufficient for our purposes. Since the BCPs used were bought and not synthesized specifically for this project we were limited to the items available from *Polymer Source Inc*. Even though their stock contains several different polymers from various material systems we were restricted to what they had to offer. This was particularly evident in the choice of R10.5 where the desired *molar S fraction* (x_s) was 64 mol-% rather than the selected 66 mol-% but the RCPs with S fractions closer to the target had fairly high PDIs. Here the author had to make a judgment call about completely pursuing x_S at the detriment of PDI or to strike a compromise by choosing the RCP with the closest x_S that had an 'acceptable' PDI - In hindsight it could be argued that it might have been better to prioritize x_S. The relatively low $\delta\gamma$ between PS and PMMA at the top surface is beneficial since it makes it less likely that the PS block will migrate and form a wetting layer; this is a problem for some BCPs consisting of an organic and an inorganic block if proper steps are not taken [12] [21]. The $\delta\gamma$ at the air/polymer interface actually almost vanishes in the P(S-b-MMA) material system at high temperatures (190-210°C [4]; 170-230°C [13]; 225°C [18]). An important factor in all these choices was that the aim of this project already from the start was considered a proof-of-concept and as such we wanted to eliminate as many potential pitfalls as possible and go with tried-and-true methods where available.

For lithographic purposes one of the most desirable qualities of a BCP is the potential for highly selective removal of a single phase - in our case the PMMA cylinders. Here P(S-b-MMA) excels since the response of PS and PMMA to a *deep ultra-violet* (DUV) exposure is quite the opposite, PS is cross-linked while the radiation causes chain scission in PMMA. The PMMA can later selectively be dissolved with *acetic acid* (AA), leaving behind a cross-linked PS mask with hexagonally close packed pores where the PMMA cylinders used to be. This property is the strongest reason why we went with this material system however the future potential of using P(S-b-MMA) in conjunction with SIS was also tantalizing. SIS is performed in an *atomic layer deposition* (ALD) machine and entails selectively growing a hard mask e.g. Al_2O_3 inside one of the phases – here the PMMA. The principle reason for using SIS is that the dry-etch selectivity can be improved dramatically but for it to truly be useful in this project the inverted composition with PS cylinders in a PMMA matrix would have been more appropriate. Such a composition is far less common in literature and moreover a different composition of the brush layer would likely be needed. The reasons being that a PS matrix is often desired (since the PMMA easily and selectively can be removed) and the perpendicular orientation is observed in a far narrower window of annealing parameters and RCP brush layer compositions for the 'inverted' BCP composition.

When choosing R10.5 three factors were mainly considered: i) M_n, ii) x_S and iii) PDI. As previously mentioned the desired x_s was $\approx$ 64 mol-% based on the results obtained in [22]. They concluded that the largest h_{BCP}-windows containing perpendicular cylinders in an asymmetric P(S-b-MMA) was obtained for a P(S-r-MMA) brush composition falling in the range $x_s \in [0.62, 0.66]$ with the largest window occurring for $x_{S;RCP} = 0.64$. Essentially, h_{BCP} can take on a wider range of values and the BCP layer will still adopt the perpendicular orientation if a brush layer with this composition is used. They furthermore found that the optimal $x_{S;RCP}$ in the RCP is fairly independent of the $x_{S;BCP}$ in the BCP but that the size of the h_{BCP}-window increases with higher compositional asymmetry [22]. If instead a cross-linkable RCP containing 1 mol-% *glycidyl methacrylate* (GMA) was chosen the ideal $x_{S;RCP}$-range would shift to $x_{S,RCP} = [0.63,0.73]$ [14]. Another approach tested in [14] was to incorporate a small amount of a third monomer containing a reactive –OH group instead of just having a single terminating one. Thus a large number or possible anchoring sites were created along the entire backbone of the polymer chain. The monomer used was *2-hydroxyethyl methacrylate* (HEMA) and the addition of 1 mol-% shifted the x_s-window, generating perpendicular cylinders, to $x_{S,RCP} = [0.63,0.74]$. The compromise between $x_{S;RCP}$ and *PDI* has already been accounted for but a judicious choice of M_n is presumably also important. Again, only a few M_n options were available and a value close to those found in [19] [23] [16] [22] was selected. At that time the reasoning was thusly: A high M_n means a larger polymer and if the density of grafting events is independent of this parameter then a larger M_n would translate into a thicker RCP layer remaining after the graft and wash. However, it is highly questionable is such an assumption would be valid since a polymer does not readily adopt a stretched out conformation due to the loss of entropy it would entail. Instead it forms a 'tangled-up ball' which might in a sense restrict the access of the terminating –OH group to the surface for high M_n chains and thus slow down by sterically hindering the grafting reaction. For this reason a low M_n RCP might have an easier time forming a

covalent link to the surface but the lesser size could mean a reduced areal coverage even if the density of grafting events might be higher.

The low $\chi_{PS,PMMA}$ ($\chi_{PS,PMMA} = 0.03$ [21] as compared to $\chi_{PS,PDMS} = 0.14$ [21] or $\chi_{PLA,PTMSS} = 0.46$ [24] all at RT) and limited dry-etch selectivity are the main objections to using the P(S-b-MMA) material system. As we have seen the former sets the resolution limit, interface width and potentially the upper annealing temperature allowed.

1.3 Equipment and Processing Techniques

1.3.1 Techniques of inducing desired morphology and orientation

The BCP polymer chains, in the solid film formed by spin-coating, have at *room temperature* (RT) virtually no long range mobility. They are thus frozen in the (presumably) disorganized state present in the BCP solution as the solvent evaporates during the spin-coating process. In order to allow the chains to self-assemble into the thermodynamically most stable conformation and thus adopt the desired morphology the mobility has to be sufficiently increased. This occurs during what will be referred to as the "anneal" and in this project two principle approaches have been used: i) heating and ii) exposure to solvent vapour.

As the BCP film is heated the polymer chains gain more and more thermal energy eventually overcoming the immobilizing restrictions imposed by entanglements and chemical interactions between neighbouring chains. Examples of such interactions include polar-polar, van der Waals and the interaction between conjugated systems such as the phenyl groups in PS. The *glass transition temperature* (T_g) is an important number in polymer physics and is generally considered the demarcation point at which larger segments of the polymer chain can start to move in a coordinated fashion [25]. Some movement (relaxation) is possible even below T_g but it is mainly rotation around single bonds of less sterically hindered side groups [25]. The kinetics improve as the temperature is raised further and for acceptable processing times a wide margin to T_g is desired but as mentioned previously the upper usable *annealing temperature* (T_a) is set by either the decomposition temperature of the BCP or the temperature at which $N\chi_{PS,PMMA}$ falls below the segregation limit (i.e. the temperature above which organized phase separation no longer occurs). Additionally, there might also be a limiting temperature window in which the efficacy of the brush layer is acceptable. In this project four different heat sources for thermal annealing purposes have been used: i) a *rapid thermal processing* (RTP) machine (UniTemp GmbH, RTP-1200), ii) a vacuum oven (Heraeus VT-6025) and to a lesser extent iii) regular lab ovens (Salvis LA, TC40) and iv) hotplates. Henceforth "RTP" will refer to either the machine or process depending on context.

The other approach of increasing chain mobility is by exposing the BCP film to solvent vapours during a so called *solvent vapour anneal* (SVA). The solvent vapour will permeate the film and cause it to swell as the smaller solvent molecules interjects themselves between the larger polymer chains. The looser network generated by the swelling lends the chains greater opportunity for movement even at moderate temperatures and the solvent molecules can be seen as providing lubrication. The advantages of SVA are that the process is energy effective since it does not require the high temperatures of the thermal techniques and can thus also extend the scope of BCP lithography to include more heat-sensitive BCPs. The most prominent downside is that it usually involves hazardous, or downright toxic, solvents that need to be handled, stored and disposed of in a controlled and safe manner - special ventilation and safety equipment is necessary. Moreover, there can easily be issues with process stability and BCP film de-wetting if stringent control over the relevant parameters is not exerted.

The morphological effects of SVA is harder to predict than for thermal anneals since the number of possible interactions multiplies and several χ-parameters are needed to thermodynamically model even the simplest of BCP systems with a single pure solvent additive. The amount of solvent in and swelling of the film is moreover a function of time, temperature, choice of solvent(s) and its vapour pressure etc. It is also likely that a single solvent will interact more strongly with one of the blocks and that the degree of swelling of this block therefore will be larger than that of the other. Such a shift in relative block volume could push the 'effective f_A' into the regime of another morphology in Figure 3 b) [4] [13]. It is also conceivable that the solvent interacts with both blocks fairly equally but that the presence of the solvent can mitigate the immiscibility between blocks and thus undermine the thermodynamic drive to phase separate [13]. One way is to use a mixture of two different solvents that selectively interacts with only one of the blocks respectively but again the number of χ-parameters and possible interactions increase exponentially. The presence of the solvent can furthermore create free surface preferentiality, screening of undesired surface interactions and the swelling can also affect commensurability conditions as L_0 might now be larger than the intrinsic bulk L_0 [13]. The solvents will swell the polymer film and effect both d_{cyl} and L_0 and upon termination of the SVA the solvent will quickly evaporate and the 'swollen' BCP pattern can get trapped in a state different from that of the thermodynamic equilibrium.

However, the thermodynamic considerations might not be the only or even the most important ones during a SVA. Research [21] suggests that the kinetics of evaporation at the conclusion of the SVA plays a pivotal role in which morphology and orientation is finally adopted in the annealed BCP film. The process of evaporation is here believed to create an ordering front that moves vertically through the BCP layer and achieving the right evaporation rate is paramount for the success of the process. The evaporation rate can be adjusted by controlling the removal rate of the solvent rich atmosphere or by the use of a "topcoat" e.g. a polymer layer on top of the BCP that the solvent molecules first must diffuse though before escaping into the atmosphere. The evaporation rate could theoretically be controlled by changing the permeability and/or thickness of this topcoat [21].

1.3.1.1 Rapid Thermal Processing (RTP)

In this project the RTP was used for grafting RCP brush layers and thermal annealing of BCP films.
The RTP is versatile and has the ability to achieve very high temperatures (>1000°C) at exceedingly high *heating rates* (dT/dt). The complete RTP program can consist of an arbitrary number of steps where the degrees of freedom for each step include time, temperature, heating/cooling rate and chamber gas flow. The sample is placed on a carrier wafer inside a quartz housing and the heat can be applied either from above or below by means of powerful halogen lamps. Quartz is a 'chemically inert' material that can withstand the rapid changes in temperature without shattering. The heat is applied from below during normal operation and the temperature of the carrier wafer is monitored by a thermocouple that provides feedback to the heating elements. However, the effective feedback is different depending on which heat source is selected; when using heating from below you need to factor in an initial temperature overshoot during the ramp-up but once the target is reached the feedback loop is very effective at keeping the *annealing temperature* (T_a) to within 1-3°C of the target. Contrary, when heating from above the feedback loop is highly effective at suppressing the initial overshoot but causes large temperature fluctuations ($\geq \pm 5$°C) around the target value. A useful combination is probably to use the "TOPHEAT" option during ramp-up and heating from below once the intended T_a is reached. However, a different strategy was used during all RTP runs (where TOPHEAT is not explicitly stated) namely to perform the ramp-up in three distinct steps. The first step is heating with a rate of 18°C/s to a T 10-20°C below T_a to make sure the overshoot will not exceed the target. This is followed by a short stationary phase to allow the overshoot to start to cling off before finally slowly ramping up to the intended T_a with the rate 1°C/s. The *annealing time* (t_a) is per definition set to from once T_a is reached to the initiation of the cooling step.

The cooling rate is far slower than the heating rate and is essentially dictated by the capabilities of machine. The RTP has an active cooling system based on internal pipes carrying 20°C water. The T versus t is logged during the entire RTP cycle and when comparing the cooling curves from multiple samples it is clear that the shape of the curve depends on both T_a and t_a. Not surprisingly it takes longer to cool from a higher T_a but less obvious is that below a certain t_a there is also a t_a-dependence. Essentially, this stems to the fact that for short anneals the entire mass of the RTP will not have time to reach its equilibrium temperature. To avoid additional risk of oxidative damage the samples were not unloaded until the thermocouple read ≤50°C (i.e. overly cautious). For reasons of safety and machine longevity there is an upper time limit for a single RTP run before cooling has to be commenced, for $T_a \leq 400$°C this limit is set at 60 min.

One of the more useful features of the RTP, in this project, is the ability to choose between three different gas flow options. The gas flow used if not otherwise explicitly stated is 150 l/h of N_2, but there is also the option to use either 150 l/h *forming gas* (20% H_2 and 80% N_2) or the "Vacuum"-setting. Unfortunately, the vacuum option more involves suction than any degree of higher quality vacuum.

Another issue that came to light late in the project is that the thermocouple inside the RTP was uncalibrated and that the actual temperature is substantially higher than the set/displayed value. The exact behaviour and extent of this offset have not, as of yet, been satisfactorily mapped out but tests using a set of calibration tapes that change colour above a certain temperature indicate that it can be as much as 30-40°C in the temperature range used in this project. **For sake of simplicity the RTP T_a-values stated in this report are those given by the RTP**. A proper survey of the offset is essential to be able to compare obtained results with literature and any attempts at technology transfer.

1.3.1.2 Vacuum Anneal (VA)

The *vacuum oven* (VO) has a maximum operating T of 200°C but unlike the RTP the time necessary to reach the set temperature is substantial e.g. 90-100 min for $T_a = 200$°C. Essentially, even the longest RTP cycle will be finished before the VO even has had a chance to reach the set-point value. The VO was used in this project to thermally anneal BCP films during vacuum conditions. Analogous to in the RTP t_a is defined from whence T_a is reached to the initiation of cooling (i.e. turning off the power). The cooling is completely passive for this oven and for T to drop below 70°C takes on the order of 3 h. The main strength of the VO is the larger chamber volume and the ability to perform extended anneals i.e. there is no upper time limit. Unfortunately, the VO is only rated for vacuum levels up to 10^{-2} mbar which even though better than in the RTP is still to be considered a low quality vacuum and there are data indicating this might be too low to obtain good ordering if the VO was used for grafting [3]. At the end of *vacuum oven anneals* (VOAs) the samples where occasionally unloaded at temperatures as high as 70-80°C but this ought to be of little to no consequence as it is still well below T_g of both polymer blocks.

The Heraeus VO was something of an unexpected windfall and prior to its discovery a custom-made ovenproof *vacuum chamber* (VC) was commissioned and then built by the instrument workshop at the *division of solid state physics* (FTF), LTH. The Viton™ o-ring used in the first iteration (v. 1.0) of the chamber unfortunately failed to completely seal the chamber at $T_a =$ 170-190°C despite it being rated for permanent operating temperatures up to 225°C. For the second version (v. 2.0) a perflouropolymer *Kalrez*™ o-ring, capable of temperatures up to 327°C, was procured and a new lid made to properly house it. One of the benefits of the VC is that it can be loaded into the regular lab ovens already present inside the ISO 5 cleanroom LNL facility. The VO on the other hand is located in an auxiliary non-cleanroom service lab which for practical purposes is cumbersome and could entail surface contamination of the BCP film. Furthermore, the sturdy construction of the VC enables it to safely withstand high vacuum levels e.g. 10^{-8} mbar even at elevated temperatures. The circumference is big enough to accommodate 2” wafers but sufficiently small to keep the time required for pump-down low. The regular lab ovens also reach T_a far quicker than the VO and the VC can be removed from the oven once the anneal is concluded and thus be cold enough to be safely opened within 30 min.

1.3.1.3 Solvent Vapor Anneal (SVA)

The apparatus used for SVA can be arbitrarily complex depending on the degrees of freedom desired in tailoring the process. The sample can be exposed to static or dynamic condition or even a combination thereof during the anneal. In this MSc project the simplest possible approach was taken, consisting of adding a few ml of solvent to a 70 ml borosilicate beaker and then placing a smaller 40 ml beaker, containing the sample, inside the larger and tightly cover the 70 ml beaker with self-sealing *parafilm M®* (a paraffin plastic film). The set-up was then left in the solvent wet bench at $T_a =$21-23°C for the *duration of the anneal* (t_a) which was defined from the sealing to the opening of the beaker. One risk with this set-up is that condensation droplets can form on the inside of the parafilm and eventually fall directly onto the sample and thus partially dissolve the BCP film. This type of SVA is sometimes referred to as “bell-jar SVA” and one problem is the lack of consistency as the resultant morphology depends on e.g. annealing time, temperature, type of solvent, swelling and deswelling rates, swelling ratio and film thickness [4].

Swelling of the film can be observed as a colour change. The composition of the atmosphere during the anneal depends on the gases initially present and the vapour pressure of the solvent which in turn is a function of temperature. The annealing conditions were more or less static with the exception of an initial and terminating transient. A higher solvent content could translate into a shorter t_a required but caution needs to be taken as it can also cause large scale rearrangements of the BCP film e.g. the creation of islands and pinholes.

More advanced static options involve first evacuating the sample chamber before the addition of the solvent(s) and thereby eliminating the partial pressures of ordinary atmospheric gases, thus creating a more solvent vapour rich atmosphere over the sample. This has been proved to substantially reduce the t_a required down to a matter of minutes for a PS sphere-forming P(S-b-MMA) BCP [26]. Dynamic conditions could be accomplished by placing the sample inside a temperature controlled flow chamber to which the solvent vapour is brought by an inert carrier gas e.g. N_2 that has been run through a bubbler with the solvent. By having multiple gas inlets to the chamber connected to separate bubblers

trough calibrated *mass flow controllers* (MFCs) the atmospheric conditions could tailored and also varied over the extent of the anneal [4].

The SVA in this project was concluded by gently removing the parafilm and sample beaker from the larger chamber vessel. All solvents used were pure and highly volatile, evaporating from the film in a matter of seconds. To further remove any lingering solvent most samples were also subjected to a 1 min *soft-bake* (SB) on a hotplate set to 80°C.

1.3.1.4 Miscellaneous

Several experiments were conducted in which two of the techniques recounted above were combined in the quest to further improve upon the ordering of the BCP film and with the expectation to harness the best properties of both techniques. Inspired by [27] [28] a couple of samples were also made in which the BCP solution contained small amounts of various surfactants in the hope that this would reduce the number of defects present at the air/polymer interface. The results of the surfactant samples are however not included in this report due to the observed detrimental effects on ordering and the lack of precision in the preparation of these alternative polymer solutions.

1.3.2 Plasma Etching Techniques

1.3.2.1 Reactive Ion Etching (RIE)

The *reactive ion etching* (RIE) system used in this project was the table-top RIE T2 System from Trion Technology. It is a parallel plate RIE system operating at the *radio frequency* (RF) f_{RF} =13.56 MHz and with a maximum RF power of 600W. It was used for surface activation, to remove the brush layer on annealed and developed samples and then to transfer the BCP pattern into the underlying SiN_x-layer.

A generic capacitively coupled RIE system consists of a grounded vacuum chamber with a platter electrode at the bottom that is electrically isolated from the rest of the chamber. The platter electrode is DC isolated and connected to the RF generator though an impedance matching network. Etching is performed during vacuum conditions e.g. 75 mTorr and with a specific flow of process gases through the chamber. The gases are usually introduced at the top of the chamber and removed trough an outlet at the bottom by a vacuum pump. The conductive chamber walls and the bottom plate respectively act as electrodes in a parallel plate capacitor and plasma is initiated by applying the RF power [29] [30]. The strong and quickly alternating electromagnetic field above the bottom plate strips electrons from the gaseous species flowing through the chamber creating highly reactive ions and radicals. Both electrons and ions move up and down in response to the RF field but the movement of the ions is far smaller than that of the electrons due to their substantially larger masses. The free electrons can further generate new charged species through high kinetic energy collisions. Some of the free electrons, traveling up and down, will collide with either the walls of the vacuum chamber or the bottom electrode. The electrons hitting the walls will be led away to ground but those hitting the bottom electrode will contribute to the generation of a large negative charge build-up due to the DC isolation i.e. the system is self-biasing. The plasma, due to its slight compositional excess of positively charged species, will be attracted to the negatively charged bottom electrode. This vertical DC self-biasing is usually [29] [31] on the order of several hundred volts and the positive ions thus impinge on the bottom electrode where the sample is positioned with directional kinetic energy. The etching thus contains both a chemical component from the reactiveness of the radicals and ions and a purely physical sputtering effect from the energetic collisions with the sample.

The Triton T2 system has five process gases connected (O_2, CF_4, CHF_3, SF_6 and Ar) and besides the flow rates of these the pressure and nominal RF power can be set depending on the sample at hand. Not all combinations of total flow and pressures are compatible though, due to the capacity of the vacuum pump. The etch rate will, as a rule of thumb, increase with higher power and/or lower pressure [29]. A lower pressure means a larger sputtering component and can also enable greater etching anisotropy, i.e. the vertical etch rate is higher than the lateral, due to the longer mean-free-path (average distance between scattering events of the reactive species).

1.3.2.2 Plasma Preen (PP) Asher

Instead of using either a typical capacitively or inductively coupled plasma generation set-up, the *Plasma Preen* (PP) asher uses higher frequency ($f = 2.45$ GHz) microwave radiation to create the plasma. It was used for surface activation prior to the brush graft and thinning/removal of polymer as well as the contamination generated during the RIE process of SiN_x. The construction is essentially a modified microwave oven with a water-cooled aluminum bottom plate. A silicone gasket runs along the periphery of the plate and the vacuum chamber is formed by placing an upside-down Pyrex™ dish over the gasket and evacuating through holes in the aluminum plate. Other holes provide the process gas which in our case was oxygen but could also be e.g. argon. The PP asher was operated at 5 mbar O_2 in this project i.e. at a substantially higher pressure than would normally be used in the RIE. One severe limitation is that continuous plasma generation is only allowed for 60 s at a time before the Pyrex™ dish needs to cool down for a couple of minutes before it can be used again. The advantages are that it, generally, is far more available and less time-consuming to operate than the RIE but can of course not compete with the RIE when it comes to process control and versatility. The main uses of the PP asher is to thin/remove resists, organic contaminants and to some extent metal oxides; the latter is mainly removed through the physical sputtering action of the impinging ions. A *Faraday cage* (FC) can be placed over a sensitive sample to protect it from both exposure to microwave radiation and the sputtering component otherwise present. The cage removes the electric field directly below it and neutralizes positive ions so that the etching mainly occurs due to neutral radicals [32]. Aside from polymer removal and thinning, the PP asher has been used for purposes of surface activation in this project.

1.3.3 Deposition and Growth Techniques

1.3.3.1 Plasma Enhanced Chemical Vapour Deposition (PECVD)

(Inductively coupled) plasma-enhanced chemical-vapour deposition (IC)PECVD was used to deposit the insulator/dielectric *silicon nitride* (SiN_x).

In ordinary *chemical vapour deposition* (CVD) the energy required to break the chemical bonds in the gaseous precursors is supplied by heating the substrate to fairly high temperatures e.g. 600-800°C [33]. The chemical reaction is initiated and sustained at/above the substrate surface where the material deposition thusly occurs. Only the surface in contact with the substrate is heated to minimize unwanted deposition on the interior surfaces of the reaction chamber. The precursor gases in our case are *silane* (SiH_4) and *ammonia* (NH_3) but unfortunately ordinary CVD is not an option due to the high temperatures needed. The primary goal with this process is to deposit SiN_x on an epitaxially grown InAs layer and InAs start to decompose at substantially lower temperatures - hence the need of PECVD which is generally performed at 250-350°C [33].

During our PECVD process the substrate was held at 250°C and the chemical reaction was instead facilitated by generating a plasma in the flowing process gases. However, instead of the *capacitive coupling* (CC) used in the Trion RIE, the MicroSys 200 PECVD machine utilizes *inductive coupling* (IC) to generate the plasma. IC means that a RF signal is used to excite a coil inside which the precursor gases flow. Generally there are two major advantages to using IC over CC: i) higher plasma densities are possible and ii) the ability to separate the plasma generation from the biasing of the substrate electrode [34]. The electrode biasing controls the kinetic energy with which the reactive species impinges on the surface. The MicroSys 200 can be used both for plasma dry etching or deposition depending on the process parameters e.g. RF power, pressure and choice of process gases. PECVD gives a conformal deposition with comparatively high deposition rates [34]. In this project we aimed for a 10 nm *SiN_x layer thickness* (h_{SiNx}) but the deposition of such a thin layer proved to be tricky due to the combination of short process times and start-up transients in the plasma. The consequences are low reproducibility in terms of layer thickness and composition stoichiometry. Another disadvantage with using PECVD for SiN_x deposition is the *hydrogen* (H) contamination of the film. The hydrogen can be bonded to both Si and N atoms and affects IR and UV absorption, stability, mechanical stress present and electrical conductivity [34].

1.3.3.2 Atomic Layer Deposition (ALD)

Atomic layer deposition (ALD) was used to deposit *silicon dioxide* (SiO_2) on SiN_x as a thin SiO_2 layer on top of the SiN_x was deemed necessary due to an observed variability in grafting efficiency of R10.5 on the PECVD SiN_x surface - despite the use of various surface activation techniques. The deposited thickness was merely 15-18 Å and the purpose was to increase the number available -OH-groups on the surface.

The main characteristic feature of ALD is the sequential nature of the process. A typical ALD process contains two gaseous precursors, e.g. A and B, but unlike in other CVD techniques both precursors are never present in the reaction chamber simultaneously. The deposition proceeds instead through sequential and self-limiting "half-reactions" of calibrated duration and separated by one or more purging steps. A complete ALD cycle thus consists of at least four schematic steps: i) introduction of precursor A, ii) evacuation and/or purging with an inert gas e.g. N_2 or Ar, iii) introduction of precursor B followed by iv) another chamber evacuation/purge [35]. Steps i) and iii) can further be broken down into the adsorption of the gaseous precursor to the substrate and chemical reactions that covalently anchor the precursor remnant to the sample surface. The self-limiting aspect of the process stems from the fact that only one precursor is present in the chamber at any one time and that there is a limited number of reactive sites available on the sample surface. The duration of the precursor exposure steps depends on the time necessary for the precursors to reach and interact with all sites on the sample which in turn are functions of e.g. temperature, size and aspect ratio of the surface features [35]. In each ALD cycle a monolayer of the final compound is deposited and this offers layer thickness precision on the Å-level. ALD is the technique of choice for deposition of highly conformal ultra-thin layers [35]. Another feature for some materials is the ability to control the stoichiometry in the film [35].

There exists a substrate temperature window in which an ALD process can be used successfully but it is generally substantially lower than other CVD techniques, usually $\lesssim 350^{\circ}C$ [35]. At too low temperatures the reaction kinetics are poor and the precursors can condensate on the substrate; at too high temperatures you run the risk of thermal decomposition and a too high precursor desorption rate [35]. The precursors used in our deposition of SiO_2 were *bis-diethyl-amino-silane* (BDEAS) and water vapour and the substrate temperature was 250°C.

1.3.3.3 Selective Area Metal Deposition: Thermal Evaporation + Lift-off

A lift-off procedure is a common method of area-selective deposition of metal on a substrate surface. Traditionally, a stack of two resist layers of differing etch properties are used, where the second (uppermost) layer contains the pattern. In the case of two polymer layers the first (bottommost) layer needs to have a low solubility in the solvent of the polymer in the second layer, otherwise the first layer will be completely or partially removed during the application of the second layer. To attain high yield and reproducibility it is furthermore important that there is a sufficient etch selectivity between the layers to obtain an undercut in the first layer of the pattern in the second layer. Once a vertical profile containing the undercut has been implemented e.g. Au is blanket-deposited via either evaporation or sputtering. The undercut is necessary to avoid the formation of a continuous Au layer instead of isolated shapes of the original pattern on the substrate. Evaporation is preferable for this application due to the higher deposition anisotropy stemming from the longer mean free path of the Au atoms. The higher pressures used during sputtering causes a greater number of scattering events and consequently a shorter mean free path and a more conformal deposition. Moreover, the metal targets used during sputtering are fairly large compared to the smaller more spot-like sources used in thermal evaporation. This results in a less collimated beam of matter (given the same distance between the metal source and the sample) and again a higher conformality. The last step is to dissolve the first polymer layer and at the same time "lift off" all layers on top, including the excess Au. The success of the "lift off" step can be jeopardized if the undercut is not sufficient and enough Au has been deposited on the sidewalls to connect the top Au layer with the Au on the substrate. Then any or all of three different scenarios can take place: i) the top Au layer is anchored hard enough for it not to be released unless more forceful methods such as a *ultra-sonic bath* (USB) is used. Even if the top Au layer is released it is highly probable that ii) some of the surface pattern will be ripped off or iii) unwanted parts of the sidewalls will break off and remain on the sample. Implementing the undercut in a dense pattern by means of a wet etch is not always possible due to the isotropic nature of the etch, risk of pattern collapse due to surface tension and the lack of process control. There is a distinct risk of completely undercutting the pattern and thus dislodging the top layer before the Au deposition. In such cases dry etching is the way to go due to the higher anisotropy possible.

1.3.3.4 Selective Area Metal Deposition: Electrodeposition

In this project electrodeposition was used to deposit Au at the bottom of the etched openings in SiNx-layer. Electrodeposition offers several theoretical advantages [36] over a traditional lift-off involving thermal evaporation: i) drastically reduced material consumption due to the complete deposition-selectivity toward conductive surfaces and since there is no need for time consuming sample preparation steps or high vacuum ii) a high throughput can be achieved. Furthermore, restrictions on iii) height and/or iv) pitch of the Au particles are no longer imposed by the undercut in the lift-off layer. The use of inorganic masks in combination with rip-off techniques also enables v) substrate reuse. The nature of the process moreover vi) allows for patterns containing more complex geometries and higher aspect ratios. The reduced material consumption, higher throughput and opportunities for substrate reuse all contribute to a reduced cost of implementing an array of Au seed particles for NW growth. During thermal evaporation metal is not just deposited over the entire sample but also on other surfaces inside the chamber and even though some of this metal can be recovered, if it is a dedicated system, the loss is considerable. A material consumption reduction by a factor of more than 300 has been demonstrated [36] by using electrodeposition instead of lift-off even after Au recovery in the latter process has been factored in. The factor will be higher for a sparser pattern but not dramatically so as most of the loss occurs to the chamber walls.

However, there are also some disadvantages; for example to deposit a fixed amount of Au in each cylinder (from run-to-run) the deposition time or current needs to be adjusted based on the BCP pattern quality (i.e. the total area of exposed InAs substrate) of the sample. The substrate furthermore needs to be conductive and a more complicated set-up is needed for p-doped substrates where holes instead of electrons are the dominant type of charge carrier.

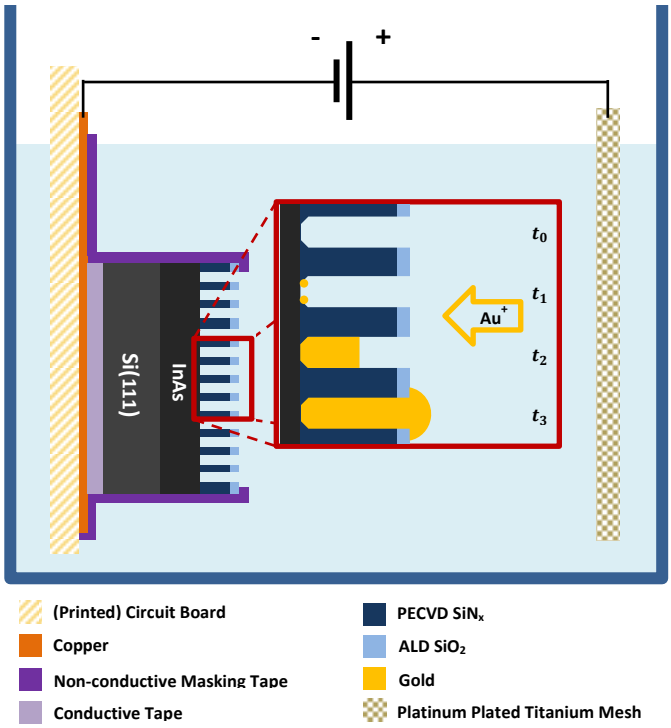

Figure 4: Schematic diagram depicting the electrodeposition process. t_x are time coordinates where $t_0 < t_1 < t_2 < t_3$. t_0 = prior to onset of current, t_1 = nucleation, t_2 = filling of cylinders and t_3 = 'mushrooming'.

The electrolyte used in this project was a cyanide-based 24K Au solution with a purity of 99.9% but other chemistries are also available [37]. The process should to be reliable as long as the Au content is kept above 80% of its initial value and the pH (5.8) and temperature (35°C) is kept within 5% of theirs [36]. The set-up consisted of two electrodes submerged in the electrolyte and connected to a current source, see Figure 4. The substrate was mounted on a printed circuit board with conductive tape (3M) and great care was taken to mask all other exposed conductive surfaces (on the cathode) with another non-

conductive tape in order to avoid unwanted deposition. The sample substrate served as the cathode during the process while the anode consisted of a mesh of platinum-plated titanium. A nominally constant current was used and the deposition was concluded by rinsing the sample in deionized water and drying it with a N_2-gun.

1.3.3.5 Metal-Organic Vapour-Phase Epitaxy (MOVPE)

Metal-organic vapour-phase epitaxy (MOVPE) is an epitaxial technique used to grow e.g. crystalline semiconductor layers or as in our case NWs and where at least one of the group III or V metal atoms are transported to the growth surface by a metal-organic precursor. Generally group III precursors consists of the metal atom with alkyl radicals attached, while those of group V more often are hydrides; however MO group V source alternatives are available [38]. To be used in the MOVPE process the precursors must have a reasonable vapour pressure at RT or below, high purity, low affinity for oxygen and water vapour but ideally also have low toxicity and cost [38].

A generalized MOVPE set-up consists of a reaction chamber, a susceptor for holding the sample, a heating system (usually IR lamps or RF coils), a gas mixing manifold and finally a scrubber to neutralize the removed gases. The working principle is based on the fact that the precursors are stable at RT but will decompose (a.k.a undergo pyrolysis) at higher temperatures [38]. In its simplest form the precursors will decompose from the heat supplied from the susceptor and some of the released III/V atoms will adsorb to the surface, see Figure 5. A portion of the adsorbed species will re-evaporate (desorb) and leave the chamber but the rest will diffuse along the surface until they find the energetically most favourable position which generally entails replicating the already present crystal structure of the substrate. The complete growth mechanism is more complicated by far and involves multiple gas phase and surface reactions. The entire process is principally governed by thermodynamics, kinetics and hydrodynamics [38], where the thermodynamics details the forces trying to restore equilibrium, kinetics the reaction rates and hydrodynamics the mass transport of reactants to and from the surface.

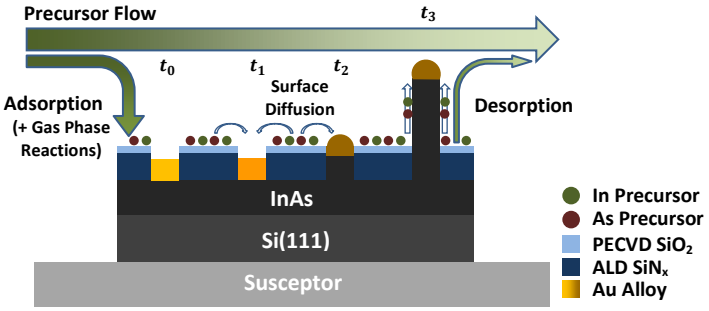

Figure 5: Schematic diagram depicting the MOVPE process. t_x are time coordinates where $t_0 < t_1 < t_2 < t_3$. $t_0 =$ prior to precursor flow, $t_1 =$ precursor surface diffusion + absorption into Au particles, $t_2 =$ supersaturation reached and deposition of InAs initiated and $t_3 =$ growth of NWs fuelled by precursors from gas-phase and diffusing up along NW shaft.

Depending on circumstances any of the three can be the limiting factor and if the *growth rate* (GR) is plotted as a function of temperature three growth regimes can be identified. At low temperatures the kinetics limit the GR and the GR increases with increasing T. At very high Ts desorption of reactants and parasitic pre-reactions limits the GR [39]. The mass transport is the limiting factor in-between these two regimes and the GR is here fairly independent of T generally making it the preferred region of operation. Low pressures are often used in the chamber to avoid unwanted gas phase reactions [38].

The main strengths of MOVPE are the versatility, reproducibility and high growth rates [38]. One staple of MOVPE is that it can be used to create both stable and meta-stable compounds since the growth processes often are far from equilibrium, opening up for tailoring of semiconductor properties by tuning the composition [39]. Other advantages are the freedom to design the precursor molecules depending on the situation and the ability grow layers of almost any compound on top of each other as long as the critical thickness is not exceeded. Actually the strain introduced due to differing lattice constants offer yet another degree of freedom to tailor electronic and optical properties of the structure. The contender, molecular beam epitaxy (MBE) can create sharper interfaces but has lower GR, requires ultra-high vacuum and has difficulties growing phosphides [38].

In this project InAs NWs were grown on a SiN_x masked InAs epitaxial layer using catalytic Au seed particles. This is a form of foreign metal catalysed growth (Au is not part of the grown compound nor consumed in the process) in which the Au seeds initiate and guide the growth and directly control both NW diameter and orientation [5]. This manner of growth is usually referred to as the vapour-liquid-solid (VLS) mechanism as the precursors/atoms are supplied in vapour form and then diffuse along the substrate and NW surfaces and eventually get dissolved in the Au particles forming a liquid alloy. The liquid alloy eventually becomes supersaturated of the dissolved species leading to the precipitation of semiconductor material at the triple phase boundary [5]. The lowest-energy surface for precipitation is then the semiconductor surface beneath the particle leading to growth in this direction. The phase of the metal particle formed during growth and properties such as interfacial energy with the semiconductor, surface energy/tension, and the diffusivities of the growth species will affect the process and the outcome e.g. growth rate and direction and crystal structure [5].

Au is by far the most used foreign seed metal and the reason for its success is believed to be: i) its and its alloys moderate melting points, ii) resistance to oxidation and other parasitic reactions and iii) the high diffusion coefficients of other elements in the metal [5]. Other foreign metals are being evaluated for the potential as seed particles due to i) cost concerns, hope to implement/influence ii) doping profile and iii) crystal structure, iv) expand the MOVPE parameter space and/or v) create novel compounds but also since vi) Au is incompatible with Si based CMOS processing [5]. Au contamination generates mid-gap electronic states in Si, has a high solid diffusivity and is incredible hard to remove from exposed fabrication equipment [5].

Other ways of growing NWs are *selective area epitaxy* (SAE) and self-seeding where growth primarily occurs on unmasked regions of the substrate in the former and the latter entails seed particles composed of a metal constituent of the final semiconductor compound. For III-V compounds it is generally the group III metal as these have low melting and high boiling points [5]. SAE has issues with crystal defects and achieving high aspect ratios i.e. the radial and vertical growths cannot be isolated as it is near impossible to fully suppress growth in radial dimension. Self-seeding (and SAE) can create extremely clean growth processes but the parameter space is smaller as there is a distinct risk that the particle will be consumed in the process if the conditions are not right [5].

1.4 Evaluation Techniques

1.4.1 Ellipsometry

Ellipsometry is mainly used to obtain film thicknesses and optical constants (e.g. n and k) but can also be used to characterize other material properties that involve a change in optical response such as composition, crystallinity, roughness and doping concentration [40].

Ellipsometry measures the change in polarization, of an incident reference beam of light, induced by the light-matter interaction with the sample. Polarization is the spatial and temporal behaviour of the electric field component of a light beam and of particular interest is its orientation in relation to the plane of incidence as the light hits the sample. The polarization can be represented by a time-dependent vector which further can be broken down into two orthogonal components, one parallel and one perpendicular to the plane of incidence; these are denoted the p- and s-components respectively. Ellipsometry is primarily concerned with the relative change of these components which is represented by an amplitude ratio (Ψ) and a phase change (Δ) [40]. The satisfaction of Maxwell's equations imposes different boundary conditions for p- and s-polarized light at an interface between two materials. The amount of light being reflected or transmitted at the interface will depend on polarization, the *refractive indices* (n_1, n_2) of the materials as well as the angle of incidence (ϕ_1), see Figure 6. The fate of the p- and s-components are independent and can be calculated separately by finding the respective *Fresnel reflection* (r_p, r_s) and *transmission* (t_p, t_s) *coefficients* [40].

A typical sample suitable for ellipsometry consists of a substrate with one or more thin layers on top. The overall light reflected off the sample will be the result of the interference of multiple light beams. At each interface, part of the light will be reflected and the rest transmitted and the total path of a particular beam will depend on the number of reflections and the layer thicknesses. To model the behaviour it is important to keep track of both the amplitude and the phase of the light beams emerging at the top surface. The latter can be tracked by defining the *film phase thickness* (β) which is a function of the physical film thickness, the wavelength, the refractive index and incidence angle [40].

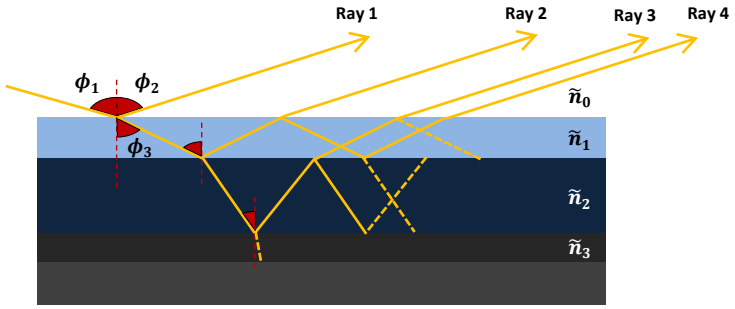

Figure 6: Selected rays schematically traced in a sample composed of multiple thin layers. Dashed lines represent ray paths that have been ignored for simplicity.

Some aspects of light-matter interaction can be described by a complex refractive index ($\tilde{n} = n + ik$) consisting of the *index* (n) and the *extinction coefficient* (k). $n = \frac{c}{v}$ is the ratio between the *speed of light in vacuum* (c) and the *phase velocity* (v) of light in the material while k describes the loss of energy during propagation through the material. The λ-interval used during the ellipsometry measurements on polymeric films in this project was $\lambda = [400, 900]$ nm and was chosen since the polymer layers can be considered transparent i.e. $k \approx 0 \Rightarrow \tilde{n} = n$ in this spectral region. IR absorption is commonly caused by excitation of modes of molecular vibration, phonon vibration and of free carriers [40]. Electronic transitions between energy levels generally account for absorption in the UV region.
A material is generally dispersive i.e. $n(\lambda)$ has a wavelength dependence and this can be accounted for by either tabulating values of $n(\lambda)$ or mathematically model the λ-response of n. The *Cauchy relationship:*

$$n(\lambda) = A + \frac{B}{\lambda^2} + \frac{C}{\lambda^4}$$

is often used for transparent materials but some caution is required since it is not constrained by the Kramers-Kronig consistency and can therefore produce unphysical dispersion [40]. The Cauchy dispersion models for B82, B67 ($A = 1.5366, B = 0.0082, C = 0$) and R10.5 ($A = 1.5357, B = 0.0069, C = 0$) were extracted from multiple measurements on samples with relatively thick polymer layers since *the signal-to-noise ratio* (S/N) generally is higher when measuring on thicker films. This can be seen by the tendency of the A, B and C coefficients respectively to converge towards specific values as the measured film height is increased.

The ellipsometer used (J.A. Woollam, M2000VI) schematically consists of a light source, a polarization generator, sample holder, polarization analyser and detector. The light incident on the sample was linearly polarized (45°) and multiple *angles of incidence* (α_i) were used in collecting the spectroscopic data. The experimentally measured shift in polarization of the reference (incident) light beam is then compared to predicted values generated by modelling the sample structure and applying the Fresnel equations. Regression analysis is then used to fit the unknown parameters (e.g. layer height and $n(\lambda)$) in the model so as to get the best agreement between the experimental and theoretically generated data. *Mean squared error* (MSE) is used to quantify the discrepancy and the lowest value corresponds to the best parameter fit, i.e. the theoretical model is iteratively adjusted so as to most accurately comply with the observed polarization shift. Unfortunately, if the model deviates too far from the actual sample behaviour the regression can get caught in a MSE local minimum instead of finding the global one. Another risk is that the obtained values reflect the mathematically best solution but not necessarily the physically most correct one, which is why a good initial model is required.

Ellipsometry is, hands down, the most frequently used characterization/verification technique in this project and has the advantages of being i) fast, ii) reliable, iii) having sub-nm accuracy (given a good model), iv) not requiring vacuum conditions and v) being able to take measurements on samples containing complicated stacks of layers. The main drawbacks are: i) that prior information is needed to formulate an adequate initial model, ii) a lack of spatial resolution due to the size of the measurement spot and iii) limited to thin thicknesses for absorbing layers [40].

1.4.2 Scanning Electron Microscope

The construction and operation of a *scanning electron microscope* (SEM) will not be outlined here; instead only operational parameters relevant to the special case of imaging polymer and SiN_x/SiO_2 layers will be discussed. The SEM was used to evaluate BCP pattern quality and the efficacy/results of the RIE pattern-transfer, electrodeposition and NW growth.

One of the most important parameters is the *acceleration voltage* (V_{acc}) which directly affects the energy of the *electrons* (e^-) in the incident beam. All other things being equal, a higher V_{acc} is affiliated with greater resolution since the magnetic lenses can focus the beam into a tighter spot size on the sample and less e^- scattering and divergence of the beam occurs in the column. Unfortunately, there are several trade-offs with a high V_{acc} [41]: i) a reduced ability to image surface microstructures due to a higher penetration depth of the e^- and hence a larger interaction volume i.e. more electrons backscatter and *secondary electrons* (SE) are generated in a bigger volume and escape from a larger surface area. The detector thus detect e^- from a larger area even though the spot-size is smaller. However this is a truth with modifications since if V_{acc} is increased sufficiently the e^- penetrates deep enough for the *backscattered electrons* (BSE) to never reach the surface, however for polymeric samples this is not generally an option. The reasons being that polymers as a rule are insulators and sensitive to ionizing radiation. The poor conductivity can lead to a local (positive or negative) ii) charge build-up that sets up an electric field with field-lines radiating out from the surface [42]. The electrostatic field affects incoming electrons so as to either attract or repulse them. If the charge-up is positive e^- will be attracted and the imaged area will appear darker but more relevant to this project is the negative charge build-up causing the incoming e^- to deviate, scatter and interact over a larger area. This manifests as brighter regions with reduced resolution; the image can easily become so saturated that it is hard to make out any features. Both the degree of iii) induced damage and iv) surface contamination also increase with V_{acc}. The e-beam is a source of intense ionizing radiation and can cause damage to a polymer structure by inducing chemical reactions or imparting kinetic energy and heat to the sample and if T exceeds T_g pattern deformation is likely to occur. Finally, v) edge-effects are more pronounced at higher V_{acc} as more of the interaction volume becomes exposed to a surface when the volume gets larger. Besides, potentially enabling higher resolution, raising V_{acc} will also lengthen the depth of field

(DOF) i.e. making it possible for features in both the foreground and background to be in focus simultaneously. All polymer films in this project were imaged using a Hitachi SU8010 SEM set at $V_{acc} = 1$ kV whereas 15 kV were more often used for the SiN_x/SiO_2 covered samples due to their reduced sensitivity.

Other crucial parameters are the beam (I_b) and probe (I_p) currents, where I_p is the part of I_b making it down to the sample [43]. The spot-size is positively related to I_b i.e. if I_b is increased then the spot-size follows suit and the resolution suffers. A low I_b also means reduced charging effects and potentially less sample damage/contamination but comes at the price of a lower S/N. A low S/N will manifest as a grainy image but can to a large extent be compensated for by increasing the detector integration/capture time [41]. A single I_b- value was not used in this project, instead I_b was varied based on observed sample charging, magnification level and in the course of minimizing astigmatism – sometimes changing I_b can resolve problems with astigmatism that (practically) cannot be corrected for by adjusting the stigmator. An author-formulated hypothesis is that you can get caught in a local astigmatism minimum and a convenient way to find the global minimum is to change I_b and redo the stigmator calibration procedure. I_b was in the range [5, 20] mA where the smaller values were a necessity for thicker polymer films due to more severe charging effects present.

The *working distance* (WD) is the distance between the bottom of the objective lens and the specimen [43] and has a profound effect on resolution and DOF. A shorter WD generally gives better resolution (up to a point) but the trade-off is a reduced DOF. WD$= [3, 4]$ mm was used for polymers while WD$= [7, 8]$ mm was found to be more suitable for the SiN_x/SiO_2 covered samples.

In imaging the samples post-electrodeposition, a 30° tilt was often used to gauge the protruding height of the Au particles. 30° is convenient since all height measurements taken in the SEM only need to be multiplied by 2 to obtain the correct physical height. Tilting can increase edge-effects and can influence shadowing effects – particularly if a SE detector is used. Shadowing effects are caused by the fact that e^- escaping from a surface facing the detector will more easily be collected and that surface will then appear brighter. An in-column detector was primarily used in this project.

At high magnification sample- as well as focal drift can be large obstacles in obtaining high quality micrographs and are particularly troublesome when charge build-up is an issue. The problem can sometimes be addressed by increasing WD (and hence DOF), reducing I_b and/or the exposure time. A short capture time is also generally desired at high magnifications to avoid radiation induced damage or conversely deposition of contamination; both can seriously affect the observed pattern structure and dimensions. The damage will first act to blunt sharp edges and degrade the cross-sectional profile of the developed polymer film. Contamination stems from the e^--beam's ability to initiate polymerization of hydrocarbons present in the vacuum and on the sample surface and will act to reduce the diameters of the etched cylinders by deposition on the sidewalls. The contamination will furthermore charge positively causing the image to progressively darken to the detriment of image uniformity with respect to brightness and contrast.

Charging effects can also be combated by improving the grounding of the sample e.g. making sure to use fresh conductive carbon tape to secure the sample to the stub. Another way is to coat the sample with a thin layer of metal or other conductive material that will form a ground plane i.e. the free electrons in the layer will redistribute so as to eliminate the external field. The coating does not dissipate the accumulated charge but instead closes the field lines so that they do not radiate out from the surface in a disruptive manner [42]. However, the latter approach is not really applicable in this project since it would put an end to further sample processing and the polymer pattern feature sizes are sufficiently small for the observed dimensions to be substantially altered for even for a thin coating. Unfortunately even when imaging almost identical samples, obtaining good pictures involves a process of parameter trial-and-error interleaved with repeated focus and stigmation corrections.

1.4.3 Water Contact Angle (WCA)

The *water contact angle* (WCA) of a water droplet on a solid surface depends on the wetting conditions of that surface. On a hydrophobic surface the droplet will be almost spherical (large WCA) i.e. minimizing the interface between the two phases while it conversely will adopt a flat drawn out conformation on a hydrophilic one where the favourability of the inter-molecular interaction between the water molecules and the substrate rivals that among water molecules.

To obtain the surface energy multiple liquids are generally needed; however WCA can be used probe relative changes in surface energy. In this project WCA was investigated as a means of characterising the changes in wetting conditions induced by the grafting of a brush layer. The brush layer is here a random co-polymer of styrene and MMA and with a higher WCA than pure Si i.e. the idea is that the efficacy of the graft procedure could be evaluated not just by the grafted layer thickness but also of the change in WCA compared to Si.

The WCA was measured using a static sessile drop method on a Biolin Scientific Theta Lite tensiometer. The software on the computer controlled camera set-up ascertains the shape of the deposited droplet of purified water and the WCA is obtained as the boundary condition to the Young-Laplace equation. The values presented in this report are the averages of the 12-13 measurements taken during the first second after the droplets were deposited on the surfaces.

1.4.4 ImageJ Processing

ImageJ is a powerful tool for extracting data from images and it was primarily used in this project to count the number of cylinders in SEM micrographs (with standardized zoom settings) of annealed B82 films and to calculate and display 2D *Fourier transforms* (FT) of said images. Furthermore, positions of local maxima corresponding to the cylinder diameter and pitch periodicity were identified in the FTs.

In order to count the number of cylinders a brightness/contrast threshold transformation first had to be performed and here either the “Huang” or default option was used depending on which was deemed best. When counting the cylinders the result can be filtered based on cross-sectional area and circularity, where the latter is defined as $Circularity = 4\pi \cdot \frac{[Area]}{[Perimeter]^2}$ and adopts values between 0 and 1; 0 being an infinitely elongated polygon and 1 a perfect circle. Only the area filter was applied since including a meaningful filtering based on circularity entailed a too grievous loss of “good” cylinders while simultaneously clearly elongated ones were included. The upper and lower area limits were 255 and 700 nm^2 corresponding to diameters of 18 and ≈30 nm respectively for perfectly circular cylinder cross-sections. Overlays of the counted areas in the SEM images and the FTs are available on request and examples from a good sample is found in Figure 7. A lot of additional information about the distribution of counted cylinders as well as for individual ones can easily simultaneously be obtained e.g. area, perimeter, center of mass, shape descriptors, skewness, Feret’s diameter and a fitted ellipse just to mention a few options.

The FTs were generated using the *Fast Fourier Transform* (FFT) tool and when identifying the maxima the noise tolerance was adjusted for each image so as to include a value corresponding to the location of the rings. A ‘fuzziness’ in the original image will affect the Fourier coefficient corresponding to the cylinder diameter more than that corresponding to the interdomain distance. The FTs contain rings rather than points due to the multiple defects and the fact that the cylinders present form multiple small grains with different orientation. An analogy would be comparing a polycrystalline material to a single crystalline one where the former FT contains rings and the latter sharp points.

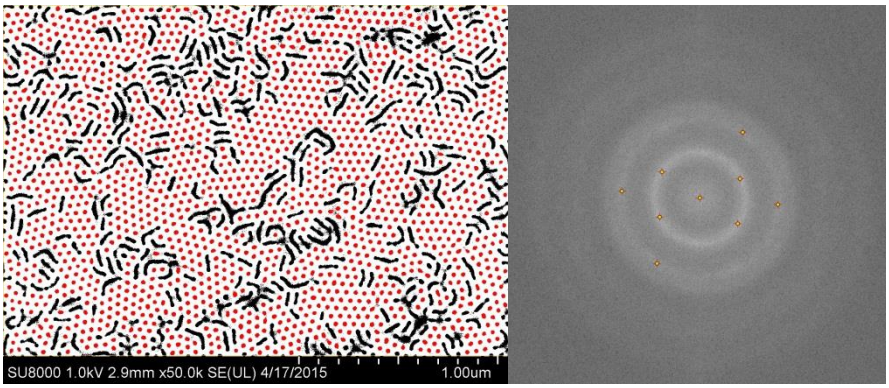

Figure 7: ImageJ processed SEM with cylinder count overlay (left) and FFT of original SEM (excluding black border at bottom).

It should also be mentioned that care have been taken to always exclude the label bar from the image area on which the FFT is performed, however the program sometimes included it during the *cylinder count* (CC) which is evident from the overlays but the addition is 2-3 cylinders in a total count of usually >1000 i.e. negligible compared to image quality parameters. Unfortunately, both the cylinder count and the FTs are heavily influenced by the degree of focus and contrast in the original SEM images. If either is found lacking the threshold procedure generates 'grainy' images that are hard for the program to interpret. Another significant source of error is that vertical cylinders surrounding a defect often will be lumped together with the defect during the count and thus be overseen; defect rich samples will therefore have a lower CC than they deserve.

The original intention was to extract and display statistical data summarizing at least the area and circularity distributions of the cylinders counted in a sample image to get a more nuanced picture of the pattern quality. Ideally the sample should have the highest possible CC and infinitely narrow distributions of cylinder area and circularity. As for the FTs the idea was to obtain and compare the magnitude of the coefficients corresponding to diameter and pitch but also to calculate the *full width half maximum* (FWHM) of the rings to get yet another sense of the pattern quality. With all these measurements the hope was to obtain representative values making objective sample comparisons possible but unfortunately the image quality/settings just vary too much. The CC was the only parameter that felt sufficiently robust to use in sample comparisons but even that is found lacking i.e. you cannot solely rely of the CCs, a subjective evaluation is alas still necessary.

(In hind sight: If the patterns had been better then a 'standard' Matlab script could have been used to obtain the *lattice orientational correlation length* (ζ), i.e. a measure of the average distance between defects or put another way – grain size, for comparative purposes.)

Part II
Experimental

2.0 Preface to Experimental Work in Part II

The conducted experimental work described below is subdivided into separate experiments where *Experiment I-V* were conducted on inexpensive Si or SiN_x/Si and aimed to develop a procedure for reliable BCP annealing and RIE pattern-transfer. In *Experiment VI* the best developed method was applied to 'sharp' samples of the desired (and more expensive) sample stack. These 'sharp' samples were then used in calibrating and testing the final processing steps consisting of electrodeposition and MOVPE growth of NWs.

For orientation, *Experiment I-III* relates to *STAGE 1* and *2* in Figure 2, *Experiment IV* to *STAGE 3*, *Experiment V* to *STAGE 4*, *Experiment VII* to *STAGE 5* and *6* and finally *Experiment VIII* to *STAGE 7*.

2.1 Preparation of Polymer Solutions

All R10.5 and B82 films were spun-cast from toluene solutions while anisole was the solvent used for B67; all concentrations stated are in weight-%. To ensure complete dissolution of the polymer (R10.5 and B82) in toluene the sealed vessel with the polymer-solvent mixture was subjected to powerful agitation in the form of an extended (≥20 min) *ultra-sonic bath* (USB) at elevated temperatures (30-50°C). Filtering the sonicated solution (once cool) through a 0.1 μm PTFE filter was found to be a necessity due to a high content of particulate matter in the polymer samples purchased from *Polymer Source Inc.* The anisole based B67 solutions used here were prepared by diluting already available high conc. stock solutions, again followed by filtering.

2.2 Experiment I: Grafting – Time and Temperature Dependence

The sample sequence in A1.1 illustrates the importance of having an adequate *R10.5 (brush) layer thickness* ($h_{R10.5}$) beneath the B82 film to obtain the perpendicular orientation and an acceptable degree of order. The sequence constitute a meta-analysis with samples collected from various experiments, all were however annealed in the RTP at $T_a = 250$°C and have approximately the same $h_{B82} \approx L_{0,B82}$. Therefore keep in mind that the samples have not been processed in precisely the same manner but the differences are of such a nature that they not ought to influence the degree of ordering in a marked fashion (substantiated later).

Three trends are observable: i) for $h_{R10.5}$ ≤5.9 nm no 'significant' amount of vertical cylinders can be observed and the corresponding samples are thus of no practical use in this project. The darker areas in the micrographs are regions where cylinders run parallel to the substrate whereas the lighter areas appear to have a disorganized mix of orientations. ii) The areal proportion of light to dark regions seems to increase with higher $h_{R10.5}$. At a macroscopic level no difference in wetting behaviour/adhesion of the B82 was observed during *spin-coating* (SC) or reflected in the MSE of the pre-anneal *ellipsometer measurements* (ellips.) It is feasible that a height differential exists between the light and dark regions, potentially as a consequence of large scale polymer migration during the anneal but since no AFM (or profilometer) scans were performed, either before or after the anneal, this remains a conjecture. Somewhere in the interval $5.9 < h_{R10.5} \leq 6.6$ nm proper vertical cylinders start to appear; this is in agreement with [18] [17] that made the same observation but with a RCP containing 61 mol-% S instead of the 66 mol-% in R10.5. If the transition occurs abruptly or gradually in this interval is not evident but the latter part of the A1.1 sequence iii) suggests that a higher $h_{R10.5}$ is affiliated with a reduced number of defects and hence a higher density of usable cylinders. Again, it should be emphasized that slight differences in processing exist between the samples that in theory could skew the observed trends but results of later experiments suggest that these variations are of minor importance.

Surface activation is intended to increase the density of –OH groups on the substrate surface available for R10.5 grafting and is performed prior to R10.5 application. As far as surface activation for Si samples is concerned, the 'gold standard' in literature is an extended immersion in heated acidic Piranha solution (3:1 H_2SO_4:H_2O_2, $T = 80$°C, t ≥30 min) and this was used for all samples in *experiment I* (Exp. I). Exp. I was an attempt to replicate the RTP grafting results found in [17] and identify the *time* (t_{graft}) and *temperature* (T_{graft}) dependence, during the RTP grafting process for this particular machine, of $h_{R10.5}$. The process flow was as follows: surface activation→ SC an (presumed) excessively thick R10.5 layer (≈ 30 nm) →soft-bake on hotplate (1 min, 100°C) → ellips.→ RTP Graft→ ellips.→ toluene USB (wash)→ ellips. ($h_{R10.5}$). Contrary to later process flows the spun-cast R10.5 layer was here also measured before and after the RTP graft and a slight thickness reduction, see A1.2, was observed that seems to increase

with T_{graft}. Speculative explanations are: elimination of remaining solvent and film porosity, a change in refractive index and/or conformational relaxation of the polymer chains.

The time evolution of $h_{R10.5}$ (always refers to the ellipsometer measurement taken after toluene wash) was mapped at $T_{graft} = 250°$, 280° and 310°C and is presented in Figure 8 and tabulated in A1.3. In the probed parameter space a strong T_{graft}- and a weak t_{graft}-dependence are observable and $T_{graft} = 280°$, $t_{graft} = 600$s was concluded to be a quick and effective combination when compared to the extended (24-48h) lower temperature (170-190°C) grafting, in vacuum conditions, that frequently occurs in literature e.g. [3]. Multiple samples were grafted with this t-T combination and the dashed line in Figure 8 runs through the median value. To confirm the effects of temperature two samples were grafted for $t_{graft} = 600$s at $T_{graft} = 265$°C and 295°C respectively i.e. 15°C above and below the previously best value. At both temperatures $h_{R10.5}$ was lower than at $T_{graft} = 280$°C. As mentioned previously, all temperature ramp-ups in the RTP were at nominally $dT/dt \approx 18$°C/s on the suggestion of [18] [17] unless otherwise stated. To verify the efficacy of this value three samples were grafted at 280°C but with lower ramp-up rates (5 resp. 10°C/s), see Figure 8.

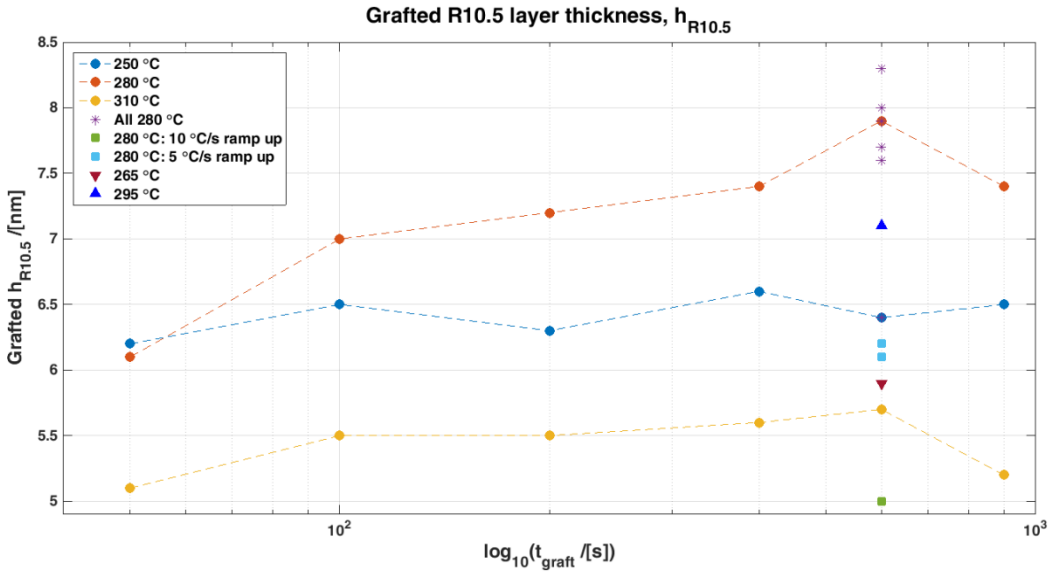

Figure 8: The dependence of $h_{R10.5}$ on RTP graft time and temperature.

There is a large caveat to the execution and interpretation of the results in Exp. I, namely the persistence of the effect of the surface activation treatment. From both discussions with supervisors and later experiments it became apparent that the effects of a surface activation quickly fade with time and that surface activation, R10.5 SC, RTP graft, wash and even BCP SC and anneal should all be performed in rapid succession to obtain the best results possible. Unfortunately, the full realization of this was brought home first later in the project. Table A1.3 summarizes essential data concerning all stages of the experiment. All samples were R10.5 SC within minutes of the completion of the Piranha treatment but after that the samples were dormant for varying amounts of time at points along the following process flow, see A1.3. Age_1 refers to the period between R10.5 SC and grafting while Age_2 represents the interlude between the graft and the R10.5 wash. The sample age is particularly pronounced for the supplementary samples probing the effects of alternative T_{graft} and dT/dt.

Another objection is that a large $h_{R10.5}$ has been treated as synonymous with a successful minimization of $\delta\gamma$ and hence as the layer's ability to induce the perpendicular orientation. This premise seems to be supported by the sample series in A1.1 but a more accurate means of evaluation would be to complete the process flow up to and including the B82 anneal, development and SEM inspection. It is possible that t_{graft}, T_{graft} and dT/dt affects e.g. the conformation of the grafted R10.5 and thus possibly its ability to exhibit surface neutral wetting. Furthermore, a high T could induce thermal degradation or other 'parasitic' chemical reactions again affecting the final properties of the grafted R10.5 besides the $h_{R10.5}$.

One additional way of gauging the properties of the exposed surface of the grafted R10.5 layer was to measure its WCA and the results are displayed in Figure 9 where WCA has been plotted as a function of $h_{R10.5}$ and the samples have been differentiated by colour according to T_{graft} and dT/dt. A linear regression suggesting a weak positive relation between WCA and $h_{R10.5}$ has also been included in Figure 9. The reliability of the fit is low due to the substantial spread in data, possible originating from surface contamination. It is furthermore highly questionable if the sensitivity of the WCA measuring equipment even extends to one decimal point.

Essentially, the only clear-cut conclusion from this experiment is that RTP grafting, of R10.5 to a surface activated Si substrate, at 280°C for ≥10 min seems to be a viable alternative to the time-consuming options found in literature.

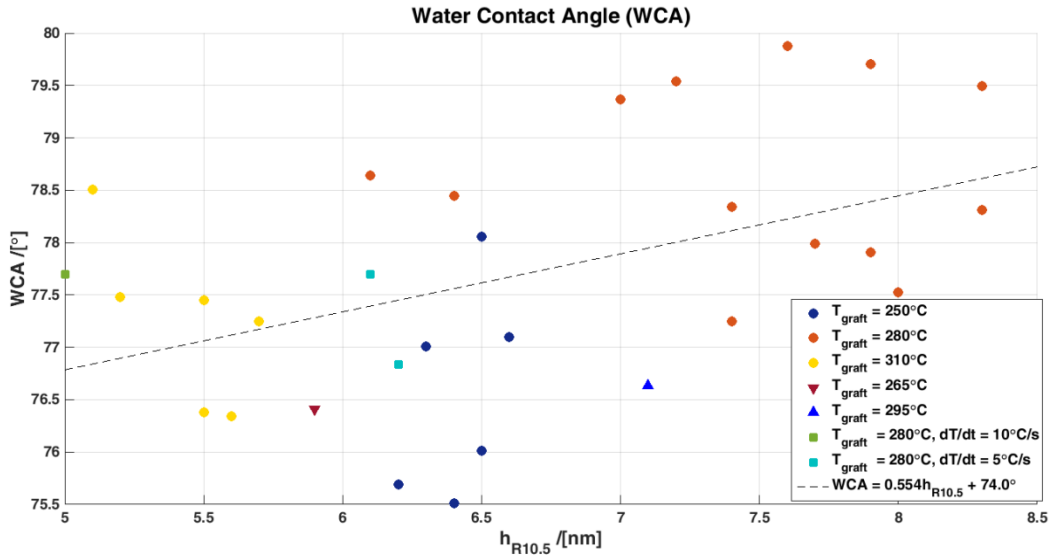

Figure 9: WCA as a function of $h_{R10.5}$, colour differentiated by T_{graft}.

2.3 Experiment II: Grafting – Efficacy of Surface activation Techniques

During the course of the project it became evident that surface activation prior to grafting is absolutely essential in obtaining a high grafting density. The Piranha treatment is an effective way of removing organic and some metallic contaminants as well as increasing the number of –OH groups on the surface [3]. Unfortunately, besides being highly time-consuming the process involves the heated mixture of a strong acid (H_2SO_4, >98%) and a powerful oxidizer (H_2O_2, 30%) and as such requires rigorous safety precautions. It is therefore highly desirable to identify a faster and safer alternative. Figure 10 summarizes the various surface activation treatments evaluated for this purpose in Exp. II.

None	Piranha	Plasma Preen	Plasma Preen	Triton RIE	Ozone Cleaner
- REF.	- 3:1 (vol.) H_2SO_4:H_2O_2 - 80°C - 40 min	- 5 mbar O_2 - **With** FC - 3 x 60 s	- 5 mbar O_2 - **No** FC - 3 x 60 s	- 150 mTorr - 40 sccm O_2 - 50 W (Nom.) - 90 s	- >250°C - 500 sccm O_2 - 10 min

Figure 10: Surface activation treatments and settings used.

The piranha treatment was compared to oxygen plasma treatments in the *Plasma Preen* (PP) and Trion RIE respectively, exposure to ozone during elevated temperatures but also reference samples without any additional treatment. The PP was used both with and without the accompanying F*araday cage* (FC). All samples were grafted in the RTP with the best settings identified in Exp. I (280°C, 10 min). The results are depicted in Figure 11 while the relevant details can be found in A1.4; observe especially that some data points overlap in Figure 11 and that the lowest value in the Piranha set can be explained by a visible patch, in the center of that sample, in R10.5 film prior to RTP graft.

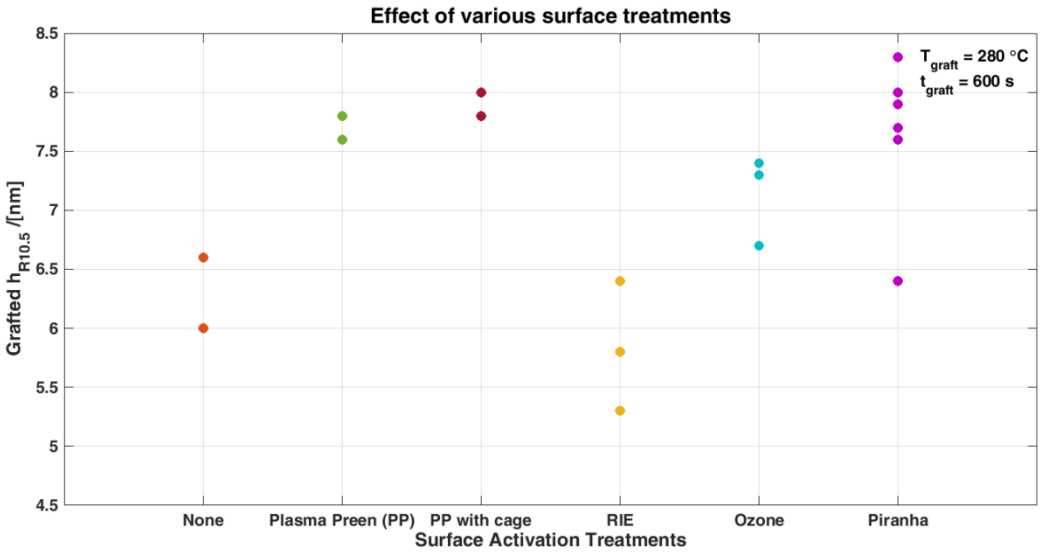

Figure 11: $h_{R10.5}$ as a function of surface activation treatment.

Two things jump out: i) even though Piranha was used on the sample with the highest $h_{R10.5}$ there only seems to be a slight difference between using Piranha and the PP with FC i.e. this appears to be a viable alternative. Unexpectedly, ii) the RIE treatment gets the lowest score, it actually performs worse than not having a treatment at all. It is highly questionable if this actually is the case or if the RIE surface activation merely affects the substrate in such a way as to render the ellipsometer model inapplicable.

Initially two samples of each alternative treatment were prepared but the *thickness of the native oxide* (h_{SiOx}) was not measured before or after the treatment, instead it was presumed to be 15Å (a reasonable assumption for untreated Si(100)). The ellipsometer measurement of $h_{R10.5}$ on RIE treated samples then gave $h_{R10.5}$ in excess of 9 nm which was both surprising and very encouraging but once the folly of not measuring h_{SiOx} before and after was pointed out to us one additional sample of each treatment was prepared. The measured h_{SiOx} from these samples were deemed representative of the treatments and subsequently **used retrospectively on the previous samples in constructing the ellipsometer models**. It is these 'corrected' values that are recounted in Figure 11. The RIE treatment had a profound effect on h_{SiOx} almost doubling it (+16Å), while the others only induced moderate changes (approx. ± 1Å). For treatments other the RIE it would be injudicious to make any categorical statements as to whether h_{SiOx} increases or decreases following the treatment based on the limited data points - you never measure on exactly the same spot in the ellipsometer and natural sample variations and uncertainties affiliated with the measurement itself cannot be ruled out as the explanation. It is debatable if the measured increase in h_{SiOx} post-RIE is solely related to an increased layer thickness or if other parameters enter into it. It is conceivable that stoichiometry (i.e. oxygen content), 'crystal structure' and surface roughness is affected making the native oxide ellipsometer model inadequate. The actual $h_{R10.5}$ for the relevant samples might instead be ascertained by making a scratch in the film and measure the step height in either an AFM or a profilometer. However, care must be taken so as not to simultaneously severely scratch the underlying substrate which would skew the step height. Most of the objections raised in Exp. I are valid also in Exp. II.

2.4 Experiment III: BCP Annealing (Order induction)

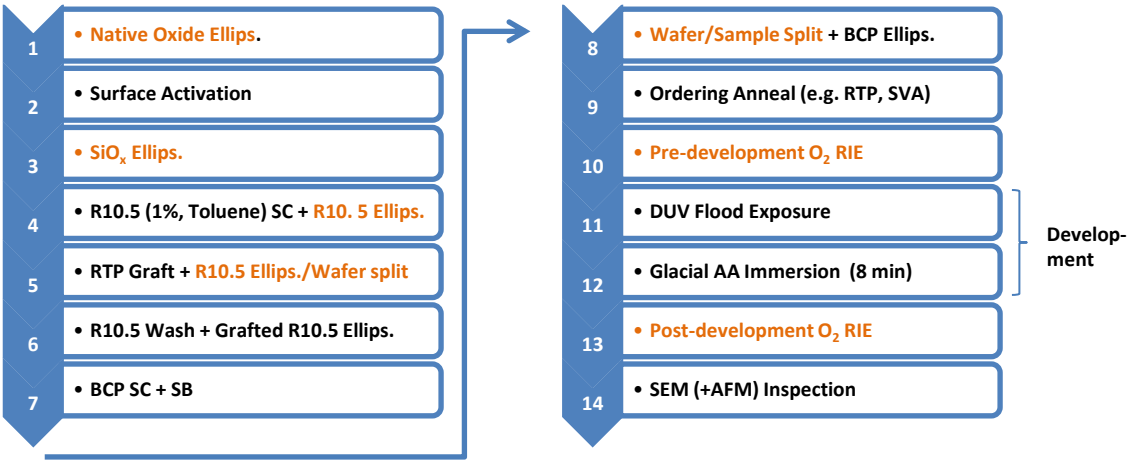

Figure 12: Schematic process flow for annealing investigations.

Figure 12 outlines a generalized process flow for the samples included in *the annealing experiment* (Exp. III). Steps marked in black are crucial while those marked in orange are optional and the number and combination of 'orange steps' can vary from sample to sample. As indicated in Figure 12, when processing a larger sample e.g. a full 2" wafer the sample can be split into smaller pieces at, at least two instances along the process flow. Either after the graft but before the wash or after the BCP spin-coating and *soft-bake* (SB) depending on intended further processing. In the first instance it is beneficial to do the split prior to the wash since it offers a convenient way of minimizing particulate contamination generated during the split. At the later instance the split results in multiple near identical BCP covered samples, something of particular interest when comparing e.g. annealing methods/parameters since important variables such as $h_{R10.5}$ and h_{BCP} can be eliminated as causal agents. One important sample nomenclature used in this project is "W#" where the "W" refers to the fact that the substrate is a full 2" Si(100) wafer and the "#" represents an identifying number. When the parent wafer subsequently is split the name is appended with a capital letter that is specific to the individual daughters e.g. W2A.

At this point it is prudent to make a statement about vigilance regarding variable inconsistencies (primarily for $h_{R10.5}$ and h_{B82}) in the entire sample pool presented and referred to in the rest of this report. An appreciable number of sample sequences have been compiled from experiments originally intended to map the effects of something else. It is a sad fact of life that the processing of some samples, for a host of reasons and a number of which is beyond your control, fails somewhere along the way. This coupled with a natural variation from sample to sample introduce highly undesired uncertainties which can be used to call into question the observed trends that the series aim to illuminate. Moreover, the direction of the experimental work has altered numerous times based on results of previous experiments and new literary finds. If a sense of fragmentation is conveyed that is why.

SEM micrographs with several discrete levels of magnification (scale bar: 5 μm, 2 μm, 1 μm, 500 nm and 200 nm) were acquired of all samples. Special care was taken to make sure that all images with the same scale bar actually have the same degree of magnification in order to be able to make comparative studies. Images of higher or lower levels of magnification were also obtained for samples exhibiting film inhomogeneity and/or finer details respectively. The images presented are those that the author believes are most informative and representative of the sample at hand.

Before embarking on this annealing odyssey a few words should be mentioned about the development step mentioned in the process flow above. The standard wet development includes both a DUV flood exposure (step 11) and a glacial *acetic acid* (AA) immersion (step 12). The DUV exposure was performed without a photolithographic mask in a Karl Süss MJB 4 DUV Mask aligner with an intensity of 9.5 mW/cm^2 at $\lambda = 254$ nm. The *total DUV dose* (D) used in literature varies wildly between references,

from 0.35 J/cm^2 [16] to 4.5 J/cm^2 [18] [19] which might suggest that the exact dose is of less importance. Below a certain value this actually seems to be the case, as indicated by the series in A2.1. The maximal practically usable radiation dose at this intensity, substrate and h_{B82} falls somewhere in the range $D \in [2.28, 5.7[$ J/cm^2 and at $D = 5.7$ J/cm^2 the dose is definitely too high since the PS structure has 'visibly' (in the SEM after development) started to decay. However, identifying the location of the upper boundary is more of academic interest rather than practical use, far more important is finding the lowest possible dose corresponding to an appropriate balance between induced chain scission of the PMMA and cross-linking in the PS domains. A low dose is generally preferable since it requires less processing time and it allows the P(S-b-MMA) system to be used in conjunction with other more DUV sensitive polymers and/or substrates.

The W26 reference sample had quite bad ordering so samples W26C-F where instead used in a DUV dose test. D was progressively decreased, in steps of 0.57 J/cm^2 (corresponding to 1 min exposure time), from 2.28 to 0.57 J/cm^2 and then all samples were immersed in AA for 8 min and inspected in the SEM, see A2.1. No appreciable difference can be detected among the samples, however these are only top-view images and the "*Automatic Brightness and Contrast* (ABC)" tool in the SEM interface was used in their capture. Cross-sectional views of the polymer films are needed to ensure that the PMMA in the cylinders is removed all the way down to the R10.5 layer. It is feasible that the degree of induced chain scission decreases with film depth and that the PMMA at the bottom of the cylinders cannot be properly dissolved during the AA immersion if the dose is too low. Attempts were made to image the ≈ 40 nm cross-section of the developed B82 polymer layer but it proved exceedingly difficult and no good images were obtained. Since no polymer damage is evident at 2.28 J/cm$_2$ (4 min) this value was used as the standard exposure dose despite the indications that a lower one probably would have been sufficient.

The author actually managed to destroy the first two sample sets by using too high D and therefore an e-mail correspondence with Federico Ferrarese Lupi, one of the principle authors of e.g. [17], [19] and [23], was initiated. He shared his experience of a technology transfer of BCP lithography from one lab to another, and according to him the appropriate D depends on the intensity of the light. A high intensity can cause degradation of the PS structure even if no damage is induced for the same D but at a lower intensity. The intensity used in this project was 9.5 mW/cm^2 i.e. almost double that used in [18] (5 mW/cm^2 at $\lambda = 253.7$ nm for 15 min). Essentially, a high DUV intensity needs to be compensated for with a lower D.

The purpose of the AA immersion is to selectively dissolve the PMMA domains and the selectivity of this wet process is very high. The duration of the AA bath was taken directly from [17] and contrary to the DUV exposure no real harm seems to come from leaving the samples in the AA too long. The PS matrix essentially behaves analogous to a negative photoresist (i.e. cross-links) and when working with such resists, changes in feature and pattern dimensions usually need to be considered since some shrinkage often is affiliated with the cross-linking process. No efforts have been made in this project to see if a similar process occurs during the DUV exposure of P(S-b-MMA) but it would be interesting to see if d_{cyl} can be tailored by varying D, even though the effect is probably too small to be of any practical use. However, the dimensions are not the only factor that could be influenced by D, perhaps the dry etch resistance of the PS mask can be improved somewhat by identifying the optimal D.

Before continuing with the annealing experiment we feel it is once again appropriate to jump the gun and take a look at some already annealed samples of B82 and B67, see Figure 13, in order to verify the pattern dimensions listed in Table 2. According to this, indeed limited, sampling $L_{0,B82} \in [46.0, 49.7]$ nm, $L_{0,B67} \in [37.1, 39.4]$ nm, $d_{cyl,B82} \in [23.9, 28.5]$ nm and $d_{cyl,B67} \in [20.1, 22.7]$ nm i.e. all obtained measurements are approx. 3 nm larger than stated in Table 2. This is presumably explained by sample size, selection bias, image and pattern quality as well as where you define the cylinder boundaries. The L_0:s are particularly important to keep in mind during the upcoming experiments as theory tells us that the relation between L_0 and h_{BCP} is relevant for pattern orientation.

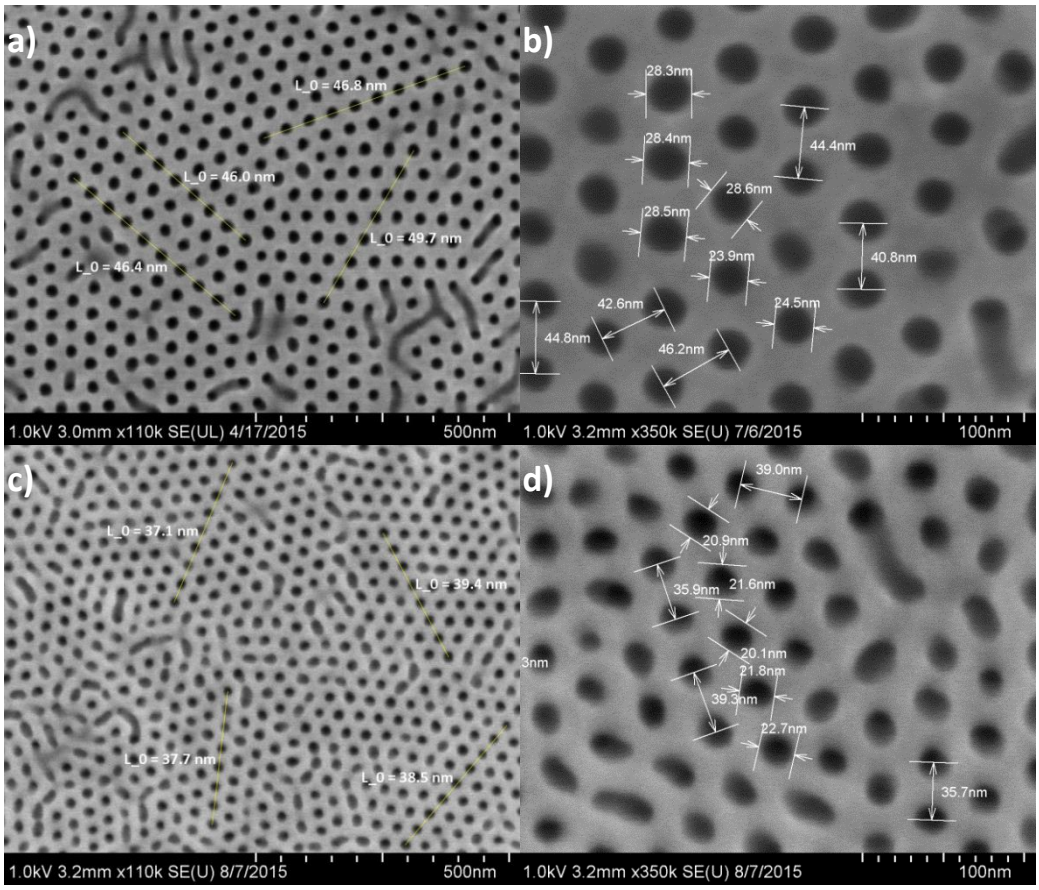

Figure 13: Interdomain distance (L_0) and cylinder diameter (d_{cyl}) of self-assembled B82 (a, b) and B67 (c, d) films.

2.4.1 B82 Polymer

2.4.1.1 B82: RTP Anneal

2.4.1.1.1 B82: RTP T_a-sweep at fixed t_a

The first RTP annealing experiment was to roughly survey the parameter space for the B82 polymer with regards to T_a and hence a temperature sweep was performed keeping t_a fixed at 1h (the maximum allowed in the RTP). The sample sequence can be found in A2.2 and a limited representative selection in Figure 14; both an upper and lower T_a boundary is clearly identifiable. For $T_a \leq 190$°C the pattern is highly irregular with a low density of vertical cylinders. A high degree of ordering on the other hand was observed in the wide interval $T_a \in [210, 260]$°C where the best value, at the time, where deemed to be $T_a = 250$°C. Solely based on *cylinder count* (CC) 230°C should be the better option but there seems to be a tendency for larger grain formation at the higher temperatures i.e. the pattern defects appears to go from being fairly evenly distributed to occur more in clusters. Granted, this is a highly subjective statement but could be verified/disproved by calculating the *lattice orientational correlation length* (ζ) which is a measure of the distance over which the long-range positional order is statistically lost i.e. a measure of grain size [16] [19]. $T_a = 270$°C teeters on the edge of being included in the stable temperature window but the initial seeds of temperature defects appear to be present in these samples. A more categorical statement can be made for $T_a \geq 280$°C where the ordering clearly has started to degrade and large areas of lying cylinders are visible. As previously mentioned this might be attributed to a higher $\delta\gamma$ towards the R10.5 between the blocks, 'degrafting' of R10.5, a reduced thermodynamic drive to phase separate or perhaps initial stages of thermal degradation of either polymer.

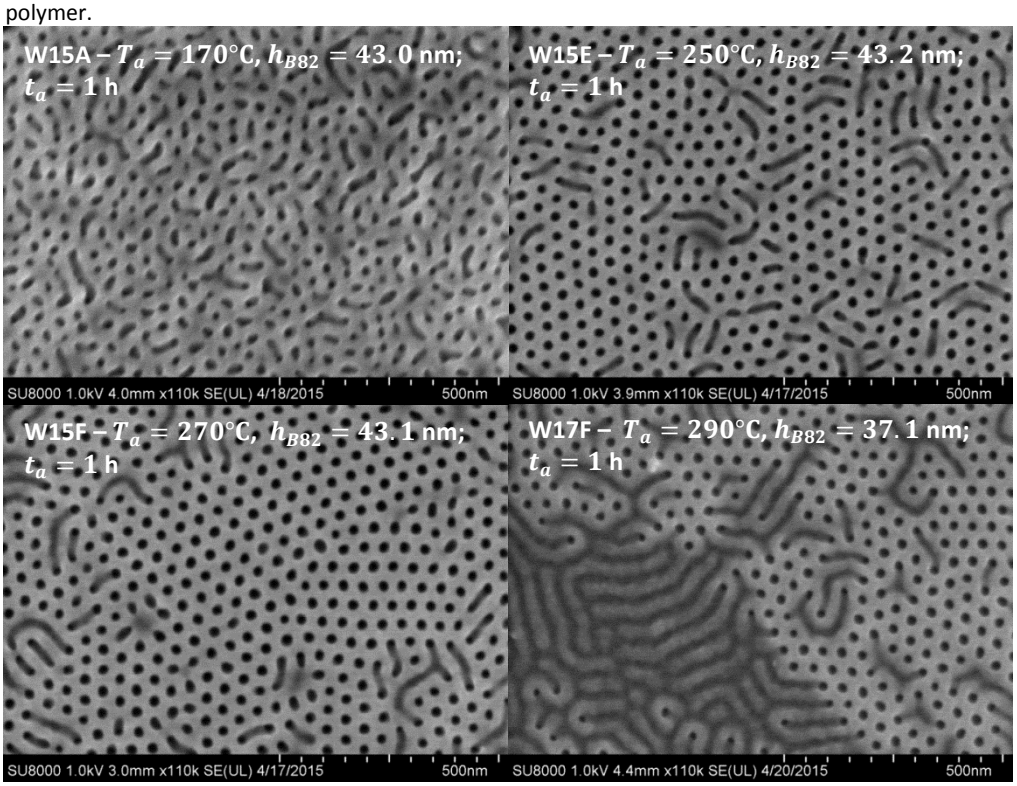

Figure 14: Effects of T_a - SEM images of selected representative B82 samples.

2.4.1.1.2 B82: RTP t_a-sweeps at fixed T_a

Order induction is a kinetic process, with thermodynamic limitations, and it is therefore more than likely that the key to obtaining good ordering lies not only in identifying a suitable T_a but rather combinations of T_a and t_a. Furthermore, for purposes of streamlining the process flow it is highly relevant to see how far you can dial back t_a and still get an acceptable polymer pattern. With this in mind, detailed time-sweeps at $T_a = 210$, 230 and 250°C were conducted and are recounted in A2.3-5. At $T_a = 210°$ and 230°C the pattern is perceived to improve with increasing t_a in the sense of fewer defects and more importantly, a greater homogeneity of cylinder dimensions. The differences are however modest and not borne out by studying the CCs. The t_a-sweep at $T_a = 250°$ is more extensive than the two previous ones and strongly suggests that t_a can be reduced by at least a factor of four, from 1h to ≤ 15 min, while still maintaining comparable ordering, see Figure 15 for two samples with widely different t_a.

Included in this series are also two samples subjected to two resp. three 1h RTP anneals back-to-back to investigate whether 1h simply is not enough to obtain perfect ordering - it is conceivable that 'rough' ordering can be achieved fairly quickly but that that advancing into 'perfect' ordering simply requires more time. Sample S4 ($t_a = 2$h) is remarkably good considering the limited $h_{R10.5}$ (6.9 nm), in stark contrast to S5 ($t_a = 3$h) that mainly consists of either deformed cylinders or patches of lying ones. The results of S5 ($t_a = 3$h) is unfortunately inconclusive due to $h_{R10.5} = 6.0$ nm i.e. at the lower edge of the identified $h_{R10.5}$-window containing the orientational transition to vertical cylinders. The multiple anneals experiment needs to be repeated with 'better' samples but even though the results of S4 is encouraging the need for multiple RTP runs is highly undesirable from a practical point of view.

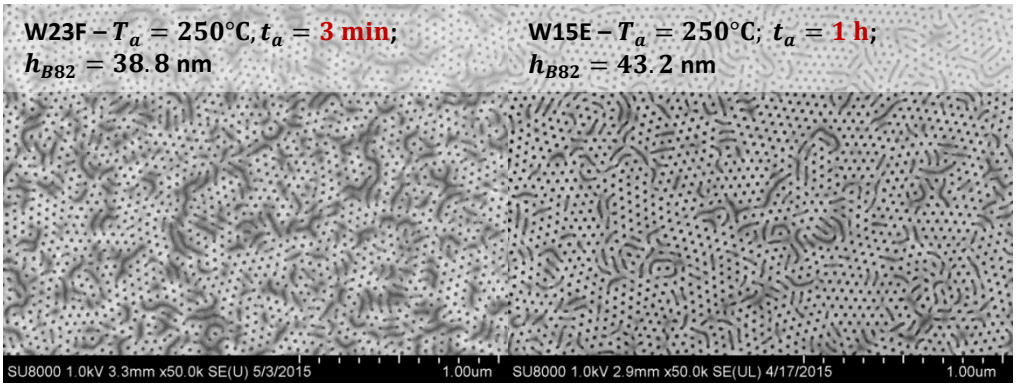

Figure 15: Effect of t_a at $T_a = 250$°C – SEM images from two selected samples with $t_a = 3$ min and $t_a = 1$h. NB: Difference in h_{B82}.

Minor forays into the previously deemed too high T_a-region (270° and 280°C), see A2.6 and A2.7, were also made to see if the induced damage could be circumvented by reducing t_a to 15 min. The improvement is less obvious at 270°C than at 280°C where the conglomerations of lying structures no longer are present. These results are more reliable since the samples came from the same parent wafers and open up the field for even shorter RTP anneals.

Before exploring more unconventional ways of using the RTP to improve the pattern quality in the B82 layer, we need to address two important questions: i) the importance of the *B82 layer thickness* (h_{B82}) and ii) whether an O_2-plasma thinning of the (remaining) B82 layer either pre- or post-development will affect the observed ordering in the SEM. As mentioned, a difference in surface tension could cause the block with the lower surface tension to preferentially migrate to the surface [13] during the anneal and this might go some way as to explain the defects that take the form of misaligned lying cylinders. It is feasible that this disturbance is only 'skin-deep' and that near perfect ordering occurs just beneath the surface layer, hence motivating the study to use O_2-plasma thinning after the anneal and development respectively.

2.4.1.1.3 B82: Effects of h_{B82}

The effect of h_{B82} is illustrated by the compilation in A2.8 (and some selected samples in Figure 16) in which all samples were annealed in the RTP at $T_a = 250$°C but unfortunately for different amounts of time but as we have seen recently this is only of subsidiary importance. It is evident that h_{B82} is an important parameter influencing the final orientation adopted. Note that all h_{B82}-values stated for annealed samples were taken prior to the anneal and hence any thinning, intentional or otherwise, is not reflected in these values.

Perhaps most notable is that a lower h_{B82} boundary, beyond which B82 lacks practical use in this project, clearly can be identified and is located somewhere in the interval $h_{B82} \in [26.6, 31.7]$ nm. At $h_{B82} = 17.8$ nm the B82 layer does not organize into a systematically ordered pattern but forms instead large 'super-domains'. The remaining PS domains post-development are more coherent and spherical in their shape than the darker regions, where the PMMA use to be, perhaps suggesting that the lowest possible free energy of a system with incomplete coverage is obtained when minimizing the PS rather than the PMMA interface. Merely based of these SEM images it is not possible to determine whether the darker areas are actually void of any remnants of B82 polymer, for that a height profile or SEM cross-sectional image is needed.

Moving down in the sequence, sample W24C ($h_{B82} = 27.6$ nm) has arguably the best ordering of any sample thus far with almost no defects and clearly visible grain boundaries. The problem is that W24C also contains large regions lacking in PS pattern coverage, something that is incompatible with down-streams processing steps such as electrodeposition and MOVPE. A speculative interpretation of the W24C results is that the low h_{B82} has allowed a large scale rearrangement of the B82 film generating thinner (dark) and thicker layer regions where the latter conforms to a commensurability condition for perpendicular cylinders. Both visual inspection and low MSE values in the ellipsometer measurements indicates that the B82 layer was uniform before the anneal. It is feasible that the high T_a and/or dT/dt in the RTP transiently can induce more internal strain in the B82 layer than what a 'gentler' 170°C VA would. Literature abounds with instances where organized morphologies have been obtained in equally thick or thinner (absolute values) P(S-b-MMA) layers [13] but where an extended lower T_a VA was used instead.

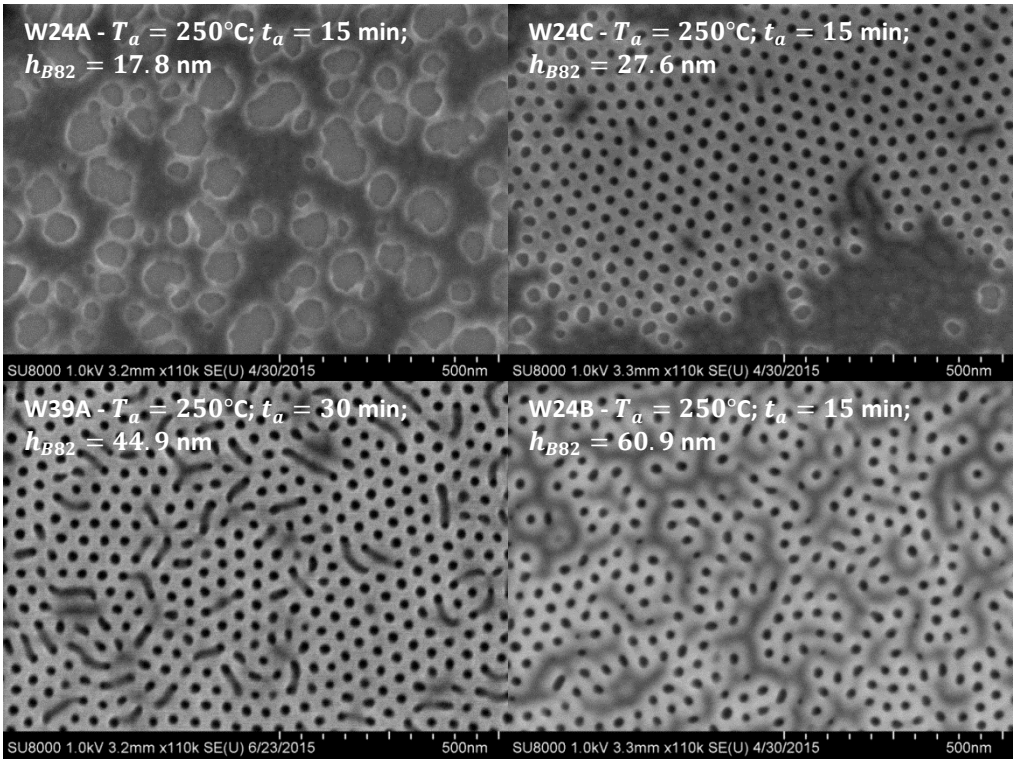

Figure 16: Effects of h_{B82} – SEM images from some selected samples.

Complete sample coverage of patterns containing vertical cylinders are obtained for $h_{B82} \in [33.7, 44.9]$ nm i.e. in a h_{B82}-window of at least 13.2 nm which bodes well for process stability. At the lower boundary some variation in d_{cyl} might be an issue. For $h_{B82} \in [60.9, 92.1]$ nm cylinders are still observable but a substantial portion of them are deformed at the surface and do not appear to be completely vertically oriented. The two samples covering this interval were, by necessity, R10.5 washed using acetone (denoted AW) instead of the normal toluene and also annealed for only 15 min. Acetone is not as good at solving R10.5 as toluene and it is unclear if/how this affects the surface neutralizing properties of the remaining R10.5 layer. It is furthermore not unlikely that the low t_a plays an integral role in the outcome since the ordering process for a thicker B82 film entails the rearrangement of more mass and hence simply might require more time. Sample W33D ($h_{B82} = 126.2$ nm) had a post-anneal O_2 RIE thinning and the observed ordering is very poor even though cylinders are visible. A likely contributing fact is that W33D was spun-cast at low speeds and thus had problems with film thickness uniformity, evident by colour variations and high MSE values in the ellipsometer measurement.

To summarize the h_{B82}-series, a high degree of order can reliably be obtained in B82 layers with $h_{B82} \in [33.7, 44.9]$ and it is feasible that the limits of this window can be increased upwards by increasing t_a and perhaps even downwards by reducing T_a and/or dT_a/dt_a and maybe compensating with a prolonged t_a.

2.4.1.1.4 B82: Effects of O_2 plasma thinning of B82 layer

The sample sequence in A2.9 aims to illustrate the effects of pre- and post-development O_2 RIE thinning respectively. For the RIE parameters used (30 W *nominal* (nom.) RF power, 20 sccm O_2, 100 mTorr) the blanket sample etch rates of PS-OH (1.2 kg/mol) and PMMA (50 kg/mol) homopolymers are 42.4 and 64.8 nm/min respectively. The PMMA:PS-OH selectivity is thus 1.53 meaning that it is not a just a thinning but also a weakly selective removal of PMMA. Based on the series of progressively more pre-development etched samples W33E, S6 and S7 perfect ordering does not appear to be lurking just below the surface; the defects we have come to expect at the top is present also at deeper levels but again be wary of the $h_{R10.5}$-values. More sure-footed conclusions can be drawn from the vacuum annealed sample W35C which was subjected to repeated post-development RIE treatments and where a reference base line was taken beforehand. The result is not the removal of defects but, as expected (due to the limited anisotropy of the process), an enlargement of d_{cyl} which eventually will cause the pattern to collapse. This problem can be mitigated by using more anisotropic etch techniques and/or parameters - lowering the chamber pressure is generally one way. The potential benefits of a post-development O_2 etch has during the course of this project only been demonstrated once, for sample W33F which was subjected to both RTP and vacuum chamber anneals. A clear defect reduction, although not an elimination, is achieved at the surface but keep in mind that the SEM image is not of exactly the same spot and that minor variation over the sample surface is to be expected. At this stage it ought to be pointed out that a minimum of two well separated spots were imaged in the SEM for each sample to reducing the risk of acquiring data from an unrepresentative local variation. Essentially, moderate O_2 plasma thinning will generally not remove defects but does also not generate new ones, motivating why some thinned samples have been included in sequences comparing the degree of pattern quality. However, in case of excessive post-development thinning cylinders will start to collapse into each other.

2.4.1.1.5 B82: 'Advanced' RTP annealing cycles

The RTP is a versatile machine with which it is possible to program complicated heating/cooling cycles, dictate rates of change, vary the gas flow etc. Previous RTP anneals consisted of three obvious steps: ramp-up, constant T and finally cooling, all conducted during a constant N_2 flow but more complicated RTP anneals were also evaluated, see A2.10.

Samples W28F and W17C constitute two attempts at multi-tiered anneals where T initially was raised to a high level to later be successively stepped down before the final cooling stage. The underlying idea being that the coarse ordering of the B82 layer occurs during the first high-T stage(s) where the polymer mobility is high. As the temperature drops the kinetics suffers but the thermodynamic drive to phase separate becomes greater hopefully enabling a finer restructuring where the defects generated earlier are 'healed out'. Unfortunately, this hypothesis was not supported by the experiments and both samples are worse or as best equal to the simpler 'one-stage' RTP anneals. Sample W27A, on the other hand, was heated to and held at 250°C for 3 min three times during a single RTP anneal and the sample was cooled in-between each heating. The idea being tested here was that it is perhaps the rapid heating

in and of itself and not just the higher T_a that is key in a RTP anneal. In A2.5 we observed that the morphology and ordering is present already after $t_a = 3.5$ min at $T_a = 250$°C and if the operative agent is e.g. a transient temperature gradient along the B82 layer thickness then perhaps repeated heatings could be beneficial. However, the degree of order once again fell short of the 'standard' RTP cycle (NB: AW).

2.4.1.1.6 B82: Heating conditions

There are two different 4" carrier wafers used in the RTP, a Si and a graphite one. The Si is the norm in this project and was used for all samples except one – W23C, see A2.11. The SEM micrographs of W23C is markedly different from what we have come to expect given the sample and other RTP parameters. The sample is dominated by a sea of densely packed lying cylinders with interspersed 'darker' islands also mainly containing the same pattern. However, in the middle and at the periphery of the islands vertical cylinders can be observed and the patches in the middle, although small, have perfect ordering. The difference in brightness is believed to stem from a height differential caused by large scale rearrangement of the B82 film but this has to be confirmed by e.g. imaging with sample tilt. The cylinders are thought to appear where vertical and/or lateral confinement makes this the most favourable orientation.

We have two highly speculative explanations as to the effect of using the graphite wafer: the first, less probable, is that carbon is introduced into the RTP atmosphere and that its presence affects the boundary conditions at the top surface. The main objection to this proposal is the low volatility of graphite at 250°C and that the RTP atmosphere is continuously replenished by a N_2 flow. The second, more credible, explanation is that graphite is less transparent than Si in the IR region, something possible affecting the sample heating conditions. The B82 would be more shielded to direct IR exposure but at the same time the wafer ought to heat up quicker if the temperature feedback loop cannot compensate and in fact the small time-lag between the set and actual temperature during ramp-up is smaller when using the graphite wafer. The observation from the T_a-sweep that the morphological orientation shifts from vertical to horizontal when T_a gets too high is also indicative.

The results above motivate looking into the exact nature of the ramp-up to T_a e.g. the magnitude of dT/dt and from which direction the heat is applied. Series A2.12 partly addresses the effects of dT/dt and includes besides the standard rate of 18°C/s also 5 and 10°C/s. It would be interesting to complement the series by testing a higher rate as well but from these samples we can conclude that, for purposes of ordering, the rate seems to be of marginal importance as long as $dT/dt \leq 18$°C/s. Identifying the highest practically usable rate would be of interest in the quest to reduce the overall processing time for industrial application of BCP lithography.
Normally the heat is applied from below but the RTP has a "TOPHEAT"-option which as the name suggests entails applying it from above. The sample is exposed directly instead of through the carrier wafer and the change in heat source location could feasibly affect the evaporation process of any residual solvent in the R10.5 and B82 films. Since the thermocouple responsible for the feedback contacts the carrier wafer from below a small time-lag might be introduced if the PID does not anticipate this. The investigation of this option is found in A2.13 but again reveals no 'magic bullet'. Sample W35A, annealed at $T_a = 250$°C for 15 min with TOPHEAT during the ramp-up, has indeed a decent cylinder density but more interestingly is the formation of islands of highly ordered vertical cylinders. However, it is probable that this is just another example of film rearrangement and confinement effects and the sample would proceed to adopt the fingerprint pattern if t_a was just a little bit longer. In an attempt to avoid island formation while using TOPHEAT both T_a and dT/dt were reduced for samples W35D and W39C but no identifiable gain can be reaped from heating from above rather than from below.

2.4.1.1.7 B82: Effects of atmosphere during anneal

To fully explore all aspects of the RTP parameter space we must also scrutinize how the composition of the atmosphere during the anneal affects the orientation. It is well established that proper chamber cleaning and pre-conditioning are crucial in obtaining reproducibility in epitaxy and some sensitive etch processes. The RTP has multiple users using it for e.g. cross-linking BCB or to thermally process III-V structures and high-k dielectrics, it is thus not unreasonable to think that some spill-over occurs from run to run. A high-T chamber pre-conditioning could in theory remove volatile compounds and thus hinder them from interfering with later processes. An attempt, see A2.14, was made to see if this concept extends to RTP annealing. Two samples from the same parent wafer were annealed with

identical RTP settings, one before and one after the chamber pre-conditioning. The pre-conditioning consisted of running the RTP at 800°C for 5 min and ashing of the Si carrier wafer. Both samples have issues with poor ordering but the 'after sample' is markedly worse than the 'before sample'. This experiment needs, of course, to be repeated for verification but if the results stand the underlying reason needs to be looked into further.

The extent and composition of chamber contamination will vary but there are controllable ways of changing the atmosphere by choosing the gas flow, if any. All available options: i) 150 l/h N_2 (standard), ii) 150 l/h forming gas and iii) "vacuum" were tested, see A2.15. All samples came from the same parent wafer but even the reference (N_2) had more defects than reasonable to expect. That said, a comparative study can still be made and forming gas appears to perform on par with N_2, not surprisingly since N_2 is the main constituent of the gas mixture. The "vacuum" option entails more suction than any higher degree of vacuum and that sample had worse ordering. It is interesting to see that the number of lying cylinders on the surface is higher and that they seem to form clusters. It is feasible that this is caused by either changes in surface tension due to the presence of oxygen or simply oxidation of the surface layer. The divergence in ordering will presumably increase with t_a.

A somewhat naive attempt at shielding samples from oxygen induced damage/defects during annealing in the RTP and regular lab ovens was also made, see A2.16. In the food packaging industry aluminum foil is used as an oxygen barrier to extend the shelf life of consumables. With this in mind, four samples where individually tightly wrapped in double layers of ordinary household Al foil and the edges were sealed by multiple sharp folds. Although the packages were not hermetically sealed, it will take substantially longer to refresh the atmosphere over the samples. This method does not remove the oxygen already present inside the packages but (partly) block the access of new molecules. Both the RTP and the regular lab oven were loaded with two samples each, one with a thinner B82 ($h_{B82} < L_{0,B82}$) and one with a thicker B67 layer. The standard N_2 flow was used during the RTP anneal and not surprisingly the samples look no different from equivalent samples without the wrapping. Note that the irregularity of the cylinders on W30A (B82) probably stems from the long post-anneal O_2 thinning that all four samples went through. However, the rubber really met the road for samples W30B and W30D which were annealed in a regular lab oven (no vacuum) at $T_a = 190$°C for 24 h. The thinner B82 sample suffered extensive damage where most of the remaining PS formed large irregular islands. In-between these islands smaller isolated areas containing cylinders can be found and even though some surface microstructure can be observed in the PS islands it does not appear to be regular or have sufficient depth to be of practical use. In comparison with W35B and W34A (both annealed in a leaky vacuum chamber, see A2.19), the fact that regions of cylinders were obtained at all might indicate that the Al actually had a barrier effect - just not as effective as hoped. The thicker B67 sample exhibits an interesting potpourri of morphologies with most of the surface covered by solid islands and a lamellar structure beneath which what appears to be cylinders can be glimpsed. Some of these observations can probably be explained by the Al coming into contact with the BCPs.

If oxygen has detrimental effects for the ordering process it is possible that limited damage can be induced during the standard 1 min 100°C hotplate SBs following the R10.5 and B82 SCs. The likelihood of this being the case is small but completely forgoing or carrying out the SB at a lower temperature could allow slightly more of the solvent to remain in the polymer layers up until the anneal. If the process of evaporation is important for ordering then this might be a way of reducing the density of defects. Besides a standard processing reference, one sample was not soft-baked at all while the other was baked for a longer time (3 min) but at a substantially lower temperature (50°C), see A2.17. Here the samples cannot share processing steps other than the surface activation and as such have different $h_{R10.5}$. Setting this aside, no clear improvement seems to come from altering the standard SB procedure even though the CCs suggest this.

2.4.1.2 B82: Vacuum Anneal

The most common form of thermal anneal found in literature is performed using a VO, usually for 24 to 48 h. A selection of VOA B82 samples from the same parent wafer is presented in A2.18. Samples W39D and W39B were annealed at $T_a = 190$°C for 6h and 24h respectively and the latter has a higher degree of order thus indicating a time-dependence even after 6h. The VO was pushed to its limits by running sample W39F at the maximum temperature 200°C for 48 h and despite a fair number of cylinders the experiment is deemed unsuccessful due to large scale film non-uniformities. The oven was pumped-down for at least 15 min prior to turning on the heat, the T_a ramp-up takes >90 min and great care was

taken to make sure the samples were not unloaded before T had dropped below 70°C. These three samples in no way constitute a thorough investigation but the conclusion drawn is that even the best sample here is no better than what can be obtained using the RTP for a fraction of the time. However, if a more suitable combination of t_a and T_a can be identified VOA has the advantage of parallelism due to size of the oven which in turn would partly negate the prolonged t_a.

The VO is only capable of low quality vacuums, 10^{-2} mbar at best, and to truly test the merits of the VA higher vacuums are required. This is one of the reasons why a custom-made oven-proof *vacuum chamber* (VC) was commissioned and built for this project. The chamber was pumped down using a combined membrane and turbo pump. Sample W34A was annealed at $T_a = 190$°C for 24h and was the first attempt at using the chamber and the result, see A2.19, was catastrophic – the remaining PS was collected either in large homogenous masses or found in tendril-like 'archipelagos'. The sample was furthermore covered in a white transparent slightly greasy film upon completion of the *vacuum chamber anneal* (VCA). At the time this was attributed to contamination deep inside crevices of the metal welds and the disassembled chamber was both washed with acetone in an USB and baked to remove all volatiles. The duration of the second VCA (with W35B) was also 24 h but was carried out at $T_a = 170$°C instead and this time no discoloration or greasy deposition was observed. However, the B82 film looked visible thinner at a cursory visual inspection. The SEM revealed that the PS once again formed homogenous domains but that these this time were small and fairly evenly distributed in the film. The most likely scenario, as the author sees it, is that the chamber had a small leak somewhere. If the leak had been substantial the turbo-pump would not have been able reach and maintain the set-point 1500 Hz. This is supported by the fact that no sound, from air rushing in, was heard when the valve was opened after the chamber had cooled down. Since 24h is plenty of time for the pressure to equalize given the small volume of the chamber, even for a modest leak, t_a was reduced to 2h for the next sample (W35C). W35C exhibits ordering comparable to the better RTP samples but since the magnitude of the leak was unknown the true potential of VA remains elusive.

One way of getting around this obstacle was to place the chamber on a hotplate and having it continuously connected to the vacuum pump to mitigate the leak. The chamber was loaded with W35F and pumped down for 15 min before putting it on the hotplate, set at 200°C for 6 h. The higher T_a was used to compensate for conductive and radiative heat losses since the heat now only is applied from below and not from all sides as in an oven. Considering that $t_a = 6$ h i.e. a factor three longer than for W35C the results of W35F is remarkable bad, in fact the appearance is very much reminiscent of that of the low T_a samples obtained during the first RTP T_a sweep. This led us to think that there might be a temperature offset between the actual temperature and the hotplate setpoint and indeed this suspicion was confirmed by using an IR probe on the unloaded hotplate. It turns out that there was approximatively a 30°C offset and that the T_a in fact was closer to 170°C. Attempts to repeat the experiment while compensating for the offset was made but unfortunately the severity of the leak improved with chamber usage and the attempts had to be aborted since the desired vacuum levels could not be reached. The leakage is believed to be caused by the inability of the Viton® O-ring in the lid to completely seal the chamber and the problem got progressively worse despite the O-ring being rated for a maximum continuous operating temperature of 225°C.

Before the magnitude of the leak was fully realized the VC was used in an experiment of note where sample W39E was placed inside the chamber which was then pumped down and put inside the VO, see A2.19. Due to the leak the vacuum level would decay but since the chamber was inside the VO the level could never drop below 10^{-2} mbar. This approach was also believed to come with an additional advantage, namely the option to remove the chamber from the oven while this was still hot. The oven takes several hours to cool to a safe unloading temperature whereas the chamber only needs about 15 min. Previously the chamber was able to maintain acceptable vacuum levels for at least 2 h, as evidenced by W35C, and despite the worsening of the leak the vacuum was thought to endure for at least 15 min. If this was the case the time required for loading and unloading the vacuum oven would have been substantially reduced making the entire process far more time effective. The results of W39E is especially indicative when compared to sample W39B that came from the same parent wafer and was annealed with exactly the same settings except for the addition of the vacuum chamber. W35B was left to slowly cool down in the vacuum oven upon completion of the anneal while the quicker method outline above was used for W39E. The difference is quite remarkable with a far greater number of lying cylinders on the surface of W39E. The interesting question is of course why and there are at least two potential explanations: i) if the leak was big enough, substantial amounts of oxygen would have been

present during the cool down and there would have been a high temperature window of opportunity for film rearrangement. The second explanation is that ii) the cooling rate in and of itself might be an important factor in the ordering process. Maybe a slow cooling is better than a more abrupt one and perhaps a natural way of implementing the idea behind the multi-tiered RTP programs. In hindsight the effect of cooling rate seems less probable when considering the good ordering of VCA sample W35C ($t_a = 2$h).

2.4.1.3 B82: Solvent Vapour Anneal

The image set in A2.20 illustrate the first venture using *solvent vapour anneal* (SVA); five pure solvents (anisole, toluene, THF, acetone and IPA) were used and the anneals were performed at RT for 24h. Anisole, toluene and THF are all routinely used to make solutions of P(S-b-MMA) due to their proficiency at dissolving both polymer blocks. Theoretically the solvent molecules will exhibit a preferential selectivity in their interaction with the two blocks but these three solvents were chosen in the hope that the swollen volume ratio between the blocks would be approximately the same as without the solvent.

As stated above, in bulk melts the block volume ratio dictates the thermodynamically stable morphology but of course the introduction of a solvent complicates the molecular interplay. The aim here is to simply improve the mobility of the polymer chains and thus allow them to self-arrange at RT. Both acetone and IPA (2-propanol) in particular should have a preference towards the more polar PMMA block and is thought to swell these domains more than the PS ones.

We can observe that the resultant morphologies after the anisole, acetone and IPA SVAs are very similar, with disorganized pockmarked surfaces. For toluene lying cylinders dominate the surface, especially inside large island formations. The only solvent showing any promise was THF for which the morphology is reminiscent of low T_a RTP anneals – a number of what appears to be cylinders, although deformed, can be observed but it is unclear whether these actually propagate all the way down to the R10.5 layer. A major issue with W22C and W22D is that both THF and acetone has a low *boiling point* (BP) and a high vapour pressure causing the atmosphere in the annealing chamber to be very solvent rich. In this case that seems to translate into large amounts of solvent inside the polymer films, in fact enough to cause the polymer film to flow, become uneven or even dewet over large areas, see A2.23.

To investigate the t_a-dependence the experiment was repeated (for anisole, toluene, THF and acetone) but with an annealing time of 4 h i.e. a reduction with a factor of six, see A2.21. An additional difference is that the samples were subjected to a 1 min 80°C SB (after the SVA), the effect of which ought to be marginal as the bulk of the solvent in the film evaporates within seconds of the sample being removed from the SVA vessel. The SEM images are almost indistinguishable from those of the previous longer runs with the exception that W28B (toluene) is completely covered lying cylinders. A larger difference can be seen on the macro-scale just by visually inspecting the samples; unfortunately no overview photos were taken of the 24h SVA samples expect for W22D (acetone). However, the IPA, anisole and toluene samples had uniform films while the THF sample just looked like a more severe version of its 4h counterpart with more and larger circular dewetted areas.

Of the pure solvents used only THF showed any potential but it was clear that reducing t_a was a necessity to maintain film uniformity; therefore one more SVA sample (W27E) was prepared using THF and $t_a = 1$h, see A2.22. The integrity of the B82 film of W27E looked intact to the naked eye but the first stages of layer break-up could be seen in the SEM. As for the morphology, no improvement is evident and thus the conclusion of these SVA experiments is that new areas of the parameter space needs to be explored e.g. the effects of other solvents, combinations of solvents, T_a, pressure and evaporation rates at the end of the SVA. The first three could have been investigated with the current set-up but the latter two would have needed more specialized equipment. Some preliminary sketches of such a system were drawn up but due to time constraints they never left the planning stages.

2.4.1.4 B82: Combinations of techniques

A few combinations of thermal techniques were evaluated in an attempt to reap the best properties from both or ideally reap some synergistic effect, see A2.24. Before the VO was connected and the VC constructed samples W17D and W17E were first annealed together in the RTP (250°C, 1h) and then in separate regular lab ovens for 18 h at 100 and 150°C respectively. Sample W17D (100°C) looked no different from a regular 'RTP sample' which is not very surprising considering that 100°C falls short of T_g

for both polymer blocks. At 100°C both polymer blocks are in the glassy state characterized by virtually no long range chain mobility, only limited segmental movement. If nothing else, this sample reinforces the conclusion drawn, in 2.4.1.1.7, regarding the detrimental effects, or rather the lack of such, of the SB in a regular atmosphere. However at 150°C we are well above the $T_g s$ of both blocks and small differences can be identified: the number of defects is approximately the same as for W17D but they are now diffuse at the edges and a large spread in cylinder diameter can be observed. 150°C is still a low annealing temperature and the observations made on W17E might simply be the effects of low-level oxygen damage. We have come across sample W33F once before when discussing the merits of post-development O_2 plasma thinning and it was annealed first in the RTP (250°C, 30 min) and then in the VC (190°C, 2h). At a first glance it looks really bad but as we have seen, after a 12 s O_2 RIE the polymer pattern looks vastly better. This would be satisfactorily explained if oxygen damage was induced at the surface, due to the leaky chamber, while deeper laying parts of the film approximately maintained the ordering formed during the RTP anneal. As you remember, similar effects of plasma thinning were not observed for other 'mono-annealed' samples.

One attempt at combining RTP annealing with SVA was made with W27D, see A2.25. An anisole SVA (60°C, 20 min) was performed in-between two short RTP anneals (250°C, 15 min). This was yet another way of testing if the evaporation process is significant for the ordering by first driving off the lingering solvent during the first RTP cycle and then replenish the film with new solvent during the SVA and the finally repeat the first step. Based on the earlier SVA experiment anisole should perhaps not have been the solvent of choice. As seen in A2.25 no added value is obtained from the extra processing steps, quite the opposite in fact.

2.4.2 67 Polymer

2.4.2.1 B67: RTP Anneal

B82 was the BCP primarily used in this project but T_a-sweeps (keeping t_a fixed) were also performed with the lower MW B67 polymer in the RTP and VO respectively. Samples with $h_{B67} \approx L_{0,B67}$ and $h_{B67} \approx 2L_{0,B67}$ were used in each run, the reason being that $L_{0,B67} < L_{0,B82}$ and a low film thickness can be a disadvantage in certain processes such as lift-off and dry etching. $h_{B67} \approx 2L_{0,B67}$ could potentially be a better option provided the vertical cylinders remain sufficiently straight. The results, see A2.26, of the $h_{B67} \approx L_{0,B67}$ samples annealed in the RTP differ significantly from their B82 counterparts. B67 is clearly more T_a sensitive and the best sample (W51F) is the one annealed at the lowest temperature ($T_a = 210$°C) and even then the lying cylinders outnumber the vertical. At $T_a = 250$°C and above the samples are dominated by a sea of lying cylinders and minor islands with either parallel or vertical ones. For this type of sample, it most probably would be beneficial to reduce T_a and/or t_a and W51H (270°C, 10 min) was one unsuccessful attempt at the latter.

Diametrically different is the response, see A2.27, of the $h_{B67} \approx 2L_{0,B67}$ samples to exactly the same treatments. Perpendicular cylinders is now the main morphology but the lower T_a tolerance still makes itself known by a progressively increasing number of lying cylinders with higher T_a. In this trend the lying cylinders are not evenly distributed in the film but rather agglomerate in dark growing coherent regions. An interesting observation is that the ordering in the area between the darker regions seems to improve as these regions grow, perhaps as a consequence of lateral confinement. W50H (270°C, 10 min) reinforces the potential efficacy of high T_a low t_a anneals. It is curious to note the difference in self-assembled pattern as a consequence of h_{B67} for a given T_a and t_a. Granted $h_{R10.5}$ is 0.4 nm higher for the $h_{B67} \approx 2L_{0,B67}$ samples but the experience gained from working with B82 is that both R10.5 layer heights should be able to support a large number of cylinders in B82 films.

2.4.2.2 B67: Vacuum Oven Anneal

The results of the $t_a = 24$h VOA T_a-sweep is an almost identical replica of the RTP one – just displaced in temperature. At 150° and 170°C the morphology of the $h_{B67} \approx L_{0,B67}$ samples, see A2.28, is a homogenous mix of vertical and lying cylinders, rich in the latter, and at 190°C the familiar sea/island constellation appears. The B67 pattern of the $h_{B67} \approx 2L_{0,B67}$ samples, see A2.29, are homogenous at 150° and 170°C but with fairly poor ordering and at 190°C the pattern of dark areas composed of lying structures is already well rooted. The preliminary conclusion, based on these samples, is that RTP annealing outperforms the VOA for B67 regardless of yardstick but of course with the caveat that more combinations of T_a, t_a and h_{B67} needs to be tested. [3] found that the equilibrium morphology was present already after 1h at $T_a = 190$°C and that no further pattern improvement was gained by longer t_a suggesting perhaps that t_a primarily needs to be reduced.

2.4.3 Annealing Commentary

At this point it is prudent to call into question the prerequisites for the ordering process. It is conceivable that the annealing conditions are not the limiting factor here and hence could be tweaked in perpetuity without ever obtaining a perfect pattern. As mentioned, it could simply be that the composition of and/or combination of R10.5 and B82 just are not optimal. We have seen that the polymer samples purchased from *Polymer Source Inc.* were heavily contaminated by particulate matter and meticulous filtering of the prepared solutions was essential in avoiding streaks and spin-comets during SC. It does not seem unreasonable to think that the polymer samples also might have had other forms of contaminants e.g. homopolymers that negatively could interfere with the ordering process.

One could even go one step further and question the quality of the polymers themselves. Even if the polymers were perfect in every respect, it might simply be that the free energy cost of having ordering defects in a polymer film virtually without any lateral constraints just is not high enough. Just speculating, instead of forcing parallel cylinders into the perpendicular orientation it might simply be kinetically easier to locally rearrange h_{B82} to create a local free energy minimum that is sufficiently stable, making the global minimum less likely to be adopted i.e. the film adopts a meta-stable arrangement due to kinetic considerations. One way of making the free energy costs higher would be *directed self-assembly* (DSA), see *outlook*.

2.5 Experiment IV: Selective Block and Brush Removal Using RIE

There are essentially two ways of developing an annealed BCP sample: i) a wet development consisting of DUV exposure and AA immersion followed by a plasma based etching to remove the brush layer at the bottom of the cylinders and thereby exposing the substrate. ii) a completely plasma based (i.e. dry) etching in which a difference in etching rate of PMMA and PS is utilized to selectively remove the PMMA cylinders prior to a similar brush removal as in i). If option ii) is used then there is the option to DUV expose the samples after the BCP anneal in the hope that the DUV will induce higher etch rate selectivities and partially degrade the R10.5 prior to its removal.

In this project two dry etch chemistries were evaluated based on *etch rates* (ERs), PMMA:PS and R10.5:PS selectivities. Moderate ERs are desirable since the entire process becomes more reproducible as the relative effect of start-up transients becomes reduced. Most coveted however are high selectivities, a low PMMA:PS selectivity will translate into a thinner PS mask remaining after a dry development and more importantly an increase in the diameter of the empty cylinders/pores. Both consequences will limit the further use of the polymer pattern as an etch mask during the subsequent pattern transfer. An acceptable R10.5:PS selectivity is needed to remove the brush layer and expose the substrate without needlessly sacrificing the resolution and PS mask further.

Both chemistries tested are combinations of a fluorine based freon (CF_4 and SF_6) and oxygen. The parameter space includes several controllable variables: pressure, gas flows, nominal RF power and etch time. To map the entire space would require a lot of time and countless samples but consulting with [44] suggested that pressure and power only marginally affect the etch selectivities when using blanket samples. Blanket samples, i.e. samples covered with a uniform non-patterned polymer layer, where used in the experiments described here. The polymers used were PMMA (M_n = 50 kg/mol), hydroxyl terminated PS (PS-OH, M_n = 1.2 kg/mol), i.e. the block constituents but as homopolymers, and R10.5. The homopolymers are not entirely representative of the blocks in the B82 on account of differences in M_n and for PS the addition of an –OH group in PS-OH. The carbon to oxygen ratio in a polymer is known to affect the etch rate [45] but these polymers were the best analogous to the individual blocks that were available at the time. The main advantage of using blanket samples is that the (time-average) ERs easily can be obtained by measuring the film thickness before and after the RIE process in the ellipsometer. The drawback is that it will provide you with the best-case scenario for BCP etching as the effects of surface topography will not be factored in. Etching a high aspect ratio pattern differs from a blanket etch since the reactive species need to travel down to the confined interface and rest products in the opposite direction. Pressure will therefore most likely be a more important consideration for a patterned rather than for a blanket sample, as the mean free path is dictated by this variable.

An initial screening of each etch chemistry was conducted by keeping the pressure (100 mTorr), RF power (30W), etch time (15 s) and total gas flow (20 sccm) constant. The freon:oxygen ratio was varied by increasing the flow of the freon in increments of 5 sccm while at the same time decreasing the oxygen flow by the same amount, keeping the total gas flow constant. A clear oversight in the SF_6/O_2 screening was that only PMMA and PS-OH blanket samples were used but judging from the CF_4/O_2 results the behavior of R10.5:PS-OH selectivity seems to mirror that of PMMA and PS-OH. The tabulated values as well as plots of ERs and selectivities can be found in A3.1-4 and A3.5-9 for the screenings of the respective etch chemistries. The plots furthermore contain polynomial fits, the degrees of which are evident from the given equations. It is debatable if lower degree polynomials in some cases would have been more representative of the physics at work even at the expense of a worse fit. Trying to make the curves fit to such a low number of data points might be misleading due to the 'natural variability' of the process. A noteworthy observation is that the ER of all polymers and in both chemistries exhibits a maximum somewhere in the lower half of the freon flow scale.

Interesting, in the CF_4/O_2 screening, is that the R10.5 peak lies closer to that of PS-OH than to that of PMMA, perhaps not surprising considering S is the dominant (66 mol-%) constituent of R10.5. However, curious is that the R10.5 peak does not lay in-between the PS-OH and PMMA peaks but rather at a lower CF_4 flow than either of these. Both selectivities grow monotonously with an increasing CF_4 flow but at the same time all ERs quickly drop off in the upper half of the CF_4 flow scale. When using pure CF_4 the final etched distances are so small, particularly for PS-OH, that initial polymer film non-uniformities and uncertainties in the ellipsometer measurement will have a marked influence on the obtained ERs and selectivities i.e. a small natural variation will be greatly amplified.

In the SF_6/O_2 screening one set of samples i.e. a data point (the 10 sccm SF_6 run) was accidentally etched for 20 s instead of the usual 15 s but as the time-average ERs are calculated and compared this value was still used when fitting the trend lines. This would not have been acceptable if the discrepancy had been >5 s since the ERs appear to have a weak time-dependence. The PMMA and PS-OH ERs have been plotted in separate figures for sake of visibility since several additional data points were collected and are presented along with the screening. If the polynomial fits are to be believed, then the PMMA and PS-OH ER peaks are both sharper and occur at lower freon flows than their counterparts in the CF_4/O_2 screen; the latter might be a reflection of the higher fluorine content of SF_6. Once again the PMMA:PS-OH selectivity grows and the ERs decrease with increasing SF_6:O_2 flow ratio in the higher registers of the flow scale. Higher PMMA:PS-OH selectivity is obtained across the board for the SF_6 based chemistry but the same ER caveats apply here as for the CF_4 screening.

To verify the high selectivity at ≥15 sccm SF_6 a 90 s run was performed (at 15 sccm SF_6) and a marked drop in measured selectivity was noted and it is likely that the reduction would be even larger for higher SF_6 flows. To implement a dry development of an annealed B82 sample the PMMA blanket etched distance needs to be $\geq h_{B82}$ $(\text{here } L_{0,B82} \approx 46)$ nm and according to A3.8 this is approximately accomplished after 15 s at 5 sccm SF_6 and after 90 s at 15 sccm SF_6. The selectivity in the first option is 3.44 but only 2.88 in the second, hence the conclusion is that the high selectivities obtained during short etches at high SF_6 flows cannot be maintained when the etch time is increased to levels of practical use.

The supplemental samples were cursory tests of the assumptions made previously i.e. the effects of RF power and pressure. As expected, the ERs increase with RF power but seemingly at the expense of selectivity and a pressure reduction is affiliated with lower ERs but an unaffected selectivity and this is further born out when combining the two. These statements all need to be supported by further tests and it is feasible that the effects of RF power and pressure will depend on the ratio of process gases.

Based on the screenings, the SF_6 chemistry was deemed the most suited due to higher selectivity and a proper *design of experiment* (DOE) was formulated using the statistical software MODDE 10.1 with the intent to model (including quadratic terms) the SF_6/O_2 RIE process. Again, to limit the scope the total gas flow (20 sccm) nominal RF power (30 W) were kept constant while *pressure* (p), *time* (t) and *SF_6 flow* (F_{SF6}) were varied. The parameter space (mainly) probed was: $p \in [75, 125]$ mTorr, $t \in [15, 25]$ s and $F_{SF6} \in [2, 8]$ sccm and the *reflected power* (P_{ref}) was included as an uncontrollable variable. The F_{SF6} range was chosen based on the previous screening where the best selectivity for an adequate etch distance was obtained for $F_{SF6} < 10$ sccm. Even though the F_{SF6} level can be adjusted in increments of 1 sccm in the RIE interface, there is a practical lower limit of 5 sccm beyond which the *mass flow controllers* (MFCs) are not sensitive enough to reproduce the same flows from run to run, meaning that the etch process could be highly unstable here – at least according to other users of the RIE system. F_{SF6} values <5 sccm were however investigated since it is feasible that the variability might be acceptable if the selectivity here is sufficiently high. The t range is a direct compromise between finding an appropriate value for on one hand dry development and on the other brush removal; at the same time the etched distances must be large enough for an acceptable S/N. $p = 75$ mTorr is the lowest possible pressure compatible with a 20 sccm gas flow and hence sets the lower boundary of the pressure range.

Tabulated summaries of the raw data fed into MODDE are found in A3.10-16 (the DUV sample data were not fed into MODDE). There is a major flaw in the set-up of this experiment and that is that the samples used in the DOE trial were not DUV exposed blanket samples. It stands to reason that using DUV exposed samples would have been more prudent since i) DUV exposure is part of the wet development process that precedes the RIE brush removal and ii) the dry development might be positively influenced by the induced chain scission and cross-linking of the respective domains. In an attempt to remedy this oversight five runs with DUV exposed samples were made, four of which for comparative purposes were with the same settings as in previous runs. Alas, the effects of DUV exposure on the ERs seem to be more complicated than a simple offset but the situation is complicated by the fact that the DUV exposure appears to cause a direct thickness reduction of the blanket polymer films. This was a fluke discovery made on the samples of the last RIE run. In the four previous runs the polymer thickness was only ascertained after the SC + SB and RIE respectively but for the last an additional ellipsometer measurement was taken after the DUV exposure. The PMMA layer had collapsed by 15.9 nm (7.9%) whereas the height reductions for the R10.5 and PS-OH layers were 2.0 nm (5.08%) and 0.4 nm (0.58%) respectively i.e. the effects are considerable for PMMA, moderate for R10.5 and probably falls below the

noise threshold for PS-OH. This needs to be further verified but since all samples came from the same respective parent wafers and where exposed at the same time the DUV induced height changes where retroactively transposed onto the first four 'DUV runs'.

To return to the DOE trial, MODDE 10.1 is a powerful statistical tool that was used to model the ERs, etched distances and the relevant selectivities based on the variables found to be statistically significant or 'borderline' so. If a variable proved to be on the verge then a model fit with and without it was compared and the best fit (based on Q2) was finally selected. A3.17-22 contains relevant model data such as: i) a summary of the fits (R2, Q2, model validity and reproducibility), ii) the plotted and tabulated coefficients, iii) plots of how well the observations match up with the model predictions and iv) plots of the predicted etched distances.

Ideally all statistical parameters in the *Summary of fit* should be 1 and the reproducibility is not far off. The *reproducibility* indicates the variation of duplicate samples (replicates) compared to the overall variability [46]. R2 is an indicator of the fit of the model while Q2 is an estimate of the future prediction strength of the model and is the best and most sensitive quality indicator [46]. A model is statistically significant if $Q2 \geq 0.1$ but a $Q2 \geq 0.5$ is needed for the model to be considered 'good' [46]. *Model validity* is a test of diverse model problems and a value less than 0.25 indicates statistically significant model problems e.g. presence of outliers, an incorrect model, or a transformation problem [46]. All R2s and Q2s are ≥ 0.684 and ≥ 0.494 respectively indicating quite decent modelling of the etch rate, selectivity etc. Somewhat troubling however is the low *model validity* for a couple of the models (i.e. equations describing the phenomena). The latter might be explained by examining the prediction vs observation plots where ideally all data points should lie on the dashed line. Runs 2 and 12 exhibit the strongest deviation in several of the plots and upon consulting table A3.10 we see that $F_{SF6} = 2$ sccm in these. As mentioned above, the MFCs in the RIE are not reliable at such low flows and this might partly explain the model validity problems. By studying the coefficients the noteworthy conclusion can be drawn that not p nor p^2 or any of its interaction products are statistically significant variables i.e. the pressure (in this range) does not seem to affect the ERs or selectivities on these blanket samples.

The main purpose of this experiment was to identify the optimal RIE settings for dry development and brush removal respectively; this can be broken down into identifying the F_{SF6} corresponding to the highest selectivities and finding an appropriate t. Figure 17 a) and b) are contour plots illustrating the combined t and F_{SF6} dependence of the PMMA:PS-OH and R10.5:PS-OH selectivities respectively. The shading of the lower part of the plots, corresponding to $t < 15$ s, indicates that this is an extrapolation of the model to t outside the actually probed parameter space. Both plots contain a distinct sweet spot and based on these we conclude that $F_{SF6} = 6$ sccm should be used in a dry development process while $F_{SF6} = 7$ sccm is arguably more appropriate for the brush removal. The last statement is based on the observed trend that the maximum contour line for a fixed t seems to converge towards $F_{SF6} = 7$ sccm as t decreases. The t needed for brush removal will be fairly short i.e. well into or even below the extrapolated shaded region. A further advantage with using the higher SF_6 flow is that the ERs seems to be lower making for a more controlled process, see A3.14 (DUV4 and DUV5).

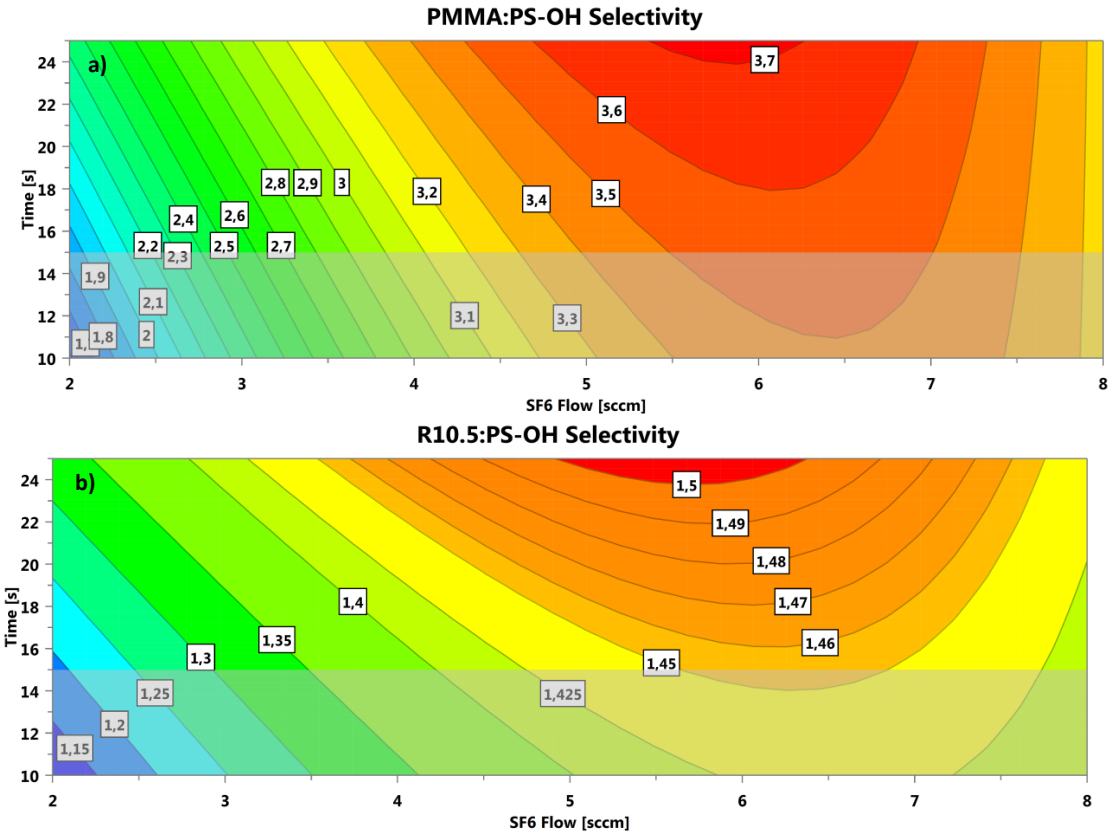

Figure 17: PMMA:PS-OH and R10.5:PS-OH selectivities (relevant to dry development and brush removal respectively) plotted as functions of F_{SF6} and t.

To identify a suitable t now when F_{SF6} has been found, model based predictions of the etched distances as a function of t have been plotted in A3.22. The plotted t-intervall for PMMA and PS-OH is that included in the DOE while it for R10.5 has been expanded with an extrapolation down to $t = 10$ s. The fact that it is an extrapolation is evident from the rapid widening of the 95% confidence interval the further we get from the probed parameter space. As it turns out we need to go to even lower t since using values in the probed t-interval would entail an excessive degree of brush layer etching (ignoring aperture effects). For that additional experiments are needed, the uncertainties accompanied with trying to extrapolate further would just be too great. Therefore some additional runs were performed (see A3.13-14, runs N18, N19, DUV4, DUV5).

Unfortunately, there was no time to try a complete dry development but the brush removal was essential for further processing. However, a natural question surfaces – how much of the brush layer remains at the bottom of the empty cylinders after a wet development? Since the solubility of PMMA in AA is increased by a DUV exposure and the fact that MMA is a large constituent in R10.5 it does not seem particularly farfetched to believe that some of the R10.5 will be removed along with the PMMA during the wet development. To test this hypothesis four old grafted samples (C9-12) from Exp. I (i.e. only covered with a grafted R10.5 layer) were put through the wet development process before re-measuring $h_{R10.5}$. The result is summarized in A3.23 and the positive surprise was that $h_{R10.5}$ was reduced to around 3 nm i.e. approximately halved. However, at this point the aging effects of grafted R10.5 layers started to dawn and to judge the effects of the DUV exposure a control test was performed were three additional samples (C1, 3 and 4) from Exp. I only were subjected to the AA immersion part of the wet development. The resultant $h_{R10.5}$ were slightly higher than for the four previous, DUV exposed, ones despite having a lower initial $h_{R10.5}$, perhaps indicating some effect of the DUV but far from conclusive. Either the AA has a stripping effect or, more likely, it is simply a question of the R10.5 chains releasing from the surface as a consequence of the wash. The working hypothesis thus far is that $h_{R10.5}$ decays as function of age and number of washes, in the sense that the anchoring of the R10.5 chains breaks over time and thus those chains will be lost during a subsequent wash. The forcefulness of the wash itself also seems to affect the layer thickness; it is easier to obtain a higher $h_{R10.5}$ by just using

manual agitation instead of an USB during the post-graft toluene wash. A more forceful agitation simply might be able rip some of the chains lose form the surface but all of these suppositions need further validation. We are now ready to proceed with more relevant samples for the overarching purpose i.e. to grow InAs NWs.

2.6 Experiment V: Pattern Transfer to a PECVD SiN_x Layer

All previous samples used to investigate the various annealing conditions have been directly on 'standard' Si(100) substrates. In the end we want to grow InAs NWs out of the Au filled openings in a SiN_x mask on top of an epitaxially grown InAs(111) layer, which in turn rests on a highly (n+) doped Si(111) substrate. This presents an immediate problem as the pores in the SiN_x mask will be defined by BCP lithography and the brush therefore needs to be able to graft onto a SiN_x surface. If reliable grafting can be achieved on SiN_x then, in theory, the entire process should be transferable and thus applicable to a wide range of substrates. This also means that the pattern transfer calibration can be performed on SiN_x-layers deposited on comparatively inexpensive Si(100) substrates.

The first step was therefore to (IC)PECVD deposit a SiN_x layer on top of five (samples WN1-5) 2" Si(100) wafers. For deposition parameters and subsequent ellipsometer measurements see A4.1-2. The aim was to deposit a *SiN_x layer thickness* (h_{SiNx}) of approx. 10 nm and trying to get as close as possible to the stoichiometric structure Si_3N_4. A measure of the latter is obtained by fitting both h_{SiNx} and the *refractive index* (n_{SiNx}) during the post-deposition ellipsometer measurement and then comparing n_{SiNx} to its stoichiometric counterpart n_{Si3N4}. According to A4.2 all h_{SiNx} overshot the targeted value, mostly so that of WN1 which is closer to 13 nm. A quite large variability is also seen for n_{SiNx} and WN1 once again distinguishes itself with $n_{SiNx} = 2.5076$ (at $\lambda =$ 633 nm) i.e. substantially larger than $n_{Si3N4} = 2.0211$ (at $\lambda =$ 633 nm). One caveat here is the moderate reliability in the ellipsometer measurement of n in such thin films. As mentioned previously, PECVD has issues with poor reproducibility and hydrogen contamination, the former being particularly important for thin layers (as in our case) since the start-up transient, including the plasma ignition, dominates the process.

The grafting conditions were examined by trying to graft R10.5 to an untreated (no surface activation) SiN_x surface (WN1B) and to one (WN1C) previously subjected to a RIE surface activation treatment (30W, 20 sccm O_2, 150 mTorr, 60s). Furthermore, B82 was also spin-coated directly onto similarly untreated (WN1A) and RIE treated (WN1D) SiN_x surfaces with the intention to verify the need of a brush-layer on a SiN_x surface. SEM images of the developed samples, see A4.4, again proved the need for the R10.5 brush but an unexpected windfall was that the RIE surface activation treatment of the SiN_x-layer only marginally improved the ordering compared to the untreated reference. All previous RTP grafting processes have been 10-20 min long but for sake of thoroughness two 1 h grafts were also performed, after a 60 s surface activating PP ash (FC), at 280°C (WN1E) and 250°C (WN1F) respectively, see A4.5. Neither of the samples surpass even the non-surface activated WN1B, in fact both are substantially worse.

Unfortunately, the encouraging grafting results on SiN_x from WN1B,C turned out not to be representative of WN2-4, see A4.6. The next intended step was to perform the complete BCP process on an entire 2" wafer and split it to obtain six identical samples that could be used for calibration of the RIE pattern transfer process, however replicating the success of WN1C proved impossible. WN2 was O_2 RIE treated, prior to R10.5 application, with the same settings as WN1C (but for 20 s longer to compensate for a strong initial spike in the reflected power) but the resultant B82 ordering was markedly worse despite the measured $h_{R10.5}$ being higher. It should be pointed out that the SiN_x layers were ellipsometer measured both before and after surface treatments to verify that they had not been removed by the treatments and to update the ellipsometer models used in later measurements, see A4.3. An interesting observation is that h_{SiNx} is almost unchanged whereas n_{SiNx} drops, perhaps a response to the oxidation of the Si in the surface layer ($n_{SiO2} = 1.4570$ at $\lambda =$ 633 nm [47]).

At this point it was unclear whether to step up or dial down the level of surface activation so both options were evaluated. A more aggressive RIE surface activation (50W, 40 sccm O_2, 150 mTorr, 120 s) was used for sample WN4A while WN3 was subjected to a more gentle ozone treatment (150°C, 10 min). The results indicate that ozone is better than the 'mild' RIE (WN2(E)) which in turn is better than the more aggressive RIE, see A4.6. The reason could be that the RIE has a sputtering component that might affect the structural integrity of the film and by extension the efficacy of the graft. It seemed that gentler was the way to go and therefore an attempt to replicate the success of the untreated WN1B was made with WN4B but severe adhesion problems during the R10.5 SC, despite several tries, prevented that. Sufficient adhesion on WN4B was achieved after the sample was PP ashed for 60 s without FC but the resultant ordering was still remarkably bad. For full disclosure it ought to be mentioned that h_{B82} was several nm thicker than expected for WN4A and WN4B which of course could affect the outcome.

The conclusion is that WN1 stands head and shoulders over WN2-4 when it comes to supporting good ordering in the B82 film. Fact is that WN1 distinguished itself already after the post-PECVD ellipsometer measurement, $n_{SiNx,WN1} = 2.5076$ was substantially higher than for the rest of the samples and could be explained by a greater silicon ($n_{Si} = 3.8771$ at $\lambda = 633$ nm [48]) content. The exact influence of the Si content needs to be investigated further but based on the limited experiments above it does not seem particularly farfetched to believe that Si-rich SiN_x-films could be an advantageous avenue of investigation. The reason why the Piranha treatment never was tested is the strong suspicion (later confirmed) that it effectively will etch an epitaxial InAs layer and thus not be compatible with the intended type of samples. Longer PP Ash (FC) treatments should however have been investigated.

In order to increase the success rate and reproducibility of the graft, a slightly more advanced two-layer stack of dielectrics, composed of a PECVD SiN_x (bottom) and an ALD SiO_2 (top) layer, see Figure 2, was deposited on wafers WN5 and WHD1; deposition parameters and ellipsometer data are found in A4.7-8. The hypothesis was that it would be easier to get a higher density of –OH groups on the SiO_2 surface then on that of SiN_x. The *SiO_2 layer thickness* (h_{SiO2}) was only on the order of 15-17Å and it is desirable to keep it as low as possible since it adds to the distance that needs to be dry etched through with limited selectivity. The substrate of WHD1 was a highly n-doped 2" Si(111) wafer and the intension was to use WN5 for pattern transfer calibration and subsequently WHD1 for calibration of the electrodeposition process. The means of surface activation was Piranha (just to maximize B82 pattern quality and hence minimize calibration uncertainties) and the grafting was actually performed twice (the first brush layer was removed by ashing prior to the second Piranha) due to a suspected contamination of two polymer solutions. The ordering on WN5, see A4.9, is far better than that achieved on WN2-4 despite the refractive index of the SiN_x being in the same range - granted Piranha was never used on those samples. A whitish discoloration appeared on WHD1 during the RTP anneal; the reason is not clear but the level of discoloration has a strong correlation to the final ordering, see A4.9, where a stronger whitish hue is affiliated with more disorder. WN5 turned out good enough to proceed with the RIE pattern transfer calibration.

The transfer of the self-assembled B82 pattern into the dielectric stack consists of two separate RIE steps: First the brush layer at the bottom of the cylinders, in the PS mask, must be removed (after the wet development) to expose the SiO_2/SiN_x stack (step 1) which then needs to be etched through to reach the surface of the substrate (step 2). In both steps a high selectivity (towards PS) and anisotropy is desired to avoid a simultaneous enlargement of d_{cyl} during the process. The SF_6/O_2 chemistry with the best RIE settings (30W, 7 sccm SF_6, 75 mTorr) identified previously was used in step 1, while a borrowed SiN_x RIE recipe (75W, 5 sccm CF_4 + 5 sccm CHF_3, 75 mTorr) was used in the second step. The SiN_x etch rate of PECVD SiN_x (deposited with the same machine) in the CF_4/CHF_3 RIE process is 100.3 nm/min on blanket samples [49]. Step 1 should be optimized to be as short as possible, while still removing all of the brush, since the presence of oxygen in the recipe makes it quite harsh on the PS mask. Some degree of over-etching in step 2 is probably beneficial to ensure break-through and exposure of the substrate. If higher control of the deposited h_{SiNx} could be achieved then the area of the exposed substrate might be tailored by the duration of step 2; such tunability might enable another degree of freedom in the formation of the Au particles during the electrodeposition and ultimately be used to counteract the loss of resolution that the pattern transfer otherwise might entail.

A simple 2x2 'High-Low' test-matrix was implemented where the duration of each of the steps can be either 'long' or 'short', where 'long' and 'short' correspond to the time necessary to blanket etch ≈200% and ≈150% of the nominal layer thickness (either h_{SiNx} or $h_{R10.5}$) respectively. h_{SiNx} is known from previous ellipsometer measurements but as we have seen the remaining $h_{R10.5}$ is probably not the as high as the original thickness measured directly after the R10.5 post-graft wash. Based on earlier tests, see A3.23, the nominal $h_{R10.5}$ was chosen to be 3.5 nm which arguably could be considered too low since those tests were conducted on old samples i.e. months had elapsed between the graft + R10.5 wash and the execution of the experiment. The addition of either 50% or 100% to what would be needed for blanket samples was to compensate for the influence of surface topology. The last step (step 3) of the experiment was to remove the remaining polymer mask by ashing the samples in the Plasma Preen for 2x60s without the FC. The samples were inspected in the SEM after B82 development (step 0) and after each transfer step, see A4.9-12.

The first thing that strikes you upon comparing the pattern of the polymer film with that transferred to the SiN_x is that the latter only contains vertical cylinders i.e. the defects are not transferred which is

nothing short of great, see Figure 18. If they had been, the yield during the following electrodeposition and ultimately the MOVPE might have been jeopardized. The diagram in Figure 19 summarizes the effect of each etch step on d_{cyl}, note that the measurements are taken of the polymer mask after steps 0, 1 and 2 while they are of the SiN_x mask after step 3. Included in this diagram are also some measurements taken post-electrodeposition, see A4.13, on the later BL9777_01 sample series. The data in Figure 19 was obtained from the manual SEM measurements seen in A.9-13, and as such has issues with limited sample sizes, image quality, subjectivity and selection bias. A more automated sampling over larger areas would have been more reliable for comparative purposes. Most troubling is the large spread in data which most likely stems from image quality, the manual nature of the measurement and the fact that the original polymer pattern was not perfect to begin with. By image quality we refer to, for example, level of focus, contrast settings and potential presence of astigmatism – all of which will affect the perceived cylinder boundary. At this point the SiN_x films were still imaged with the same SEM settings as for the polymers i.e. low V_{acc} and WD and not the higher voltages that later proved superior for this type of sample.

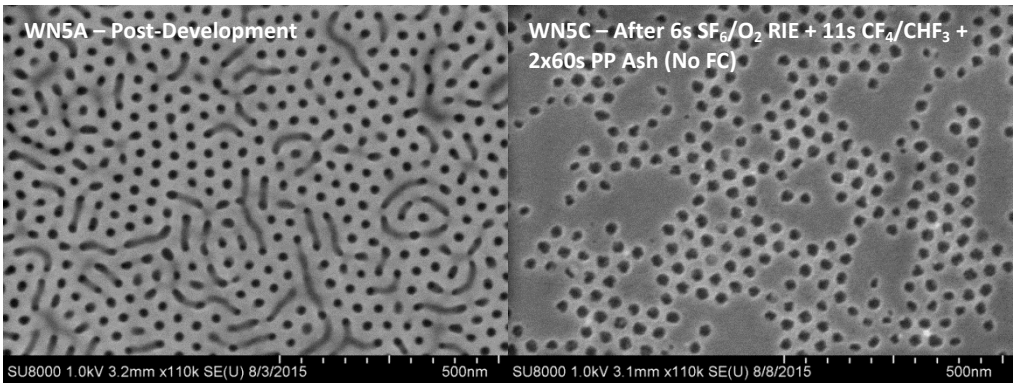

Figure 18: Pattern in developed B82 film (left) as well as the pattern transferred into the SiN_x.

Most notable is the clear d_{cyl} increase (+≈7 nm) during the SF_6/O_2 step, see Figure 19. However, the PS mask seems fairly stable in the CF_4/CHF_3 RIE and only a minor additional increase is observable, see Figure 19, which means that we can over-etch the SiN_x layer without having to fear a steep loss of resolution. Not surprisingly, a longer etch step (in steps 1 and 2) seems to lead of a larger increase of d_{cyl} but in the end what matters is the cylinder diameter in the SiN_x film. Interestingly, $d_{cyl,SiNx}$ seems to adopt approximately the same value as $d_{cyl,PS}$ when the second etch step is the longer option, while $d_{cyl,SiNx} < d_{cyl,PS}$ appears to be the case when the shorter option is used. This might indicate that the brush removal step is not sufficiently long to effectuate a complete breakthrough to the underlying SiO_2, and that the first part of the second step is spent just removing the last of the R10.5. What we are measuring here is the diameter at the top surface, but more important is the diameter of the area (if any) of exposed substrate at the bottom of the cylinders in the SiN_x layer. To find this the film cross-section needs to be imaged in the SEM, unfortunately imaging such a thin (≈10 nm) dielectric layer proved very challenging and ultimately failed despite strenuous efforts. The conclusion at the time was that the only practical way of evaluating the completion of the pattern transfer is to attempt electrodeposition and inspect if, where and how much Au was deposited. For this a highly doped substrate is needed something the WN5 daughters did not have. However, with more appropriate SEM settings (and a more conductive substrate) it is most likely possible to gauge whether SiN_x breakthrough has occurred from the contrast in a top-view image.

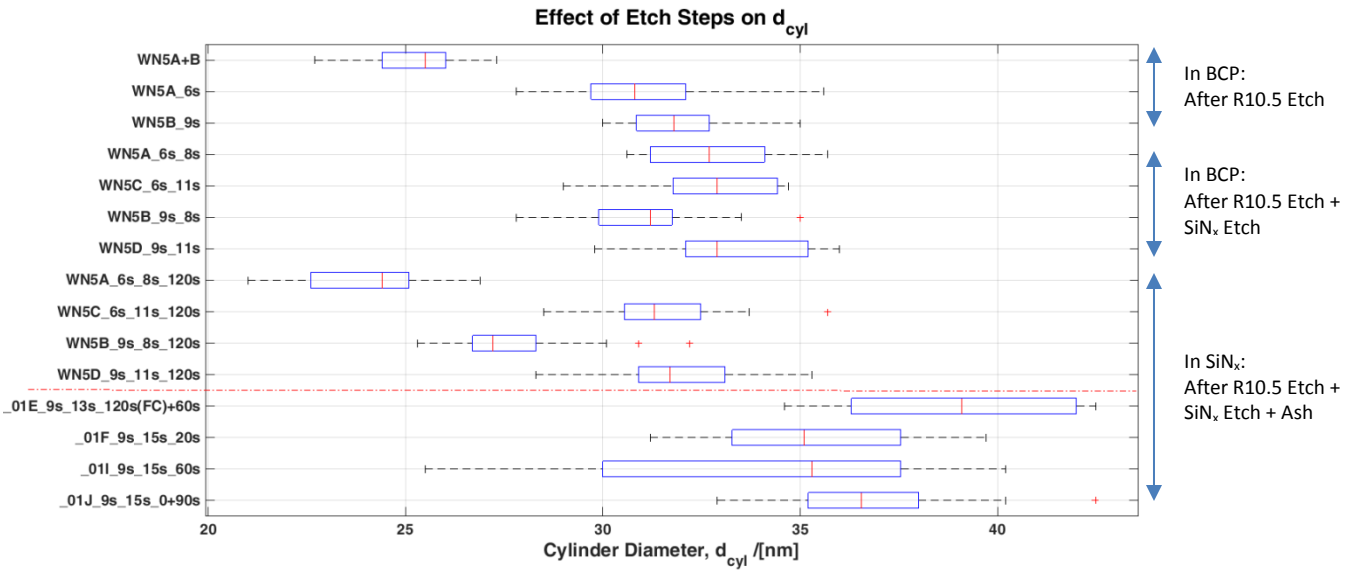

Figure 19: The effect of the RIE steps on cylinder diameter at the top surface. Data below the dashed red line in the diagram is from BL9777_01 samples taken post-electrodeposition, see A4.13. Nomenclature: sample_R10.5 Etch time_SiN_x etch time_ PP ash time. Whiskers $\pm 2.7\sigma$; box: 25, 50 and 75 percentiles; red crosses: outliers. The cylinder diameter is measured on the top surface of the remaining PS matrix after the brush removal and the SiN_x etch respectively. After the ashing the measured diameter is that of the openings (at the top surface) in the SiN_x-layer.

2.7 Experiment VI: Lithographic Method Applied to an InAs/Si(111) Substrate

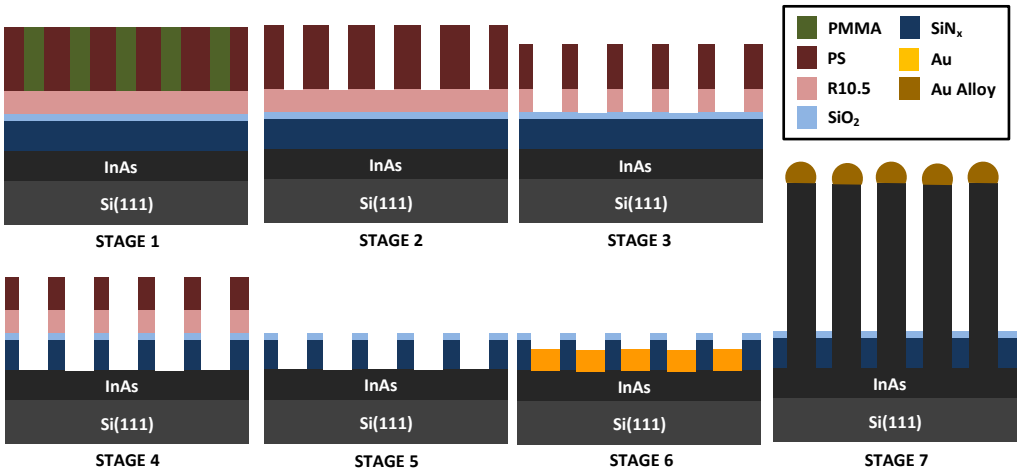

STAGE 1
0) Substrate: S1813/InAs/Si(111); S1813 = Protective Pol. Layer
1) S1813 Removal: Acetone (60°C) + Acetone USB + IPA USB
2) InAs + InAs Oxide Ellips. (264 nm InAs + 2.2 nm InAs Oxide)
3) SiN_x (IC)PECVD + Ellips. (8.5-10.3 nm)
4) SiO_2 ALD + Ellips. (17 Å)
5) Implementation of PS Etch mask, see Figure 12

STAGE 2
Sample Split + BCP Development (+SEM)

STAGE 3
SF_6/O_2 R10.5 RIE (+ SEM)

STAGE 4
CF_4/CHF_3 SiO_2/SiN_x RIE (+ SEM)

STAGE 5
Plasma Preen O_2 Ash (+ SEM)

STAGE 6
Electrodeposition (+ SEM)

STAGE 7
MOVPE of InAs NWs (+ SEM)

Figure 20: Schematic process flow of the BL9777_01 sample series.

Since the processing of sample WHD1 (the highly doped 2" Si(111) wafer with a SiO_2/SiN_x stack) failed it was decided to proceed with calibrating the electrodeposition process using 'sharp' samples i.e. Si(111) substrates with an epitaxially grown InAs layer on top. As with WN5 and WHD1 a SiN_x and SiO_2 layer was deposited on sample BL9777_01 and BL9777_02 (2x2 cm^2) using PECVD and ALD respectively, see A4.14 for ellipsometer data and Figure 20 for a schematic processing summary. No attempt to remove the native oxide was made prior to the deposition of the dielectrics. An alternative process flow was initiated with sample BL9777_04 (2x2 cm^2) where the dielectric stack was replaced with an equally thick (≈ 10 nm) ALD SiO_2 layer. The idea was to forgo with the unstable PECVD deposition and only use the highly controllable ALD process for more reproducible results but unlike with SiN_x it is questionable if SiO_2 mask is fully compatible with the MOVPE process. Thus such an oxide might have to be removed with e.g. HF after it served its purpose as an insulating layer during the electrodeposition. The principle drawbacks would be that i) some III-V growth would occur on the unmasked substrate and not just below the Au particles and ii) unrestrained by the SiN_x mask the seed particles might be more prone to conglomerate and move around on the substrate during both the pre-growth anneal and the growth proper. However, this avenue of investigation was never taken to its conclusion and will thus not be detailed further.

The Piranha treatment was tested (despite earlier raised objections) as the means of surface activation to test if the conformal SiO_2/SiN_x would shield the InAs layer from the acidic solution. The treatment had to be interrupted within minutes due to extensive sample damage to BL9777_02 which meant that no further processing of this sample was undertaken. BL9777_01 on the other hand was more or less unaffected, something verified by countless ellipsometer measurements all over the sample surface. A 3x60s PP ash with the FC was used instead and the sample was annealed at $T_a = 250$°C for $t_a = 1$ h. The sample was scribed and split into thirteen daughter samples, one 10x10 mm^2 (_01A) and twelve 5x5 mm^2 (_01D-O), prior to a wet development. For some reason the graft process was only moderately successful resulting in a far from perfect ordering in the B82 layer, see A4.15. Fortunately, the pattern

contained a sufficient number of vertical cylinders, for a proof-of-principle, to proceed with further processing.

We wanted some degree of over-etching in the subsequent pattern transfer to ensure that the substrate was exposed at the bottom; optimizing the process will be a later step. An exposed conductive substrate is crucial for the success of the electrodeposition and with this in mind the duration of the brush removal step was set to 9s while the SiN_x etch was $\geq$ 11s; for sample specific details see Table 3 or A5.2 where the particulars of the following PP ashing and electrodeposition also are listed, together with the resultant SEM images. From SEM inspections is appears that after a 15 s SiN_x etch the substrate is clearly 'visible' and, as expected, the exposed substrate area is smaller than a cylinder cross-section taken at the surface. 15 s was therefore deemed appropriate and was used for most samples but both higher and lower values were also tested. A thin SiN_x meniscus can be observed around the exposed substrate.

2.8 Experiment VII: Electrodeposition (and initial lift-off test)

2.8.1 Electrodeposition of Au

As elaborated on previously, the purpose of the ashing here (unlike with WN5x) was not really to remove the remaining polymer mask but to remove deposits of fluorocarbon polymer by-products formed during the RIE steps that might otherwise form an insulating layer on the substrate. In fact keeping the PS polymer mask could be beneficial since the physical barrier between cylinders would be larger and there would less risk of agglomeration of individual Au particles during the deposition. Theoretically the ashing could also have a negative aspect, it could induce crystal damage in the exposed substrate and more importantly cause the formation of an insulating oxide that would interfere with the electrodeposition, i.e. finding the appropriate degree of ashing was a question of identifying the golden middle ground. The attempt to find this is the reason why the ashing procedure varied from sample to sample. The backside of all samples, except the first, were also etched to ensure a good electrical connection between the substrate and the printed circuit board (via the conductive tape). During the R10.5 spin-coating some of the polymer will get on the backside and then be anchored in place during the subsequent graft and if not removed will increase the contact resistance.

A major unforeseen issue that needs to be addressed is that the physical integrity of the SiO_2/SiN_x layer became compromised during the electrodeposition and the layer was either partially or completely stripped from some parts of the sample, see A5.1. This is troubling because Au deposition will occur here as well and these regions will act as Au sinks reducing the processing yield by rendering these parts of the sample unusable but more importantly might also jeopardize the outcome in originally unaffected areas. The amount of metal deposited depends on the current level and time, an increase in either or both will lead to more metal being deposited. Essentially, a certain amount of charge corresponds to a specific amount of metal (resistive losses aside) and if Au sinks are present that means that less is deposited in the cylinders for a set time and current. Time and current are otherwise calculated based on the desired size of the Au particles and the surface density of cylinders, the total exposed substrate area in actuality. In these research settings we have the opportunity to compensate for the Au sinks by an iterative process of inspection and repetition but the stability problem of the SiN_x needs to be worked out before an industrial upscaling of the process flow. The Au sinks introduce both a hindrance to reproducibility and a higher consumption of Au, the latter of which is synonymous with higher processing costs. As of yet it is still uncertain what causes the failure of the film but the silicon-poor stoichiometry ($n_{SiNx,\_01} = 1.5644$, MSE = 10.05) is likely a contributing factor. The cyanide should not etch the SiN_x substantially but it is possible that it could interject itself between the film and the substrate and thus reduce adhesion to the point where the film locally releases from the surface.

Comparing samples _01D and _01E post-electrodeposition is quite interesting, see A5.2 (or Figure 21 for a cursory overview); _01E has been etched longer (13s vs 11s) but has received a shorter equivalent ash. Individual sample processing is summarized in Table 3. Ashing without the FC is far more aggressive, due to the presence of the sputtering component, with a PMMA ER that is approximately four times higher than with the FC. Varying amounts of Au have been deposited in almost all of the cylinders on _01D while only small amounts are found in a few of the cylinders on _01E. The longer etch time can lead to more fluorocarbon residues and that in combination with a shorter equivalent ash seems to be detrimental. Noteworthy is the variation in deposited metal from cylinder to cylinder on _01D, this is most likely related to the number of nucleation sites per cylinder. As the name suggests, nucleation sites are areas where the deposition initiates and where further deposition mainly occurs. A higher density of nucleation sites will result in a more evenly distributed Au deposit within and among the cylinders. The suspected limited number of sites on _01D can probably be put down to an insufficient SiN_x etch; the SiN_x meniscus at the bottom is quite large even after the longer 13s etch of _01E.

For _01F the SiN_x etch was stepped up yet again (to 15 s) but the ash was only 20s (No FC) and it is a clear improvement over the previous two samples. Now practically all cylinders contain Au but the location of the cylinders on the sample surface seems to play in, with almost filled cylinders in the center and a more sparse deposition along the cylinder periphery closer to the sample edges. It is unclear whether this location dependence stems from the electrodeposition or the RIE etching. In the RIE the electrical field at the sample edge can differ from that in the center, which of course could affect the ER somewhat. During electrodeposition all metal areas of the printed circuit board not covered by the sample needs to be masked and it is feasible that some of the masking tape partially might have covered the sample edges, affecting the access of the electrolyte species. Notable is that the Au in the

cylinders does not form a single coherent mass but rather is divided up into smaller globules indicating the still limited number of nucleation sites. Judging from the images, taken near the edges of the sample, nucleation seems to have occurred primarily along the border of the SiN_x meniscus and this might be related to a *microtrenching effect* during the RIE and ash. During such plasma processes a negative charge build-up can occur on the cylinder sidewalls in the insulating SiN_x layer and since the plasma has a net positive charge the reactive species are attracted, and hence deviated in their paths, towards the sidewalls. The result is that a higher number of reactive ions hit around the bottom edges of the cylinders thus locally increasing the ER there [50]. An alternative explanation to the *microtrenching effect* is that ions incident at gracing angles (>80°) with respect to the sidewalls bounce off these which thus essentially have a focusing effect on the incoming ion flux towards the base of the sidewall [50]. The presence of the SiN_x meniscus perhaps suggests that this is more of an issue during the ashing and that the elimination of fluorocarbon contamination at the bottom is more effective towards the sidewalls.

Sample _01G was ashed identically to _01F but both the SiN_x etch and current was boosted to 17 s and 450 mA respectively. The electrodeposition was performed twice due to current fluctuations during, and small Au deposits after, the first try but after the second the cylinders were well filled. The amount of Au varies among the cylinders and for some a 'mushrooming' effect is visible i.e. the diameter of the particle quickly grows when it has reached a height were it is no longer constrained by the SiN_x sidewalls. Due to the high pattern density, once mushrooming occurs it is not long before the particles become large enough to coalesce into superstructures not suited for growth of NWs.

The results of both _01I and _01J are a bit perplexing, both were etched the same as _01F but were ashed three (60 s) and four and a half (90s) times longer respectively and on top of that a higher current was used. Based on all this we expected more Au to be deposited but what we find is instead less Au despite performing two consecutive depositions. The lack of Au on _01J after the first run could be excused by the fact that no ashing was performed, this to verify the supposition that fluorocarbons were a real and not just hypothetical concern. At this point one might argue that the culprit could be an insulating oxide due to the prolonged ashing but that would be at odds with the results of _01D, _01K and _01L, all ashed 2x60 s (No FC) and where the last two belong to the best three samples generated. It is conceivable that the rinsing and SEM inspection in-between two runs might contaminate the surface in some way that negatively affects the second run but it seems a bit farfetched.

As mentioned, the best samples (_01K and _01G), with regards to deposition amount and distribution, were obtained using a 2 x 60 s ash (No FC) and it seems that this is a suitable level and that oxide generation is less of a problem than fluorocarbon contamination and hence the emphasis should be on removing the latter; the optimal balance between the two will likely vary with the choice of epitaxial III-V layer. Furthermore, the exact effects of the ashing need to be ascertained, from the previous investigation of various surface activation treatments it seemed that ashing only marginally affected the SiO_x thickness and even a possible net reduction was hinted at. It is also feasible that a steady state thickness, of sorts, can be reached where the oxidation of deeper lying III-V semiconductor is counteracted by a continual removal at the top surface by the sputtering action. Sample _01L was etched and ashed identical to _01K but the electrodeposition was performed twice due to low current levels during the first run. Here the mushrooming effect is even more pronounced than on sample _01G.

	Etching and Ashing			Electrodeposition	
Sample	$t_{SF6/O2}$ **/[s]**	$t_{CF4/CHF3}$ **/[s]**	t_{O2Ash} **/[s]**	$I_{dep.}$ **/[mA]**	$t_{dep.}$ **/[s]**
BL9777_01D	9	11	120	350	10
BL9777_01E	9	13	120(FC)+60	350	10
BL9777_01F	9	15	20	350	10
BL9777_01G	9	17	20	450	10+10
BL9777_01I	9	15	60	1^{st}:450+2^{nd}:240	1^{st}:10+2^{nd}:10
BL9777_01J	9	15	1^{st}:0+2^{nd}:90	450	1^{st}:10+2^{nd}:10
BL9777_01K	9	15	120	450	10
BL9777_01L	9	15	120	<450	10+5

Table 3: Summary of etch, ash and electrodeposition parameters of individual samples.

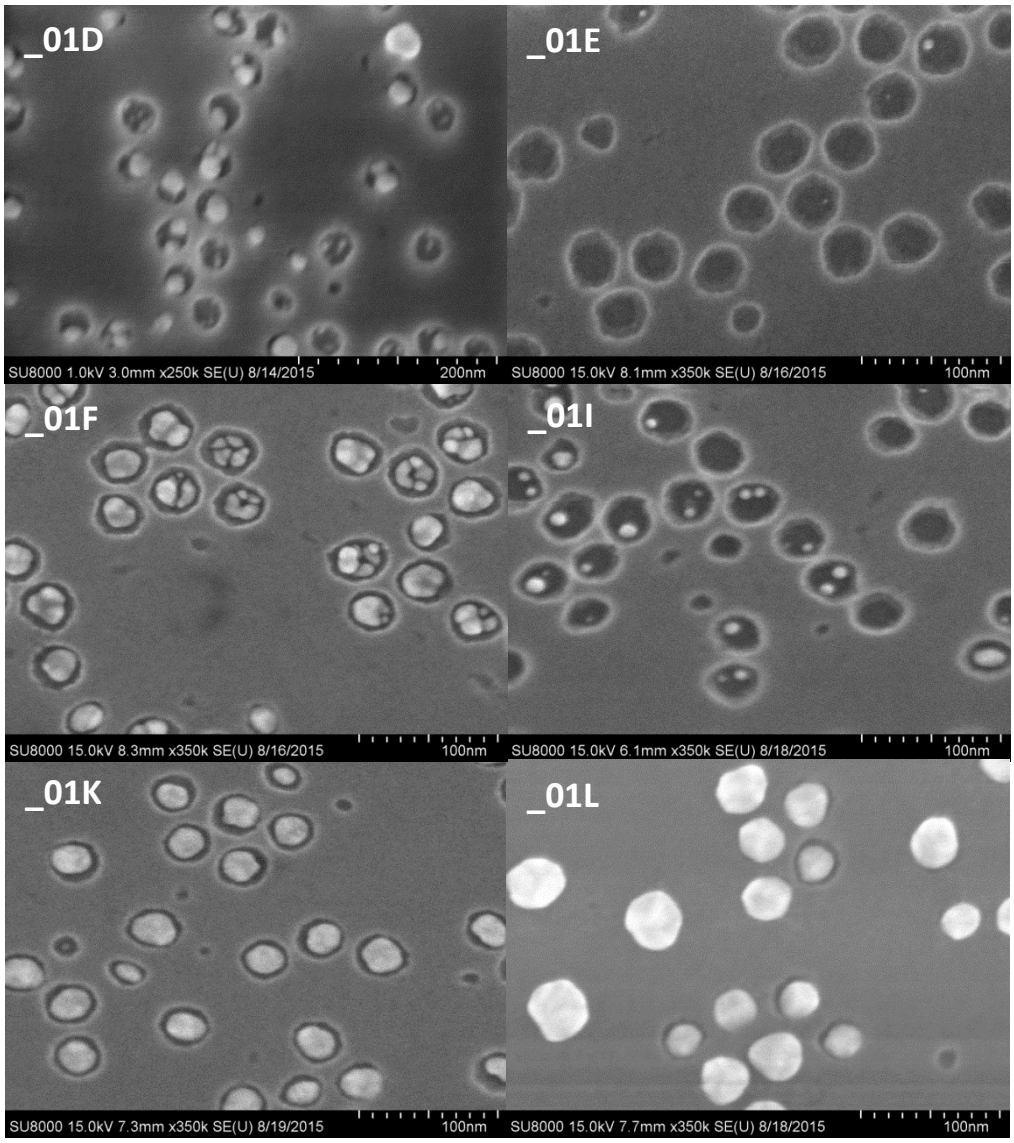

Figure 21: SEM images of selected samples post-electrodeposition. NB: Different scale for _01D.

2.8.2 Initial test of thermal evaporation + lift-off

Two initial tests of implementing a lift-off procedure was performed on regular Si substrates with a grafted R10.5 layer and a RTP annealed B67 film ($h_{B67} = 73.0$ nm $\approx L_{0,B67}$). The samples were RIE etched (30W, 7 sccm SF_6 + 13 sccm O_2, 75 mTorr, 9s) post-development to remove the brush layer and approximately 7 nm Au was thermally evaporated onto the samples using a Pfeiffer Classic 500 evaporator. The fist lift-off attempt was made using heated (90°C) Remover-1165 but the Au layer did not release from the sample surface despite prolonged immersion and manual agitation. The result of the second attempt using immersion in heated (80°C) Piranha solution was markedly different, the Au peeled off within seconds of the sample being exposed to the acidic solution but the sample was still left in the solution for a full 10 min. No additional agitation e.g. USB had to be used but as alluded to previously the Piranha solution is not compatible with InAs containing samples although the technique might be useful in various DSA applications. For InAs samples an alternative lift-off chemistry has to be identified.

The results of the attempted Piranha lift-off is illustrated in Figure 22 but although the top Au layer peeled off successfully only sparse irregular Au deposits were left on the substrate. The most probable explanation is that the same R10.5 RIE treatment was used as for samples with a thinner B82 film i.e. the brush removal was more suited for cylinders with a larger aperture and lower h_{BCP}: d_{cyl} aspect ratio.

Essentially, the working hypothesis is that not all of the R10.5 was removed at the bottom of the cylinders prior to Au deposition and when the sample was exposed to the Piranha solution the R10.5 beneath the Au particle was dissolved as well causing even the desired Au particles to release from the surface. An alternative explanation is that the evaporated Au layer formed a more or less continuous film due to the lack of a proper lift-off layer (and hence undercut) i.e. the desired Au particles on the substrate were fully connected to the top Au layer and were essentially 'ripped off' during the procedure.

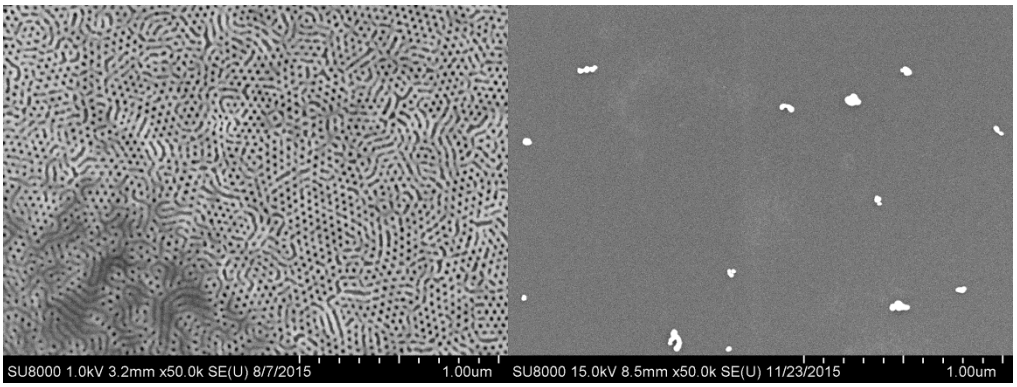

Figure 22: Sample W50C after B67 development (left) and thermal Au evaporation + Piranha lift-off (right).

2.9 Experiment VIII: MOVPE Growth of III-V NWs

All steps recounted thus far have in one way or another been leading up to this attempt at growing InAs NWs using the Axitron 200/4 MOVPE set-up and selected samples from the BL9777_01 series. We managed two runs with three samples in each - two BCP defined samples and one EBL defined *growth test* (GT) sample. One 'good' sample with completely Au filled cylinders and one 'bad' with only small scattered deposits were chosen to be included in each MOVPE run for comparative purposes; _01K, _01I and GT_10551 were included in the first run (#10551) while _01L, _01J and GT_10552 were used in the second (#10552). The MOVPE process can be subdivided into a pre-growth Au anneal and the subsequent growth of InAs NWs. The time and temperature for the Au anneals differed between the two runs while the settings for the growth step were kept identical. The essential processing parameters are listed below:

Step 1: Au Anneal
Run #10551: 5 min at 420°C in AsH_3
Run #10552: 10 min at 550°C in AsH_3

Step 2: InAs growth
Preformed at 420°C for 600 s. Later cooled in an AsH_3 atmosphere.

Process gas	**Flow /[sccm]**	**Equivalent Molar Fraction**
Tri-methyl indium (TMIn)	20	2.79E-06
Arsine (AsH_3)	2.5	1.92E-04
V/III Molar Ratio		69

In the post-electrodeposition SEM images we observed that the Au in a cylinder generally originated from multiple nucleation sites which later coalesced as these seeds grew into each other. The annealing step is meant to allow the Au particles to form a cohesive mass and adopt a more spherical geometry. The precursor process gases were tri-methyl-indium (TMIn) and arsine (AsH_3) and an equivalent V/III molar ratio of 69 was used.

Unfortunately, the sample variability imposed during the electrodeposition propagated into the MOVPE process and all samples contain a medley of defects but also plenty of NWs of various dimensions, see *Appendix 6* (A6) for a collection of SEM images from each sample and Figure 23 for a cursory summary. All overview pictures evidence problems with homogeneity over the sample area which likely originates in the SiN_x damage induced during the electrodeposition. The relative brightness between areas can in general be attributed to the local density of grown InAs features on the surface, where lighter areas are affiliated with a higher yield of NWs. However, this does not hold true for all areas and it is likely that the thickness of the remaining SiN_x layer also affect the perceived brightness. Areas with no, or only a thin, insulating layer will appear darker due to the conductivity of the InAs/Si(111) substrate.

Upon doing a cursory overview of all of the results you find that the samples with Au filled cylinders, which after the electrodeposition were considered the prime candidates with the highest probability of success, actually fared the worst. In practically all categories of characterization such as: yield of initiated seeds, density of NWs and number of defects the samples with sparse Au deposits (_01I and _01J) outperform the, up to this point, reigning favourites (_01K and _01L).

Notable when studying sample _01K is the large number of non-germinated Au seeds and the variation in NW height even in neighbouring structures. A substantial number of defects can also be found on the surface and a recurring shape is the steep pyramid oriented at an angle or nearly parallel to the substrate. The shapes of the defects are otherwise erratic with an almost 'flowing' character. Some larger structures can perhaps be explained by agglomeration of adjacent seed particles or structures growing into each other. The NW diameter (d_{NW}) range for this sample was found to be $d_{NW} \in [30.7, 39.7]$ for a small sampling in a region near the sample edge.

_01I, the second sample in the first run, had a comparatively low number of defects which strengthens the hypothesis that several of the defects observed on _01K were caused by pooling of Au and since far less Au was present on the surface of _01I this would be less likely to happen.

As before, areas with different growth patterns can be identified, some without any growths what so ever (despite the presence of seeds) and others densely populated. Particularly interesting is that one area can contain thin tall NWs while the region next to it have shorter but thicker ones. The transition between these areas is not gradual but rather abrupt, more or less form one row of NWs to the next. It seems reasonable that such an abrupt diameter increase stems from the presence of larger Au particles prior to the MOVPE rather than from any mechanism in that process. In which case the cause ought to be found in either the original B82 pattern or in the faltering SiN_x film integrity during the electrodeposition. The degree of SiN_x etching will likely depend on the straightness of the cylinders in the polymer etch mask; if the propagation of the cylinders through the film follows a curve then some of the reactive etch species following a vertical trajectory will be intercepted by the sidewalls before reaching the SiN_x surface. In this scenario the exposed substrate area would be smaller and less Au would be deposited in these cylinders, ultimately birthing thinner NWs. It does not strike us as farfetched to think that the lengthwise orientation of cylinders through the film exhibit at least some short range order i.e. if one cylinder is bent then it seems probable that its immediate neighbours also bend in a similar fashion.

The other explanation involving the stability of SiN_x is perhaps more likely due to the size and uniformity of the distinct areas but no height or contrast step can be distinguished on the substrate at the transition. However, an interesting observation opens up for a third option: all of the thin NWs have a substantially larger diameter at the base that then quickly reduces into the thinner 'steady state' value. The height of this transition is comparable to the height of the thicker NWs, perhaps suggesting that these are merely a pre-stage that eventually would 'sprout' a thinner spire given more time. The measured thin and thick NWs had diameters in the range [13.5, 20.6] nm and [25.8, 36.7] nm respectively.

Looking at GT_10551, present in the same run as _01K and _01I, reveals a lot of defects similar to those found on _01K indicating that the MOVPE conditions might partly be culpable and this was the principle reason to why both temperature and time were increased in the Au annealing step in the second MOVPE run (#10552).

Sample _01L had larger seed particles than _01K, a fair number exhibiting a clear mushroom profile. Even though stray NWs can be identified most nucleated growths have either an amorphous or pyramidal shape where the latter start out with a wide base that gets thinner either stepwise or progressively. Some of the pyramidal features are vertically oriented but most run at an angle or parallel to the substrate. Large areas of the sample are completely barren, with none of the abundant Au seeds nucleating a growth. Due to the larger seeds more pooling of adjacent Au particles is observable and the higher annealing temp might also have been instrumental in this. Three of the SEM images of this sample in A6 illustrate what is believed to be one of the previously mentioned Au sinks. The middle of this 'gash' ought to have had a layer or at least multiple deposits of Au after the electrodeposition and judging from the large growths in this area it would seem that the Au has formed individual droplets that acted as seeds. This might go some way as to explain the large variation in diameter of the germinated structures in the 'gash' but equally interesting is the dense growth bordering the defect and that peters out to the usual sparsity within 10-15 μm. Just speculating as to the cause, it might be that less Au is deposited in the surroundings to an Au sink due to a local depletion of the electrolyte and as we have seen during these MOVPE conditions less Au seems to work better. It is feasible given the dense pattern (small precursor collection area) and MOVPE conditions that the large Au particles simply cannot accumulate enough precursors to reach supersaturation and thus germinate InAs growth. The 'disadvantage-of-large-seeds argument' is however hard to reconcile with the fact that comparatively gigantic structures started to grow within the Au sinks.

Not surprisingly, sample _01J is very reminiscent of _01I with a high yield of NWs. Areas of distinctively different brightness were observed which were labelled 'light', 'dark' and 'black' in order of dwindling brightness. Going from 'light' to 'dark' only seems to be a matter of NW density, where the 'light' areas have a higher value, and even though the same density trend is observable in the 'dark' to 'black' transition a 'colour' change of the substrate is also evident. The presence of defects in the SiN_x film (or alternatively in the InAs epitaxial layer) is likely the causal agent here. In a small sampling, NW diameters ranging from 11.9 to 25.4 nm were found and obtaining the lowest value measurement proved difficult. One interpretation is that the electron bombardment in the SEM is sufficient to cause the NW to vibrate due to its low mass and flexibility.

Growth test GT_10552 does contain some defects but the levels appear to be lower than for the GT included in the first run.

To round up, we managed to grow InAs NWs from arrays of Au seeds, defined by BCP lithography, using MOVPE and thus achieved our overarching goal with the project. In these experiments smaller seed particles led to higher NW yields and fewer 'defect' features on the substrate post-MOVPE. However, even our largest particles are not exceptional, literature abounds with NWs grown using far larger seeds (but with a greater pitch) so there are clearly more factors involved. Most likely the MOVPE growth conditions need to be tailored based on the size and pitch of the Au seeds; perhaps changing any or all of the following parameters might resolve the issue: time, temperature, chamber pressure, absolute flow rates or equivalent V/III ratio.

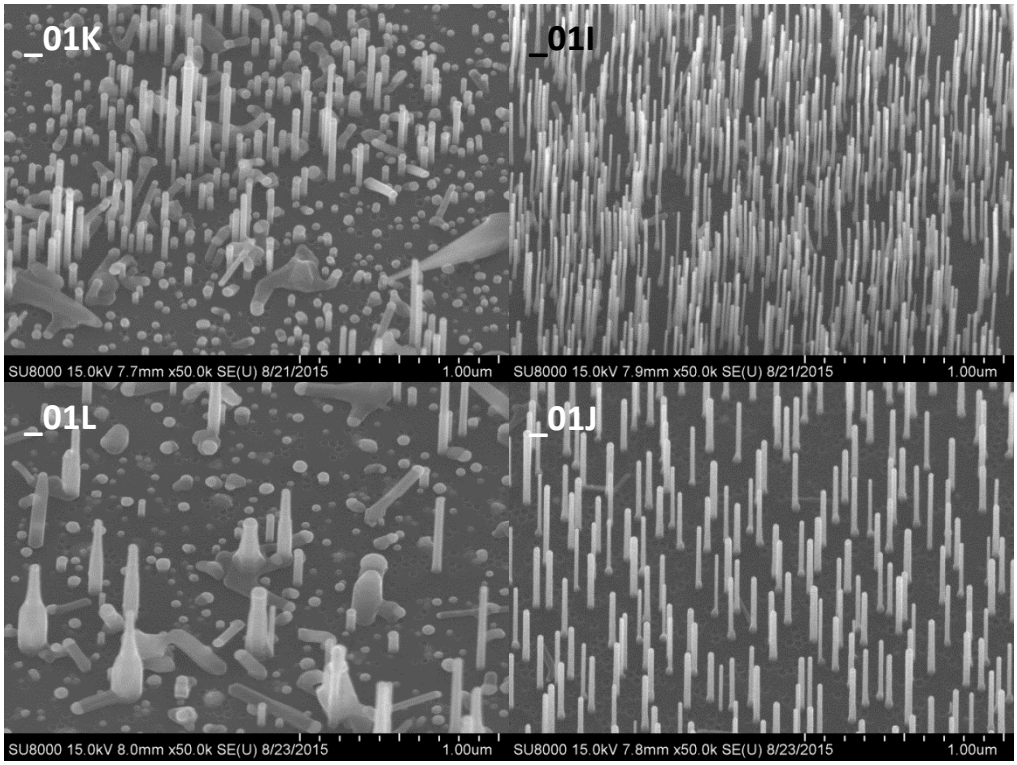

Figure 23: Selected SEM images of the BL9777_01 samples post-MOVPE. NB: Different length scales.

Part III

Project Evaluation and Outlook

3.1 Summation, Discussion and Conclusions

During the course of this project we have developed and proved the viability of a quick and inexpensive process flow, based on BCP lithography, for the production of dense arrays of Au particles over large areas. From there we took it one step further and demonstrated that the Au particles can be used as catalytic seeds in a MOVPE process to grow InAs NWs on a SiN_x masked InAs/Si(111) substrate. This, no doubt, has been a successful proof-of-principle but it is evident that extensive optimization is necessary before any industrial size up-scaling.

One thing that has become evident during this project is the importance of the brush layer on the resulting morphology and orientation of annealed B82 films. For the RCP brush polymer R10.5 used here, $h_{R10.5} \geq 6.6$nm is required to obtain a decent density of vertical cylinders and the ordering moreover seems to improve with increasing brush thickness - at least up to a point. The believed reason being that a thicker brush layer more effectively screen the BCP from the preferentially PMMA wetting Si surface. However, excessively high $h_{R10.5}$ values (>8.3 nm) could result from ungrafted polymer remaining on the surface as a consequence of an inadequate post-graft wash. The use of R10.5 as a brush layer requires grafting, i.e. a condensation reaction between a terminal –OH group in the polymer and another on the substrate surface, that covalently anchors the polymer to the sample. The ellipsometer measured $h_{R10.5}$ is a measure of the density of graft events and polymer conformation (for a given MW). To ensure the success of the grating process the number of –OH groups needs to be increased on the sample surface prior to polymer application and RTP graft, something here referred to as surface activation.

In this project we investigated several means of surface activation and came to the conclusion that heated Piranha solution is the best option for Si samples. This method, unfortunately, is not compatible with InAs containing samples which essentially disqualifies it for future elaborations on this project. Even though the jury is still out regarding the RIE, it would seem that the PP asher with the FC is the next best option and it has the additional benefits of being both faster and safer than the Piranha treatment. The PP asher can only sustain a continuous plasma for 60 s before needing to cool for 5 min and in this project the surface activation treatment consisted of three consecutive runs making the total processing time substantially longer than need be. It is also of interest to be able to remove the sample from the plasma chamber quickly since the effect decays rapidly. An Emitech K1050X asher is available in the NanoLund clean room facility and this might be a good alternative since it has no time constraints and offers higher flexibility with regard to RF power, O_2 and Ar flow and comes with a faraday cage unlike the RIE.

The experience gained during this project suggests that all BCP processing steps, from surface activation to anneal, should be performed as quickly as possible in a back-to-back process flow. The reason being that the R10.5 brush appears to experience aging effects even after the RTP graft and wash - not the polymer in and of itself but rather its anchoring to the substrate. Essentially, this means that an old sample cannot be washed in an organic solvent without losing most of brush layer and if such a sample was to be spin-coated with the BCP some of the R10.5 would be dissolved and intermingle with the B82 perhaps with detrimental consequences for the ordering process.

The RTP was otherwise found to be a fast and convenient way to perform the graft due to the inert atmosphere, high temperatures and the fast heating rates possible. $T_{graft} = 280$°C for $t_{graft} =$ 10-20 min and with a heating rate of 18°C/s was found to be a practical and effective grafting program. If the ellipsometer measured $h_{R10.5}$, post-graft and wash, is ≤ 5.9 nm then further processing is futile because the resultant pattern might not contain any vertical cylinders at all; if this happens the sample can sometimes be ashed and successfully reused but far from always. The capricious nature of the grafting procedure, i.e. the fact that $h_{R10.5}$ can vary wildly from sample to sample and in the end you get what you get is at this stage probably the largest hindrance to the fidelity of our version of BCP lithography.

Based on the findings of [22] it is likely that a P(S-r-MMA) version with a styrene fraction closer to 64 mol-% would be better at creating a neutrally wetting surface but the grafting issue would remain. An alternative approach is to use cross-linkable RCPs that do not need to be grafted to the surface but rather form an insoluble cross-linked mat after e.g. heat or DUV exposure. Given sufficient adhesion for spin-coating this would open up for quicker, more reliable and substrate insensitive surface neutralization. The main drawback would be the difficulty in keeping the thickness down while

maintaining a structurally cohesive layer, the former being important because it needs to be etched through with limited selectivity; even so this will probably prove to be an advantageous avenue of research if adopted.

The total DUV dose (intensity 9.6 mW/cm^2 at $\lambda = 254$ nm) used during the course of BCP development appears to be flexible at least from 0.57 to 2.28 mJ/cm^2 but eventually as the dose is increased further the PS mask will start to break down as well as the PMMA. Higher doses can most likely be used if the intensity is lower.

After extensive thermal annealing experiments in the RTP, regular lab oven, vacuum oven, ovenproof vacuum chamber and even combinations thereof the conclusion is that the RTP outperforms all other options when it comes to both speed and ordering; although it is too early for a definitive call before the new vacuum chamber iteration (v. 2.0) has been tested. The RTP enabled ordering process for B82 seems to be incredible stable with regards to both time and temperature. A large T_a processing window stretching from 210°C to 270°C was identified but care has to be taken to reduce t_a correspondingly when venturing into higher temperatures. It is likely that the temperature window can be broadened if t_a is kept very short which actually would be beneficial from the point of cost effectiveness and might counterintuitively also mean shorter cooling times since the RTP will not have time to reach its equilibrium temperature before the cooling is initiated. The basic pattern emerges very early (for the T_a:s above) but cylinder cross-sectional shape and diameter tends to converge towards an equilibrium value as the process proceeds. Both the vacuum chamber and the vacuum oven at $T_a = 190$°C for $t_a = 2$h and $t_a = 24$h respectively performed comparable with the RTP but these anneals were, at least, between a factor of 2 and 24 longer; their main advantage is the ability to include multiple wafers in a single run. There have been indications that a low level presence of oxygen during the anneal (or cooling) might be related to the formation of lying cylinders on the surface, whereas higher levels (or prolonged exposure at high temp.) can cause direct polymer damage that manifests as large homogeneous masses of PS post-development.

The attempts at SVA using pure solvents at RT and atmospheric pressures were all unmitigated failures; even the best samples, using THF, fell short of the worst RTP annealed sample. Just speculating, the problem might have been the use of single pure solvents that either dissolve both blocks or just have a slight selectivity towards one of them; such a solvent might undermine the immiscibility between blocks - the corner stone of BCP lithography. It might have been better to use a mix of two strongly selective solvents, in a calibrated ratio, each favouring one of the blocks respectively. Using low BP solvents with high vapour pressures means a higher solvent content in the atmosphere above the sample and this might speed up the process; at the same time care has to be taken to limit the duration of the anneal as the B82 film can exhibit de-wetting behaviour by breaking-up – something seen for both THF and acetone.

All attempts at combining the strengths of different annealing techniques, thermal and otherwise, proved less successful than a single RTP anneal. Other attempts at acquiring a higher quality pattern in the B82 film using the RTP, such as chamber pre-conditioning, use of alternative gas flows, Al foil oxygen barriers, graphite carrier wafer, multiple consecutive runs and multi-tiered programs all proved fruitless (although educational).

All comments above relate to the use of the B82 which behaved quite differently from the lower M_n B67 polymer during RTP and VOA. The ordering process in B67 exhibited a lower tolerance for high T_a which perhaps is not surprising considering the naturally higher mobility of a shorter polymer chain and the fact that $N_{B82} > N_{B69}$, $\chi \propto 1/T$ and $N\chi$ ideally should be $\gg$10. However, noteworthy and unexpected was the impact of h_{B67} on the resultant ordering at high T_a. All B67 samples with $h_{B67} \approx L_{0,B67}$ were either completely useless or heavily dominated by lying structures in the probed t_a-T_a window. The $h_{B67} \approx 2L_{0,B67}$ sample series, on the other hand, had a very high density of vertical cylinders but even here a clear trend of pattern degradation with increasing T_a was observed. The pattern degradation can be combated by reducing either t_a or T_a but fortunately reducing t_a seems to be better for ordering than the alternative. All in all it is an interesting observation that the vertical cylinder morphology appears first, later to be replaced by one where the cylinders run parallel to the substrate. It is conceivable that T_a was sufficiently high to induce thermal damage that accumulated with time and negatively could have affected the ordering process. A speculative alternative explanation is that the thermal energy is enough to break the covalent bonds anchoring the R10.5 chains thus no longer

preventing them from diffusing into the BCP layer; even though the contamination of the BCP layer by the R10.5, in and of itself, not might be crucial the loss of the surface neutral wetting might be – yet another reason why a cross-linked brush layer might be the better choice. The B67 RTP T_a-behaviour is observed for the VO as well but displaced in T_a and the transition is perhaps a bit more abrupt.

Wet development was exclusively used for the selective removal of the PMMA cylinders but appropriate settings for a dry RIE development were identified (30W, 6 sccm SF_6 + 14 sccm O_2, 75 mTorr) with a predicted (blanket) selectivity of 3.6-3.7 for a ≈45 nm layer. Unfortunately there was no time to verify the process on an actual sample and it is likely that a patterned sample will handle somewhat differently. The R10.5 etch rate and selectivity towards PS-OH was modelled simultaneously to find the proper settings for brush removal (30W, 7 sccm SF_6 + 14 sccm O_2, 75 mTorr). The SF_6/O_2 RIE DOE was a compromise between the two processes and needs to be complemented by an extension into shorter etch times for R10.5. The behaviour of the R10.5:PS-OH selectivity mirrors that of PMMA:PS-OH but at lower values, which is not that surprising considering the composition of R10.5. Removing the R10.5 at the bottom of the cylinders in the PS mask is necessary before proceeding with transferring the pattern into the underlying SiO_2/SiN_x on sharp samples. This transfer was accomplished with a CF_4/CHF_3 RIE treatment (75W, 5 sccm CF_4 + 5 sccm CHF_3, 75 mTorr) and the combination of a 9s brush removal and a 15s SiN_x etch will expose the substrate for electrodeposition when using the B82 BCP and a ≈10 nm SiO_2/SiN_x stack. The addition of the thin ALD SiO_2 was found to be a necessity for a reliable R10.5 grafting process. The PS etch mask is fairly stable in the SiN_x etch but unfortunately not in the SF_6/O_2 RIE, as evidenced by the enlargement of d_{cyl}. This loss of resolution can probably be alleviated by using an ICP-RIE system capable of lower working pressures and in which the biasing of the bottom plate can be controlled independently from the plasma generation, thus enabling higher anisotropy.

Prior to the electrodeposition of Au the insulating fluorocarbon contamination generated during the pattern transfer needs to be removed and a 2 x 60 s PP ash (no FC) was found to be the best option tested. Our initial worries about generating an interfering insulating oxide on the InAs substrate seem to have been unwarranted. More problematic were issues with the integrity of the SiN_x during the Au electrodeposition, regions exhibiting what appears to be complete and partial removal were observed in the SEM. Large areas of exposed substrate will act as Au sinks lowering the yield, increasing Au consumption and make the entire deposition less predictable. A constant current was used during the deposition but for future references it might be better to use e.g. a square-wave (tophat) signal to avoid local depletion of electrolyte species by allowing for short periods of diffusion between depositions and thus obtain more even deposition rates. Furthermore, it is feasible that a stronger initial spike could be conducive to nucleation.

In the MOVPE, both samples with filled cylinders and sparse Au deposits were used and the NW yield of the latter was substantially higher. The likely reason is agglomeration of neighbouring Au particles and that the growth conditions probably were more suited for the smaller Au seeds given the pattern density. A high density means that each seed will have a smaller collection area of precursor species. The effect of varying the Au anneal remains uncertain due to the sample to sample variability but judging from the GT samples the second option entailing a longer time and higher temperature seems slightly better. [36] found that the level of impurities and the effects of porosity of the electrodeposited particles were below the 1% detection limit (XPS) and insignificant respectively using the same electrodeposition setup (except current source) and Au solution.

By now it must be evident that this project has been a succession of compromises between mapping parameter spaces and just finding a set that works. These are of course not mutually exclusive but in hindsight some of the annealing experiment should perhaps been dropped (some not even included in this report) in favour of deeper studies of later processing steps. That said, the fact that we managed to define an array of Au particles using a block-copolymer and then grew InAs NWs means that we achieved the goal of the project. Besides process optimization, several exciting future lines of investigation have been identified (listed below) with the potential to improve the reliability and expand the scope of BCP lithography.

3.2 Outlook: Future Lines of Investigation

3.2.1 Directed Self-assembly

As the name suggests *directed self-assembly* (DSA) entails creating the proper boundary conditions that will guide the self-assembly process towards a desired pattern/orientation; examples include various forms of lateral confinement and manipulation of surface wetting properties. Confinement involves imposing a specific geometry on the BCP film in which the total free energy of the system for a particular morphology and orientation is substantially lower than the alternatives. This specific configuration will then be thermodynamically favoured and hence more likely to be adopted. It is simultaneously a way of making the free energy costs affiliated with an ordering defect substantially higher. Examples for a cylinder-forming diblock BCP are i) 'trapping' the BCP between sidewalls distanced in such a way that an integer number of cylinders fit snuggly in-between or ii) creating arrays of pillars on the substrate, prior to BCP SC, with a pitch that is close to multiples of the intrinsic BCP interdomain spacing (L_0) - sometimes referred to as density multiplication (and an excellent way of combining BCP lithography with NIL) [4]. Another degree of freedom is obtained by tailoring area-specific brush layers such that e.g. the bottom substrate exhibit neutral wetting while laterally confining sidewalls or pillars selectively 'prefers' to interact with one of the two blocks thus adding more customizable lateral boundary conditions. Some examples of unintentional DSA was obtained during the course of the project due to Si particles, generated during scribing, that ended up on the B82 film, see Figure 24.

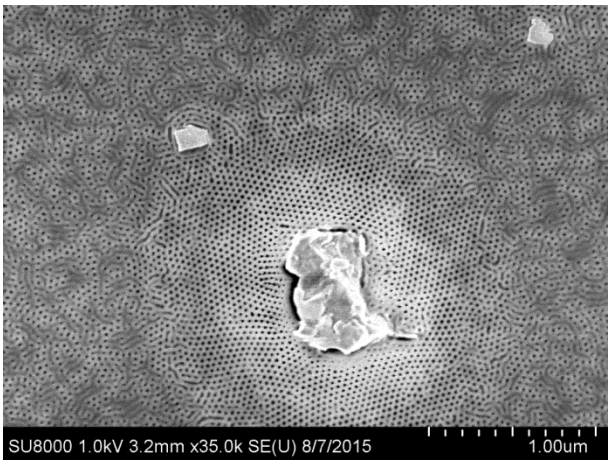

Figure 24: Si particle inducing long range order in B82 film.

The ordering seen in the image periphery is quite mediocre whereas that surrounding the large Si particle is pristine – the only 'defects' are the clearly visible grain boundaries. Interesting to note is that the same effect cannot be observed around the two smaller particles and it is tempting to suggest that i) it is the weight of the larger particle that has introduced a vertical stain or ii) perhaps the particle rests on the substrate and this periodic orientation might be the system 'trying' to maximize the PMMA-Si interaction which is more favoured than the alternative. The PMMA-Si interface might be maximized by having the cylinders run parallel to the exposed Si surface on the sides of the particle. This might go some way as to explain why the smaller particles do not induce the same effect as they simply might rest on top of the film. The PMMA-Si interface would then be maximized by having the cylinders run parallel to the bottom surface of the particle (and hence substrate). An alternative hypothesis is that the particle changes the local heating/cooling profile. It is fortuitous that the effect extends radially for more than 20 periods around the particle, suggesting that the substrate area that needs to be sacrificed for the DSA structures might be acceptable. DSA features could be implemented by e.g. EBL or NIL. Another tantalizing option might be to use a higher M_n BCP to fabricate structures that subsequently can be used to guide the ordering of a lower M_n BCP. DSA is a hot research topic at the moment and clearly a highly interesting future line of investigation.

DSA using physical guiding structures are often referred to as *graphoepitaxy* but guiding can also be achieved by chemical nanopatterning of the substrate and one interesting example of the latter is the take on *molecular transfer printing* (MTP) found in [16]. They found that $\zeta \propto h_{BCP}$ and $\zeta \propto {t_a}^{0.28}$ for samples with h_{BCP} ≈2-11L_0 when annealed at T_a =210, 230°C with ζ >1100 nm for $h_{BCP} \approx 11L_0$. They furthermore proved that it is possible to transfer the surface pattern of thick films containing large

grains to thinner ones by means of MTP. MTP here entails mixing the BCP with graftable PS-OH and PMMA-OH homopolymers that will be incorporated into the PS and PMMA BCP domains during the ordering anneal of the thick film. A new Si substrate is then placed on top of the 'thick film sample', clamped together in a sandwich configuration and annealed again. PS-OH and PMMA-OH in the domains will graft to the new Si substrate and thus create a chemical pattern identical to that of the surface layer of the thick BCP film. The grafted (and washed) new sample is then SC with a thinner layer of the identical polymer blend and annealed, the surface pattern serves to guide the second self-assembly so as to recreate the old pattern in the new thinner BCP film. The reason why the thick film cannot be used for lithographic purposes directly is that there is a decoupling between the interfaces in such thick films; meaning that if the substrate is treated with a neutral brush cylinders can nucleate independently at both interfaces and will not necessarily line up. Actually even if they were to align to create continuous vertical cylinders from top to bottom it is doubtful that they would be sufficiently straight for later lithographic steps such as RIE or a lift-off procedure. One upside with this approach is that a brush layer is no longer necessary for the thick film sample, used in the MTP process, as the morphology at the free surface will be dominated by the influence of that interface which at these temperatures will be neutral.

3.2.2 Supplemental Experiments

It would be interesting to perform some supplemental thermal annealing experiments, specifically: i) explore the high T_a low t_a part of the RTP parameter space and ii) use the new improved and hopefully leak-proof vacuum chamber to once and for all get to the bottom of the effects of oxygen in the atmosphere over the sample during the anneal. Finding SiN_x PECVD settings conducive to higher deposition reproducibility and mechanical stability is essential for the success of later processing steps such as RIE pattern transfer, electrodeposition and MOVPE. Finding an alternative dielectric or deposition technique that is compatible with InAs is another way to go. Performing the graft in the new vacuum chamber would be interesting due to the findings in [3] where oxidative damage to the RCP ($f_{PS} = 0.58$, M_n =11.4 kg/mol, PDI =1.64) generated pattern defects very similar to ours. Their h_{RCP} was only approx. 4 nm but that seems to have been sufficient if the vacuum level was $8x10^{-3}$ mbar or more. A h_{B69} sweep in [3] moreover implies that getting very close to $h_{B69} = L_0$ or $\frac{1}{2}L_0$ might be more important than previously expected; the defects generated for h_{B69} not conforming to commensurability were very reminiscent of ours.

3.2.3 Low M_n hydroxyl terminated P(S-r-MMA) brush layers

According to [18] effective surface neutralization can be achieved when $h_{RCP} \approx 2R_g$, where R_g is the radius of gyration of the RCP chain in a melt. R_g is a direct function of N (and thus M_n) and for M_n =1.7 kg/mol (61 mol-% S) effective grafted brush layers as thin as 2 nm were demonstrated, something that would improve the fidelity of the pattern transfer as the loss in resolution is mitigated. They furthermore identified two regimes: i) above h_{RCP} = 5-6 nm where the brush height, independent of M_n, is sufficient stop the BCP from interacting with the substrate and generate perpendicular cylinders and ii) below h_{RCP} = 5-6 nm where the efficacy of the brush is a function of both h_{RCP} and the *grafting density* (Σ). A high Σ seems to be able to compensate for the lower h_{RCP} and shield the BCP from the underlying SiO_2. A high Σ is more readily obtained for low M_n RCPs.

3.2.4 Improving the physical stability of PECVD SiN_x layer

[6] claims that the physical stability of a PECVD SiN_x layer deposited on (111)B GaAs can be improved by annealing at 600°C under AsH_3 flow with H_2 as carrier gas. This was meant to densify the dielectric mask and relieve thermal expansion-induced stresses in the film that otherwise might cause cracking and/or delamination during a later *selective area MOVPE* (SA-MOVPE) of InAs NWs. Perhaps the same is applicable for our sample stack.

3.2.5 Mixing BCPs of Different MW for Improved Pattern Quality

There is research [51] suggesting that the ordering can be improved by using a mixture of two P(S-b-MMA) BCPs of different M_n rather than, as we have done, using a single BCP. The hypothesized reason is that the smaller BCP improves the mobility of the larger by interjecting itself between the longer chains and thereby acting as a 'lubricant'. If the results can be replicated it would be an effective and basically effortless way of increasing the yield as no extra processing step is necessary. Only the BCP solution preparation would be marginally more complex. It would be interesting to study if any changes to the T_a dependent behavior will occur as we during the course of this project has seen that B67 and B82 handle

very differently. The shorter BCP should be seen as an additive to the longer and the dimensions of the adopted pattern will be closer to the intrinsic values of the higher M_n BCP.

3.2.6 Alternative Au Deposition Techniques

Due to the present problems with reproducibility in the electrodeposition procedure it would be prudent to explore alternative routes of area-selective Au deposition. As mentioned, lift-off is a tried and true method with excellent process control given the right circumstances but it generally requires the incorporation of a lift-off layer below the patterned etch mask. There are several issues that need to be considered before trying to implement such a sample stack: i) the *lift-off resist* (LOR) must have a low solubility in toluene (and/or anisole) i.e. the solvent used for the R10.5 and B82 solutions as it needs to be applied before the SC of these polymers. ii) An e.g. ALD SiO_2 spacing layer needs to be deposited in-between the LOR and the R10.5 to allow the bush polymer something to graft on to and to act as a barrier by preventing the LOR polymer chains to diffuse up into the R10.5 and B82 layers during the annealing step. Grafting directly onto the LOR might be accomplished if this layer was cross-linked but that in turn would render it useless as a lift-off layer. The best alternative would be to use a cross-linkable brush directly on top of the LOR as it would fulfil both the barrier and neutral surface wetting criterions. iii) Perhaps the main problem is that the LOR adds to the layer height that needs to be etched through with a limited dry etch selectivity. Either a different BCP or SIS (see below) might be necessary to achieve the pattern transfer without a severe loss of resolution.

If an alternative sample process flow does not entail a SiN_x layer then an even simpler Au deposition method might be possible. A domain selective Au precursor ($AuCl_4^-$) loading can be realized by a simple immersion of a self-assembled *poly(styrene-block-4-vinylpyridine)* [P(S-b-4VP)] sample in a HCl + $HAuCl_4$ aqueous solution [52]. The precursors will only bind to the protonated pyridinic nitrogen in the P4VP domains and after the BCP film is subjected to an O_2 plasma etch the only thing remaining on the sample surface will be an array of metallic Au where these domains used to be. An analogues technique might be possible, after additional functionalization, with the P(S-b-MMA) material system.

3.2.7 Polymer Solution Additives

i) Homopolymer

Adding small amounts of homopolymers, i.e. pure PMMA or PS, can offer some tunability in domain size and pitch of the BCP pattern [13]. The addition of PS homopolymer has also been found to increase the pattern quality of vertically oriented cylinders in P(S-b-MMA) films [4].

ii) Oleic acid

The addition of *oleic acid* (OA) to the P(S-b-MMA) solution used to spin-cast the BCP film has been demonstrated to be advantageous in obtaining a morphology of perpendicular cylinders (at least at the surface) [28] [27]. Due to its molecular structure, consisting of a polar head and a non-polar tail OA will act as a surfactant where the head preferentially will interact with PMMA and the tail with the PS. During the anneal the OA will rise to the surface of the BCP layer where it will position itself in the interface between domains and act to neutralize the differential surface tension and thus induce perpendicular cylinders originating from the top-surface and propagating down towards the substrate. If OA is used in conjunction with a R10.5 brush layer then perpendicular cylinders will nucleate at both interfaces and hopefully improve the pattern quality. One risk with using OA in thicker polymer layers is probably that the cylinders in the two ordering fronts might not line-up and thus no one cylinder would traverse the whole BCP layer, rendering them useless for our lithographic purposes.

iii) RCP end-linked to perfluorinated groups

RCP end-linked to perfluorinated groups can be used to neutralize the air-polymer interface as the low surface energy of the perfluorinated groups will anchor these to the top-surface and the RCP will thus bee exposed to the underlying BCP layer [4].

3.2.8 ALD Deposited Brush Layers

'Silanes' is a large family of compounds that, in theory, could be used in conjunction with ALD to form monolayer thin brush layers with conformal coverage and tailored surface energies. The general molecular structure of a silane consists of a 'head' that can be grafted to e.g. –OH groups on the substrate surface and a customizable tail that will be exposed to the BCP layer. The differential surface energy can then be minimized by judiciously choosing the chemical composition of the tail. Alternatively

the grafting ratio of two (or more) silanes with different properties could perhaps be varied to change the wetting conditions of the brush layer. This way two types of silanes might be able to act as a brush layer for different BCPs within the same material system e.g. P(S-b-MMA) or perhaps even for multiple material systems by changing the silane ratio. The fact that ALD would be used for the deposit opens for a highly controlled and hopefully reproducible process.

(3-Mercaptopropyl) trimethoxysilane (MPTS) has been found to provide neutral wetting conditions for P(S-b-MMA) as a single component SAM, but somewhat successful binary and multi-component SAMs have also been demonstrated [4].

ALD chlorides could also be used on already patterned samples to 'poison' exposed surfaces and thus prevent III-V growth on these areas during MOVPE.

3.2.9 Sequential Infiltration Synthesis (SIS)

Sequential infiltration synthesis (SIS) is yet another way of using ALD to extend the scope of BCP lithography. SIS is used on samples with an already established pattern and essentially entails growing a hard mask e.g. Al_2O_3 or AlN selectively inside one type of polymer domain. For example, SIS has been utilized on our material system, P(S-b-MMA), to selectively grow Al_2O_3 inside the PMMA domains using *tri-methyl-aluminum* (TMA) and water as precursor gases [53] [54]. The TMA will non-covalently bind to the carbonyl carbon in PMMA and this interaction will prevent those TMA molecules from being removed during the subsequent chamber purge. No corresponding interaction occurs in the PS domains and hence no TMA will remain there post-purge and when water subsequently is introduced into the chamber Al_2O_3 will only nucleate inside the PMMA domains. The precursors permeate the polymer film and the hard mask will grow inside rather than on top of the polymer film. TMA exposure, purge, H_2O exposure and another purge constitute a simple ALD cycle and the size of the Al_2O_3 growth can be tailored by the number of cycles and is not limited to the initial size of the domain. The main advantages with SIS are i) that the method can be used to substantially boost the dry etch selectivity of a BCP and ii) the final hard mask domain size can be varied with great precision meaning that a single BCP can be used to obtain the same pattern but with a range of feature sizes. For our particular BCP with PMMA cylinders the technique is not immediately useful for our purposes but perhaps for a version with the inverse composition i.e. PS cylinders in a matrix of PMMA. A dry development would then have to be used but that ought not to be a problem as the dry etch selectivity would be far higher. SIS can also be applied on other material systems and as elaborated on earlier there are good reasons as to explore other BCP systems.

3.2.10 Dedicated System for SVA

Building (or buying) a dedicated system for SVA enables new degrees of freedom to manipulate e.g. time, temperature, vapour pressure/flow, evaporation rates, chamber pressure before, during and after the anneal. [26] demonstrated that the necessary process time can be reduced from hours or days to mere minutes by first evacuating the chamber prior to the introduction of the solvent. The hypothesis is that the solvent permeates the BCP film faster and more completely when the original atmosphere first has been removed. The experiments accounted in [26] used a sphere-forming version of our P(S-b-MMA) material system but if this technique is applicable on our BCP then SVA would truly be a powerful alternative to the RTP anneal as the SVA would be as quick, if not quicker, and less energy consuming. The downside is of course the storing, handling and disposal of solvents but for our purposes only very small volumes would be needed.

3.2.11 Higher χ Material System

As explained earlier, the *Flory-Huggins interaction parameter* (χ) sets the resolution limit, defined as the smallest cylinder cross-section that can be implemented with that material system, since it allows for smaller N values; furthermore a high-χ material system enables not only greater resolution but also sharper block interfaces. Several of these contain one organic and one inorganic block, e.g. P(S-b-DMS) and P(MMA-b-DMS), which comes with the added benefit of having a higher intrinsic dry etch selectivity. Some BCPs are constructed from blocks with appreciably different e.g. electrical, magnetic and/or optical properties which would open up for new novel applications besides just lithography. These differences can also be harnessed for order induction and DSA etc. The downsides are that these generally not are as easy to work with due to large differences in surface energies and it is highly

questionable if the results obtained here at all are transferable, so in some sense you would have to start from scratch again.

3.2.12 Polymer Functionalization

Instead of completely changing material system the present P(S-b-MMA) BCP might be functionalized with groups with some desired property. Even though such a change is likely to affect the ordering etc. the difference might be modest or just a question of an offset, in which case some of the accumulated data above would still be relevant.

3.2.13 Advanced morphologies

In this project a linear cylinder-forming diblock BCP has been used but just by adding a third block containing a different monomer residue (i.e A-B-C) and varying the relative composition and χ:s (by monomer selection) a wide range of more advanced morphologies can be adopted. This of course entails synthesizing a new BCP. At least a dozen thermodynamically stable [2] more complex morphologies have been identified for a triblock BCP but this is still a fairly unmapped area of research. Furthermore, it is almost certain that the practical implementation of these morphologies would be exceedingly difficult due to long-lived metastable states and a greater deal of control will be needed [2]. Another mentioned alternative is to use the same binary material system but with a different molecular structure; instead of two blocks (i.e. A-B) three blocks (A-B-A) might be used or the linear polymer chain could be replaced by a star-shaped or branched molecular structure.

Part IV
Bibliography

4.1 Bibliography (References)

[1] M. C. Garner, "Lithography for enabling advances in integrated circuit and devices," *Phil. Trans. R. Soc. A,* vol. 370, pp. 4015-4041, 2012.

[2] F. S. Bates and G. H. Fredrickson, "Block Copolymers - Designer Soft Materials," *Physics Today,* pp. 32-38, February 1999.

[3] I. A. Zucchi, E. Poliani and M. Perego, "Microdomain Orientation Dependence on Thickness in Thin Films of Cylinder-forming PS-b-PMMA," *Nanotechnology,* vol. 21, pp. 1-5, 2010.

[4] H. Hu, M. Gopinadhan and C. O. Osuji, "Directed Self-assembly of Block Copolymers: a Tutorial Review of Strategies for Enabling Nanotechnology with Soft Matter," *Soft Matter,* vol. 10, pp. 3867-3889, 2014.

[5] K. A. Dick and P. Caroff, "Metal-seeded Growth of III-V Semiconductor Nanowires: Towards Gold-free Synthesis," *Nanoscale,* vol. 6, pp. 3006-3021, 2014.

[6] Y. Huang, T. W. Kim, S. Xiong and e. al., "InAs Nanowires Grown by Metal-Organic Vapor-Phase Epitaxy (MOVPE) Employing PS/PMMA Diblock Copolymer Nanopatterning," *Nano Letters,* vol. 13, pp. 5979-5984, 2013.

[7] M. W. Matsen and F. S. Bates, "Unifying Weak- and Strong-Segregation Block Copolymer Theories," *Macromolecules,* vol. 29, no. 4, pp. 1091-1098, 1996.

[8] Y. Mai and A. Eisenberg, "Self-assembly of Block Copolymers," *Chem. Soc. Rev.,* vol. 41, pp. 5969-5985, 2012.

[9] C. M. Bates, M. J. Maher, D. W. Janes och e. al., ”Block Copolymer Lithography,” *Macromolecules ,* vol. 47, pp. 2-12, 2014.

[10] W. J. Durand, G. Blachut, M. J. Maher and e. al., "Design of High-Chi Block Copolymers for Lithography," *Polymer Chemistry,* vol. 53, pp. 344-352, 2015.

[11] Y. S. Jung and C. A. Ross, "Well-Ordered Thin-Film Nanopore Arrays Formed Using a Block-Copolymer Template," *small,* vol. 5, no. 14, pp. 1654-1659, 2009.

[12] J. G. Son, K. Gotrik and C. A. Ross, "High-Aspect-Ratio Perpendicular Orientation of PS-b-PDMS Thin Films under Solvent Annealing," *ACS Macro Letters,* vol. 1, pp. 1279-1284, 2012.

[13] J. N. L. Albert and T. H. Epps, "Self-assembly of block copolymer thin films," *materialstoday,* vol. 13, no. 6, pp. 24-33, 2010.

[14] E. Han, K. O. Stuen, Y.-H. La and e. al., "Effect of Composition of Substrate-Modifying Random Copolymers on the Orientation of Symmetric and Asymmetric Diblock Copolymer Domains," *Macromolecules,* vol. 41, pp. 9090-9097, 2008.

[15] Wikipedia, "Surface Energy," [Online]. Available: https://en.wikipedia.org/wiki/Surface_energy. [Accessed 11 10 2015].

[16] S. Ji, C.-C. Liu, W. Liao and e. al., "Domain Orientation and Grain Coarsening in Cylinder-Forming Poly(styrene-b-methyl methacrylate) Films," *Macromolecules,* vol. 44, pp. 4291-4300, 2011.

[17] F. Ferrarese Lupi, T. J. Giammaria, S. M. Ceresoli and e. al., "Flash grafting of functional random copolymers for surface neutralization," *J. Mater. Chem. C ,* vol. 2, pp. 4909-4917, 2014.

[18] K. Sparnacci, D. Antonioli, V. Gianotti and e. al., "Ultrathin Random Copolymer-Grafted Layers for Block Copolymer Self-Assembly," *ACS Applied Materials & Interfaces,* vol. 7, pp. 10944-10951, 2015.

[19] F. Ferrarese Lupi, G. T. J, G. Seguini and e. al., "Fine Tuning of Lithographic Masks through Thin Films of PS-b-PMMA with Different Molar Mass by Rapid Thermal Processing," *ACS Applied Materials & Interfaces,* vol. 6, pp. 7180-7188, 2014.

[20] F. Ferrarese Lupi, Interviewee, *E-mail correspondance.* [Interview]. 30 Janurary 2015.

[21] E. Kim, W. Kim, K. Hee Lee and e. al., "A Top Coat with Solvent Annealing Enables Perpendicular Orientation of Sub-10 nm Microdomains in Si-Containing Block Copolymer Thin Films," *Adv. Funct. Mater. ,* vol. 24, pp. 6981-6988, 2014.

[22] D. Yeol Ryu, S. Ham, E. Kim and e. al., "Cylindrical Microdomain Orientation of PS-b-PMMA on the Blanced Interfacial Interactions: Composition Effect of Block Copolymers," *Macromolecules,* vol. 42, pp. 4902-4906, 2009.

[23] F. Ferrarese Lupi, T. J. Giammaria, F. G. Volpe and e. al., "High Aspect Ratio PS-b-PMMA Block Copolymer Masks for Lithographic Applications," *ACS Applied Materials & Interfaces ,* vol. 6, pp. 21389-21396, 2014.

[24] L. M. Pitet, S. F. Wuister, E. Peeters and e. al., "Well-Organized Dense Arrays of Nanodomains in Thin Films of Poly(dimethylsiloxane)-b-poly(lactide) Diblock Copolymers," *Macromolecules,* vol. 46, pp. 8289-8295, 2013.

[25] J. R. Fried, Polymer Science & Technology, 2nd ed., Prentice Hall, 2003, p. 154.

[26] Y. Gong, L. Yuhu, Y. He and e. al., "Solvent-Vapor-Induced Rapid Assembly of Block-Copolymer Film via Prevacuumizing," *Macromol. Chem. Phys. ,* vol. 215, pp. 1092-1097, 2014.

[27] J. Gon Son, H. Kang, K. Ki-Yeon and e. al., "Orientation Change of Diblock Copolymer Thin Films by the Addition of Amphiphilic Surfactants: Effect of Film Thickness and Surfactant Concentration," *Macromolecules ,* vol. 45, pp. 150-158, 2012.

[28] J. Gon Son, X. Bulliard, H. Kang and e. al., "Surfactant-Assisted Orientation of Thin Diblock Copolymer Films," *Adv. Mater.,* vol. 20, pp. 3643-3648, 2008.

[29] P. Etch. [Online]. Available: http://www.plasmaetch.com/reactive-ion-etching-systems-rie.php. [Accessed 11 10 2015].

[30] Wikipedia, "Reactive Ion Etching," [Online]. Available: https://en.wikipedia.org/wiki/Reactive-ion_etching. [Accessed 12 10 2015].

[31] O. Instruments. [Online]. Available: http://www.oxford-instruments.com/products/etching-deposition-and-growth/plasma-etch-deposition/rie. [Accessed 12 10 2015].

[32] T. Universal. [Online]. Available: http://www.terrauniversal.com/cleaning-systems/plasma-preen-cleaners.php. [Accessed 12 10 2015].

[33] Plasma-Therm. [Online]. Available: http://www.plasmatherm.com/pecvd.html. [Accessed 12 10 2015].

[34] Wikipedia, "Plasma-Enhanced Chemical Vapor Deposition," [Online]. Available: https://en.wikipedia.org/wiki/Plasma-enhanced_chemical_vapor_deposition. [Accessed 13 10 2015].

[35] R. W. Johnson, A. Hultqvist and S. F. Bent, "A brief review of atomic layer deposition: from fundamentals to application," *Materials Today,* vol. 17, no. 5, pp. 236-246, 2014.

[36] R. Jafari Jam, M. Heurlin, V. Jain and e. al., "III-V Nanowire Synthesis by Use of Electrodeposited Gold Particles," *Nano Letters,* vol. 15, pp. 134-138, 2015.

[37] Wikipedia, "Gold Plating," [Online]. Available: https://en.wikipedia.org/wiki/Gold_plating. [Accessed 13 10 2015].

[38] I. Garcia, B. Galiana, I. Rey-Stolle and e. al., "MOVPE Technology for the Growth of III-V Semiconductor Structures," in *Spanish Conference on Electron Devices*, Madrid, 2007.

[39] M. Behet, R. Hövel, A. Kohl and e. al., "MOVPE growth of III-V compounds for optoelectronic and electronic applications," *Microelectronics Journal,* vol. 27, pp. 297-334, 1996.

[40] J. W. Co., "Ellipsometry Tutorial," [Online]. Available: http://www.jawoollam.com/tutorial_1.html. [Accessed 14 10 2015].

[41] Jeol, "JEOL Guide to Scanning Microsocope Observation," [Online]. Available: http://www.jeolusa.com/RESOURCES/ElectronOptics/DocumentsDownloads/tabid/320/Default.aspx?EntryId=1. [Accessed 14 10 2015].

[42] H. H. T. A. Inc, "University of Toledo," [Online]. Available: https://www.eng.utoledo.edu/cmsc/downloads/docs/SEM%20Workshop%20presentation%204.pdf. [Accessed 14 10 2015].

[43] B. Hefner, "University of Minnesota - Scanning Electron Microscopy Primer," [Online]. Available: http://www.charfac.umn.edu/sem_primer.pdf. [Accessed 15 10 2015].

[44] N. Nilsson, Interviewee, *Process Engineer.* [Interview]. 2015.

[45] M. Omura, T. Imamura, H. Yamamoto and e. al., "Highly selective etch gas chemistry design for precise DSAL dry development process," in *Advanced Etch Technology for Nanopatterning III*, 2014.

[46] Umetrics, *MODDE 10.1 - Help File.*

[47] RefractiveIndex.Info, "RefractiveIndex.Info - SiO2," [Online]. Available: http://refractiveindex.info/?shelf=main&book=SiO2&page=Malitson. [Accessed 15 10 2015].

[48] RefractiveIndex.Info, "RefractiveIndex.Info - Si," [Online]. Available: http://refractiveindex.info/?shelf=main&book=Si&page=Vuye-20C. [Accessed 15 10 2015].

[49] M. Graczyk and R. Cichonski, "Shallow SiNx dry etching for NW growth on AlIIBV and Si substrates," LundNanoLab, Lund.

[50] Z. Cui, Nanofabrication - Principles, Capabilities and Limits, Springer Science, 2008, p. 255.

[51] D. O. Shin, J.-R. Jeong, Y. H. Han and e. al., "A plasmonic biosensor array by block copolymer lithography," *Journal of Materials Chemistry,* vol. 20, pp. 7241-7247, 2010.

[52] J. H. Mun, S. K. Cha, H. Kim and e. al., "Nanodomain Swelling Block Copolymer Lithography for Morphology Tunable Metal Nanopatterning," *small,* vol. 10, no. 18, pp. 3742-3749, 2014.

[53] Q. Peng, Y.-C. Tseng, S. B. Darling and e. al., "Nanoscopic Patterned Materials with Tunable Dimensions via Atomic Layer Deposition on Block Copolymers," *Adv. Mater.,* vol. 22, pp. 5129-5133, 2010.

[54] Y.-C. Tseng, Q. Peng, L. E. Ocola and e. al., "Enhanced Block Copolymer Lithography Using Sequential Infiltration Synthesis," *J. Phys. Chem. C,* vol. 115, pp. 17725-177729, 2011.

[55] J. Gon Son, H. Kang, K.-Y. Kim and e. al., "Orientation Change of Diblock Copolymer Thin Films by the Addition of Amphiphilic Surfactants: Effect of Film Thickness and Surfactant Concentration," *Macromolecules,* vol. 45, pp. 150-158, 2012.